DEVELOPMENT OF NOVEL ANTICOUNTERFEITING TECHNOLOGIES USING HEAVY METAL FREE NANOPARTICLES

A Thesis Submitted to
the Graduate School of Engineering and Sciences of
İzmir Institute of Technology
in Partial Fulfillment of the Requirements for the Degree of

DOCTOR OF PHILOSOPHY

in Materials Science and Engineering

by
Didem TAŞCIOĞLU

July 2021
İZMİR

ACKNOWLEDGEMENTS

ABSTRACT

DEVELOPMENT OF NOVEL ANTICOUNTERFEITING TECHNOLOGIES USING HEAVY METAL FREE NANOPARTICLES

Counterfeiting, the act of illegally copying a product or document, is a growing problem. Anticounterfeiting technology uses fluorescent inks that are invisible to the naked eye in daylight, but become visible under UV light. However, these inks have problems such as fading when exposed to sunlight for a long time and disappear completely. All of the existing security materials for ID cards, driver's licenses, passports, banknotes used in our country are imported.

In this study, our aim is to create a new generation of security materials and codes to combat counterfeiters and to verify the generated security codes in a simple, efficient and fast way. For this purpose, water and solvent-based nanoparticles synthesized which are non-toxic and a long-term optical stability. Security codes that cannot be detected in daylight have been created on various substrates (paper, polymer, and glass) utilizing screen printing and inkjet printing methods and using the synthesized nanoparticles. In addition, the authenticity of the security codes was checked by a commercial fiber optic based spectrometer and a handy hand-held optical device called the Quantag sensor. Thus, a verification method that can be distinguished by a simple detection device is proposed.

Furthermore, random and inimitable droplet and droplet/fiber patterns were created using the electrospinning method. Thus, unique and inimitable security codes detectable under UV light were created which may be used for anticounterfeiting. To check the authenticity of the original security codes created; images collected with a simple smartphone microscope and a database was created in which the original patterns were recorded. The originality of the random patterns was checked by comparing it with the patterns recorded in the database. In addition, the spectral information of the particle from the droplet/fiber pattern obtained was determined with a simple hand-held device. Thus, by reading spectral information from the pattern, the spectral signature of the nanoparticles was verified and thus a second-step security was created. In this way, a two-stage anticounterfeiting technology that is impossible to imitate has been developed.

ÖZET

SAHTECİLİĞE KARŞI AĞIR METAL İÇERMEYEN NANOTANECİKLER KULLANARAK YENİ TEKNOLOJİLERİN GELİŞTİRİLMESİ

Bir ürünün, belgenin veya paranın yasadışı olarak kopyalanması eylemi olan sahtecilik, büyüyen bir sorundur. Sahtecilikle mücadele kapsamında, yaygın olarak kullanılan mürekkepler gün ışığında çıplak gözle görünmezken, UV ışık altında floresan ışıma yaparak görünür hale gelirler. Ancak, bu mürekkeplerin güneş ışığına uzun süre maruz kaldıklarında solma ve zamanla kaybolma problemleri vardır. Ülkemizde kullanılan mürekkep ve kağıt dahil tüm güvenlik malzemeleri ithal edilmektedir.

Bu tez çalışmasının amacı sahtecilikle mücadele için yeni nesil güvenlik malzemelerini (mürekkepler) geliştirmek, bu malzemeleri kullanarak spektroskopik ve görüntü temelli güvenlik kodlarını oluşturmak, oluşturulan güvenlik kodlarını verimli ve hızlı bir şekilde doğrulamak için fotonik temelli teknolojileri geliştirmektir. Bu amaçla, toksik olmayan ve uzun süreli optik kararlılık gösteren suda veya organik çözgen içinde homojen biçimde hazırlanan nanotanecikler sentezlenmiştir.

Serigrafi ve mürekkep püskürtmeli baskı yöntemleri ile farklı yüzeylerde (kağıt, polimer, cam vb.) güvenlik kodları (desenler) oluşturulmuştur. Ocean Optic fiber optik spektrometre ve Quantag sensörü adı verilen el tipi optik okuma cihazları kullanılarak güvenlik kodlarının orijinalliği doğrulanmıştır. Böylece basit bir algılama cihazı ile ayırt edilebilen bir doğrulama yöntemi önerilmiştir.

Ek olarak, elektroeğirme yöntemi kullanılarak rastgele ve taklit edilemeyen damlacık ve damlacık/fiber desenleri oluşturulmuştur. Böylece sahtecilikle mücadelede kullanılabilecek, UV ışık altında görünür olan eşsiz ve taklit edilemez güvenlik kodları elde edilmiştir. Orijinal güvenlik kodlarının gerçekliğini kontrol etmek için akıllı telefon mikroskobu ile görüntüleme yapılmış ve orijinal desenlerin kaydedildiği bir veritabanı oluşturulmuştur. Elde edilen rastgele desenin özgünlüğünü veritabanı ile karşılaştırılarak belirleyen görüntü analiz yazılımı geliştirilmiştir. Ayrıca elde edilen damlacık/fiber desenler içerisinde taneciklerin spektral bilgilerini doğrulayan basit bir el cihazı ile belirlenmiştir. Böylece, desenden spektral bilgileri okuyarak, taneciğin spektral imzası belirlenmiş ve ikinci bir güvenlik basamağı oluşturulmuştur.

TABLE OF CONTENTS

LIST OF FIGURES

LIST OF TABLES

CHAPTER 1

INTRODUCTION

1.1. General Context

Counterfeiting, i.e. the act of unlawfully copying a product, document, or money, is a topic of basic and applied study as well as an economic problem because of the harm it poses to the economy and human health[1-3]. For example, counterfeiting in fields such as food, medicine, and vaccines puts the public health at risk as well as the economic damage. Apart from this, forgery of documents such as banknotes, identity cards, and passports is an important crime in the eyes of the states and causes great economic losses. In addition, significant economic losses occur when product protection and tracking are not carried out for valuable items such as jewelry or many different products such as fuel with a wide range of uses. In summary, counterfeiting is a growing and long-standing problem due to the threat it poses to the well-being and health of consumers. Considering that billions of dollars of illegal profits are created each year through counterfeiting; anticounterfeiting is extremely critical to the protection of intellectual property and the detection of counterfeit products in many applications. It becomes important to apply identity verification technologies in the fight against counterfeiting. Therefore, anticounterfeiting technologies have been developed to protect and verify the authenticity of the product or document.

Over the past few decades, numerous technologies such as radio frequency identification (RFID)[4, 5], hologram[6, 7], nuclear tracking[8], NFC tags[9], biometric markers or inks[10] with the advantages of traceability and contactless recognition have been proposed to verify the originality. These solutions differ significantly in their complexity and cost. For example, although it has the advantages of traceability to radio frequency identification (RFID), high information capacity, and contactless recognition, high cost limits its practical use, and rewritability threatens the security of stored information[11]. In addition to this, holography, which can show a completely 3-dimensional image of the holographed subject, is used as a security feature[12]. However, holography technology is

1

complex and has expensive production equipment. Using matrix barcodes such as QR codes containing product identification or tracking information is an inexpensive and effective solution[13]. But these codes are easy to copy or recreate. These can be reproduced without difficulty from the embedded message, or by scanning and reprinting an original printed code, creating a fake one. For this reason, standard printed matrix barcodes are not suitable for use to verify the authenticity of products. In summary, most of these anticounterfeiting technologies are well known and can be easily imitated by counterfeiters. For this reason, industries at risk of counterfeiting (medicine, money, documentation, food, cosmetics, etc.) have included taggants in their products to distinguish them from potential counterfeits[14]. The markers used for this application are typically invisible and have replaced traditional barcoding and hologram anticounterfeiting technologies that can be copied more easily. Taggant technology has been successfully used to reduce counterfeiting through continuous monitoring, thus preventing a crime from occurring[15]. The most important point is that these security tags are low cost to be applicable, have high coding capacity to prevent duplication, are not toxic to individuals and nature, and are detected and analyzed in simple ways[16].

When we look at the studies in the last decade, Figure 1.1 shows that there has been a significant increase in the number of studies aimed at preventing counterfeiting with the development of different materials and printing methods.

Publication year	Record Count	% of 306 articles
2010	4	1.3
2011	9	2.9
2012	16	5.2
2013	6	2.0
2014	11	3.6
2015	17	5.6
2016	23	7.5
2017	24	7.8
2018	37	12.1
2019	74	24.2
2020	82	26.8
2021	3	1.0
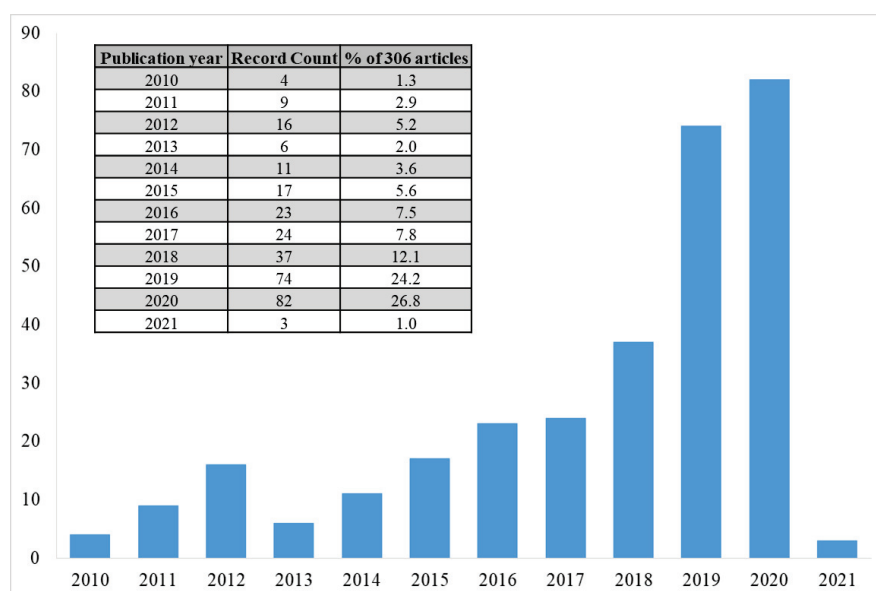
Figure 1.1. Distribution of the number of studies by years. Statistical distribution of publication records of 'anti-counterfeiting' keywords with respect to publication years. All data was collected using WoS analytics.

Recently, taggants based on optical nanomaterials have made significant progress in forensic research and traceability of products[17]. From a material perspective, we see that fluorescent-based materials and their corresponding anticounterfeiting technologies stand out due to their optical qualities, excellent security features, and difficulty of reproduction (Figure 1.2). Organic and inorganic luminescent materials, such as dyes[18], metal-organic frameworks (MOFs)[19], rare earth nanomaterials[20], semiconductor nanoparticles (quantum dots (QDs) and carbon dots)[21, 22] are emerging as attractive materials for anticounterfeiting applications.
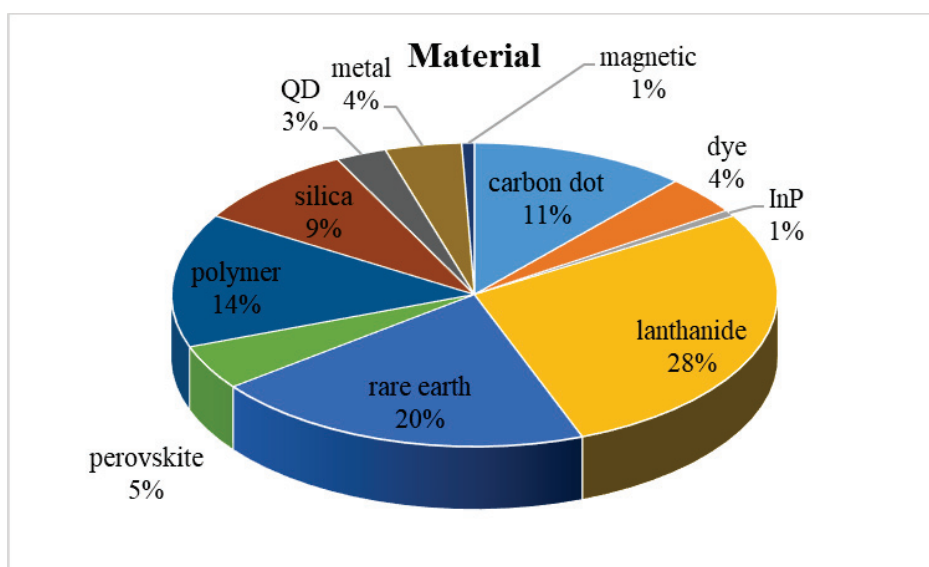
Figure 1.2. Percentage distribution of materials in security label applications in the last decade.

In literature, it has been reported that luminescent security inks generally contain organic dyes[23, 24] and lanthanide-based materials[25, 26]. While organic dyes allow for the creation of inexpensive security labels, on the other hand, these low costs and easy availability can facilitate illegal reproduction. Moreover, organic dyes have problems such as short fluorescent life and photobleaching[27]. Likewise, photobleaching lanthanide materials upon prolonged exposure to sunlight make these materials unsuitable for security printing applications. In addition, the high cost of precursor costs of lanthanide materials restricts high-scale production and prevents the security label to be developed from being feasible, as it will affect the unit cost[28, 29].

However, the quantum dots can be alternatives to organic dyes or lanthanide ion complexes[30]. Quantum dots are nano-sized particles in the semiconductor material class

which are constructed of several atoms. Particle sizes of quantum dots can be adjusted by controlling the synthesis process parameters, and the sizes typically lie between 2 nm and 10 nm (atomic diameter 10 to 50)[31]. Quantum dots exhibit outstanding optical and electrical properties due to the fact that their crystal sizes are changed[32]. Comparing with photoluminescent organic dyes, quantum dots have many advantages, from lightfastness to unique optical properties. Quantum dots have narrow emission spectra that can be adjusted by altering the size, composition, and surface chemistry of the quantum dots[33]. Unlike organic dyes having discrete emission peaks due to chemical composition, quantum dots can be tuned all over the spectrum. Besides, quantum dots have broad absorption spectra which allows them to be excited over a wide wavelength range and thus, different photoluminescent quantum dots are excited by a single excitation wavelength. With all these distinctive features, quantum dots can be an excellent opportunity to develop multi-component spectral coding mechanisms currently used in security printing technology.

Figure 1.3 shows that the printing types and distribution in the literature. Many materials for creating security labels can be easily applied as a security ink with different printing methods such as stamp printing[34], screen printing[29, 35], and inkjet printing[36, 37] for anticounterfeiting applications.
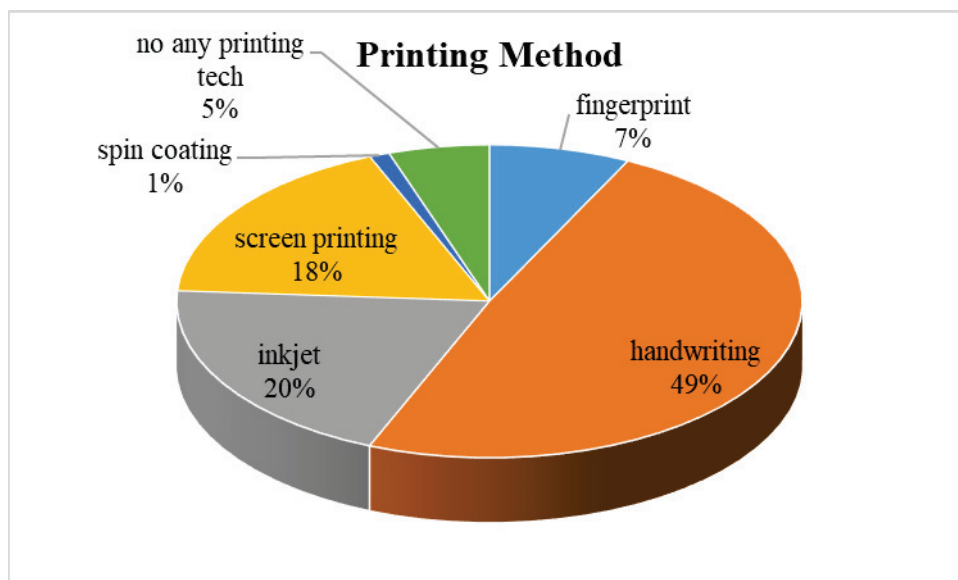
Figure 1.3. The printing types and distribution in the literature.

Despite the fact that the materials and printing techniques are so advanced, most of the luminous printed labels and patterns can still be cloned. This greatly limits high-level anticounterfeiting practices, as they are produced through a largely deterministic process and therefore the encrypted information encoded in luminescent labels/patterns is somewhat predictable[38]. Recently, it is thought that the inclusion of a security tag, such as fingerprints which allows direct and almost inimitable identification specific to each person, in the labeling of documents and products, will significantly increase the level of security and make copying impossible.

Recently, physically non-clonable functions (PUFs) based on uncertain random structures offer advanced security techniques. PUF is a physical object with a unique and fingerprint-like property[39]. The tags developed are based on the random irregularity of the object. Therefore it becomes impossible to copy and is an ideal method to prevent counterfeiting. The PUF tag is saved in a database to avoid counterfeiting and and the customer may check if a product is genuine by reading the anticounterfeiting tag and comparing the reading to those in the database. The first PUF was created in 2002 by the creation of unique random distribution patterns embedded in a polymer block[40]. PUFs developed so far are based on the optical, plasmonic, magnetic, and phase change properties of nanoparticles. Only for authentication purposes, there are some studies in the literature to create functions (PUFs) that cannot be physically cloned (Table 1.1). There are many examples in the literature where nanomaterials are randomly distributed within the material or product. For instance, polymer particles create unique optical barcodes by encoding them with different bright rare earth materials[41], in another study mentions a method of creating an optical PUF (Physical Non-Clonable Function) by 3D Printing a Photopolymer nano-suspension containing CdSe nanoparticles[42]. Although PUF labels have been developed with various materials, we still encounter some limitations of the materials. For example, certain properties such as the toxicity of Cd-based QDs or bleaching of lanthanide materials due to prolonged exposure to sunlight make these materials unsuitable for safe printing applications. Additionally, PUF tags were created that consist of randomly arranged nanofibers produced by molecular beam epitaxy from a polyaromatic hydrocarbon that can be detected using fluorescence microscopy[43, 44]. Here, the randomness is due to the angles at which the nanofibers grow and the coordinates of their endpoints. The suggested PUF labels, on the other hand, are made up of complicated organic molecules that are difficult to mass-produce and have

low physical stability. It is also claimed that security tags that could not be cloned may be generated based on the varied transportation behavior of the perovskite precursor and the irregular crystallization of perovskite during inkjet printing[45]. It was also showed that the capacity of anticounterfeiting tags could be increased significantly by adding three-dimensional height information of perovskite patterns to security tags. It has been shown that perovskite fluorescence spots that cannot be seen with the naked eye can be detected with a fluorescent microscope. However, decoding such complex PUF codes often requires more advanced and expensive equipment such as a fluorescent or confocal microscope.

In summary, counterfeiting is a very important problem for many states and companies and the research to be done in this area is very valuable. Today, with the advancement of material technologies, the optical and physical properties of nanomaterials continue to be also improved. This offers new areas and ideas in new technologies to be used in the fight against counterfeiting to researchers.

Table 1.1. Anticounterfeiting tags grouped based on material, security type and verification technique.

Material	Coding Type	Security Type	Substrate	Application Type	Reader (Verification Tech)	Ref
PbS QDs	Randomly distributed nanoparticle patterns	-	Polymer	Irradiated under UV illumination	TEM	46
Fluorescein-embedded Ag@SiO$_2$ Core–Shell NPs	Randomly distributed nanoparticle patterns	Surface Plasmon Resonance, Fluorescence, Raman Signals	Silica-coated Silicon Substrate	Shadow-mask-lithography-assisted Self-assembly	Dark-field, Fluorescence or Raman Microscope, Portable Microscope Smart Phone	47
Coordination Polymer, Cupric Bromide Complex Of Pyrazine 1,4-dioxide	Graphical And Spectral	Fluorescence Signals, 2D Graphical Information	Polymer	Lithography	Bright-field, Dark-field, Fluorescence Multifunctional Microscopy	48
-	Random Topography	Random Topography Of A Scattering Surface	Paper, Coated Paperboard, Plastics Metals	Laser Surface Authentication	RFID	49

(cont. on next page)

7

Table 1.1. (Cont.)

Material	Coding Type	Security Type	Substrate	Application Type	Reader (Verification Tech)	Ref
Polymer Wrinkles	Microfingerprints	The Wavelength Of The Ridge Patterns And The Particle Geometry	Passport, A Ring, Watch	The Lithography, Free And Spontaneous Wrinkling	Confocal Laser Scanning Microscopy (CLSM), Portable Microscope (200×) attached To an IPhone 6	14
Au NPs	Randomly distributed nanoparticle patterns	Scattering	-	Dropcast	Dark-Field Microscopy	50
Lanthanide-doped Zeolite Taggants in Polymer Film	Randomly distributed nanoparticle patterns	Luminescence	Glass	Casting	RGB Data Convert To Digital Data	51
Eu^{3+}/Tb^{3+} Phosphors	Random patterns	Scattering Luminescence	Tape	Painting	Microscope Filters 10× Camera	52
Fluorescent Proteins And Silk Proteins	Randomly patterns	Luminescence	The Surface Of Medicines	Directly Attached	RGB Data Convert To Digital Data	53
NIR-to-visible Upconversion Nanocrystals	QR Code	Luminescence	Paper	Aerosol Jet	Smartphone	54

Table 1.1. (Cont.)

Material	Coding Type	Security Type	Substrate	Application Type	Reader (Verification Tech)	Ref
Fluorescent Dye Coated AgNWs	Randomly distributed nanowires	Luminescence	PET Film	Dropping	Fluorescence Microscopy	55
Perovskite Crystal Dot	Randomly distributed NPpatterns	Luminescence	Polymer	Ink-jet Printing	Fluorescence Microscopy	45
Cd-based NPs	Randomly distributed nanoparticle patterns	Luminescence	Glass	Ink-jet Printing	The Portable Microscope For Smartphone	56
UCMPs/CDs	QR Code	Luminescence	Paper	Screen-printing	Smartphone	57
Polymer microtaggant	2D matrix-type QR Code	2D Graphical Information	Drug	Optofluidic maskless lithography system	Fluorescence microscope, Smartphone	58
UCN-encoded microparticles	Spectral	Luminescence	Pharmaceutical blister packs, currency, credit cards, etc.	Magnetic contact printing or modified inkjet methods	Smartphone	41

(cont. on next page)

Table **1.1. (Cont.)**

Material	Coding Type	Security Type	Substrate	Application Type	Reader (Verification Tech)	Ref
Metal nanostructures	Spectral and pattern	2D Graphical Information	-	Electron beam evaporator	Bright-field reflection microscope	59
Photo-responsive supramolecular polymers	QR code	Fluorescence	Paper	Inkjet printing	-	60
Microspheres	Barcode (one-dimensional Code)	Fluorescence	-	-	Confocal laser scanning microscope	61
Microfibers	Pattern	Fluorescence	Drug	Electrospinning	Fluorescence microscope	62
Gap-enhanced Raman tags	Random pattern	Raman spectrum	Transparent Scotch tape, paper	Drop-casting	Confocal Raman system	63

1.2. Problem Description and Purpose of This Study

Nowadays, in addition to the anticounterfeiting of valuable documents and certificates, increasing market volumes in many areas create enormous opportunities for counterfeiting. Traditional anticounterfeiting methods usually offer one-step security and can be deciphered by skilled counterfeiters as they are visible and are often produced according to pre-designed/set coding rules. On account of this, it has become more important to develop security tags that cannot be cloned or difficult to clone. Therefore, compared to simple labels, the trend towards labels produced by stochastic manufacturing processes has increased recently. Although the increasing material options offer researchers the opportunity to create security labels based on random distribution and difficult to repeat, expensive and specialized devices such as confocal microscopes, fluorescence microscopes, transmission electron microscopes, etc. are still needed for the verification methods of many security labels. This situation does not allow the use of security labels created with nanoparticles for the control of the originality of the product or the document in daily life. For this reason, in order to have a say in preventing counterfeiting, it becomes important to ensure that the security labels to be developed are complex and unrepeatable, as well as to check their originality in a simple and fast way.

The aim of this study is to create new generation security labels/patterns that can be used in security printing and brand protection applications and to verify the created security labels/patterns by a simple, efficient and fast way. In this dissertation, the security labels/patterns to be created by heavy metals free nanoparticles that are luminescent in the visible region and have optical stability for a long time. For this aim, we synthesized InP and carbon-based quantum dots acting as pigments in security labels/patterns to be developed. Security inks are formulated to emit in different colors with water-based carbon and solvent-based InP nanoparticles creating security labels that will be used in screen printing and inkjet printing. Besides, we checked the originality of these tags with the help of a simple device. Thus, we developed a verification method that can not be observed by naked human eye but will be distinguished by a simple detecting device.

In addition to this, in our study, we created unique security patterns with electrospinning technique apart from known printing methods. Thanks to the random droplet/fiber pattern we obtained, we produced inimitable security patterns. By the electrospinning technique, it is not possible to reproduce the same droplet/fiber pattern

even by its manufacturer, so we are able to create unique security patterns such as fingerprints that cannot be cloned. Also, the electrospinning technique offers a simple production method for the security label, eliminating the difficulty of industrial-scale production and replication. In this study, we propose a verification method, firstly, the luminescence properties of the security patterns will be determined by using a hand-held spectrophotometer to check spectral authenticity of the product or document. Additionally, the security pattern image obtained by a mobile phone will be checked and matched with the original image in the database for authentication. Therefore, the originality of the product or document can be proven by verifying the two-steps.

CHAPTER 2

DEVELOPMENT AND APPLICATION OF CARBON NANOPARTICLES BASED FLUORESCENT INKS FOR SECURITY PRINTING

2.1. Introduction

Counterfeiting of high-value things such as money and legal documents is a challenging problem worldwide[64]. Paper-based information encryption and counterfeiting prevention is a hot topic, as many important documents, including identity cards, passports, money, and checks, are currently still held on paper[65]. Different combat techniques are designed using various materials and methods to prevent counterfeiting[66-69]. Luminescent labels are one of the most popular security items to protect original documents. In the security printing sector, UV luminescent inks are commonly used as 2nd level security features, being non-visible in the daylight and become visible under UV light. Table 2.1 lists some examples of luminescent nanoparticles utilized in the production and design of luminescent security inks, the methods of their synthesis and printing procedures[70].

Table 2.1. List of the luminescent nanomaterials, synthesis and printing methods[70]. Copyright 2016 Royal Society of Chemistry

Luminescent nanomaterials	Synthesis methods	Printing methods	Ref
LaPO:Eu	Hydrothermal	Screen printing	25
Y_2O_3:Eu	Sol-gel	----	26
water based-hybrid dots/HEC	Hydrothermal	Screen printing	71
β-$NaYF_4$:Er/Yb	Thermal decomposition	Inkjet printing	72
$NaYF_4$:Er/Yb	--	AFM nanoxerography	73
CdTe	Wet- chemistry	Mask based printing	74
CdS	Wet- chemistry	Inkjet printing	75
ZnS:Mn^{2+} QDs	chemical precipitation	Handwriting	22
Carbon Quantum Dots	Thermal decomposition	Inkjet printing	76
Carbon nanodots	Pyrolysis and microwave	Simple writing by pen	77
Gold and silver np	Microwave	Screen printing	78

Among various printing methods, inkjet printing is preferred due to its minimal reagent use, direct and high-throughput modeling capability, difficulty to replicate, and ease of authentication. Therefore, complex anticounterfeit labels may be created using inkjet printing of luminescent security inks. Simply described, the inkjet printing process ejects a fixed amount of ink in a chamber from a nozzle by means of a sudden, semi-diabatic reduction of the chamber volume by means of piezoelectric action[79]. UV fluorescent inks for security printing are generally organic dye and lanthanide based, and their lightfastness in not adequate for many applications such that they bleach in time when exposed to sunlight for an extended period of time. Although studies have been made with quantum dots recently, there is no commercial product yet.

Recently, environmentally friendly carbon-based luminescent quantum dots (CD), which offer outstanding features such as biocompatibility, high chemical stability, and photostability, have attracted much attention[80, 81]. CDs are conjugated systems consisted of sp^2 and sp^3 hybridized carbon atoms[82]. CDs have many different potential applications, including drug delivery, bioimaging, solar cell, fluorescence sensors[83, 84]. Particularly, their optical properties are unique and prominent, and can be applied in a wide spectrum of security printing applications. Carbon dot based anticounterfeiting labels can be regarded as one of the hot topics among these potential areas.

CDs are conventionally synthesized via top-down or bottom-up methods[85]. The top-down method involves breaking down bulk carbon structures into nanoparticles by using arc discharge, laser ablation, chemical, or electrochemical oxidation, and etc[86-88]. Many types of carbon materials, such as graphite powder, carbon nanotubes, carbon fibers can be processed to achieve quantum dots via top-down methods[89, 90]. The Bottom-up method, on the other hand, comprises assembling various molecular precursors such as citric acid, carbohydrates, and biomaterials to form carbon based nanoparticles employing various approaches such as pyrolysis, hydrothermal, thermal decomposition and microwave synthesis[83, 91-93]. Compared to traditional semiconductor quantum dots, CD production is generally cost effective and relatively easier to scale up.

In this work, we formulated a security ink suitable for inkjet printing using carbon based nanoparticles as a color pigment to authenticate valuable documents. We preferred water-soluble carbon based nanoparticles forwhy they have high optical stability and easy synthesis methods. Security labels have been printed on paper sheets using the inkjet printing technique. The security labels printed were verified by using a low-cost,

convenient handheld optical device, called Quantag sensor developed in-house by Quantag Nanotechnologies. Here, it is aimed to detect the differences that cannot be distinguished with the eye by controlling the printed security labels with a hand sensor and thus deter counterfeiting.

2.2. Experimental

2.2.1. Reagents

Diammonium hydrogen citrate (98%), urea (99%), Polysorbate 80, TWEEN® 80 viscous liquid and Span® 80 nonionic surfactant were purchased from Sigma-Aldrich. Ethylene glycol (≥ 99%) and tetraethylene glycol (98%) were purchased from Merck. Blue luminescent carbon-based nanoparticle was supplied from Quantag Nanotechnologies.

2.2.2. Synthesis of Green Luminescent Carbon Based Nanoparticles

In this chapter, for creating new security labels we aimed to obtain carbon based nanoparticles with high photoluminescence spectra in the visible region and high experimental yield.

Firstly, diammonium hydrogen citrate and urea were mixed and ground homogeneously. The weight fraction of mixture is 1:1. Then this mixture was heated under reflux for 15 minutes in air. After the reaction, the obtained product was dissolved in water and then was purified by using centrifugation at 6000 rpm for 20 min[94, 95]. After centrifugation, the concentration of CDs solution is 9%. The quantum yield of particles was measured by 16%. The yield of this synthesis procedure was found to be 55%.[95]
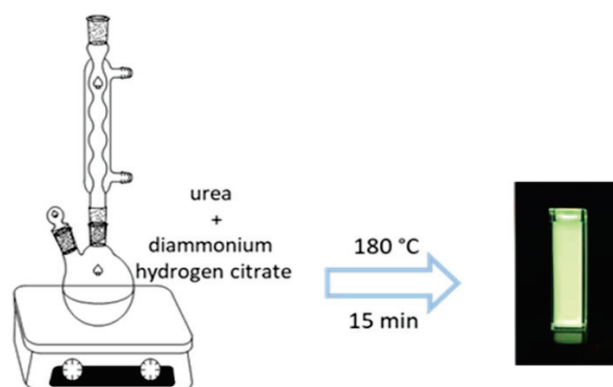
Figure 2.1. Schematic illustration of green luminescent carbon dot synthesis.

2.2.3. Formulation of Luminescent CDs Ink

Luminescent CDs ink was made by dispersing varied percentages of blue and green luminescent particles in a combination of water and water-soluble organic co-solvent based on investigations in the literature[96, 97]. To avoid clogging of the printer nozzles, organic co-solvents such as water-miscible ethylene glycol and tetraethylene glycol were used as humectants. Typically, the ink solution contains two different non-ionic surfactants (Span® 80 and Tween® 80) at a ratio of 5% in 20 ml of the mixture to increase surface wettability. To get well-dispersed CDs, the mixture was violently stirred for 10 minutes and ultrasonically vibrated for 10 minutes. After the prepared Luminescent CDs ink was filled into the ink cartridge of the inkjet printer (EPSON L382), various labels were printed on A4 paper (without fluorescence background).

2.2.4. Characterization

Photoluminescence (PL) and quantum yields (QY %) measurements were performed by Horiba-Fluorolog with an integrated sphere (Koç University). Absorbance was measured by Shimadzu UV-3600 UV-VIS-NIR spectrophotometer (Koç University). Fourier transform infrared spectroscopy (FTIR; Spectrum 100, PerkinElmer, Shelton, CT, USA) (İzmir Institute of Technology-IYTE) was used to confirm N-doped. X-ray photoelectron spectroscopy (XPS) studies were performed using a Thermo Scientific K-Alpha XPS spectrometer (Ege University). High-resolution transmission electron microscopy (HRTEM; JEOL 2100F, operated at 200 kV) was used to examine the

morphology of the CDs. Surface tension was measured by Krüss digital tensiometer K10ST (IYTE). Viscosity of the inks was measured with RheoSense microVisc (IYTE). Epson L382 inkjet printer (Quantag) was used to print security labels. Quantag sensor is a fiber optic-based device developed in-house (patent protected). It is a handheld and low-cost optical instrument utilizing fiber optical probes to detect and measure fluorescent intensity (brightness) and colors (wavelength) of inks embedded into patterns printed on substrates.

2.3. Results and Discussion

2.3.1. Spectral and Structural Characteristics Green Luminescent Carbon-Based Nanoparticles

Photoluminescence (PL) and absorption (Abs) spectra of CDs were shown in Figure 2.2. Emission PL_{max} is 532 nm and photoluminescence color of particle is green.
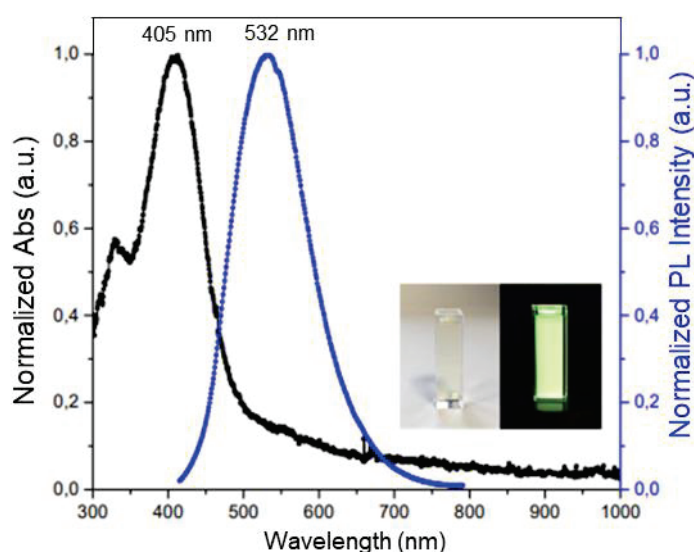
Figure 2.2. Abs (left vertical axis, solid line) and PL (right vertical axis, dash line) spectra of CDs.

The composition and surface groups of the CDs were investigated using X-ray photoelectron spectroscopy (XPS). Carbon (284.39 eV), nitrogen (399.28 eV), and oxygen (531.23 eV) are present at the surface of CDs, according to the broad XPS

spectrum shown in Figure 2.3.a. The five components of the C1s spectrum (Figure 2.3.b) may be deconvoluted into multiple peaks corresponding to C=C (sp^2 carbon) (284.26 eV), C-C (sp^3 carbon) (284.67 eV, 285,05 ev), C=N (285.72 eV), and C-N (287.84 eV). The pyridinic N (C-N-C) and pyrrolic N (N-H) groups, on the other hand, may be deconvoluted into two components with peaks at 399.39 and 400.23 eV, respectively, in the N1s spectra (Figure 2.3.c). There are additional oxygen-containing groups that may be detected on CDs' surfaces (Figure 2.3.d). Two peaks in the corresponding O1s band are associated with sp^2 (C=O, 531.02 eV) and sp^3 (C-O, 532.09 eV)[98, 99]. The presence of nitrogens was shown by XPS measurements.
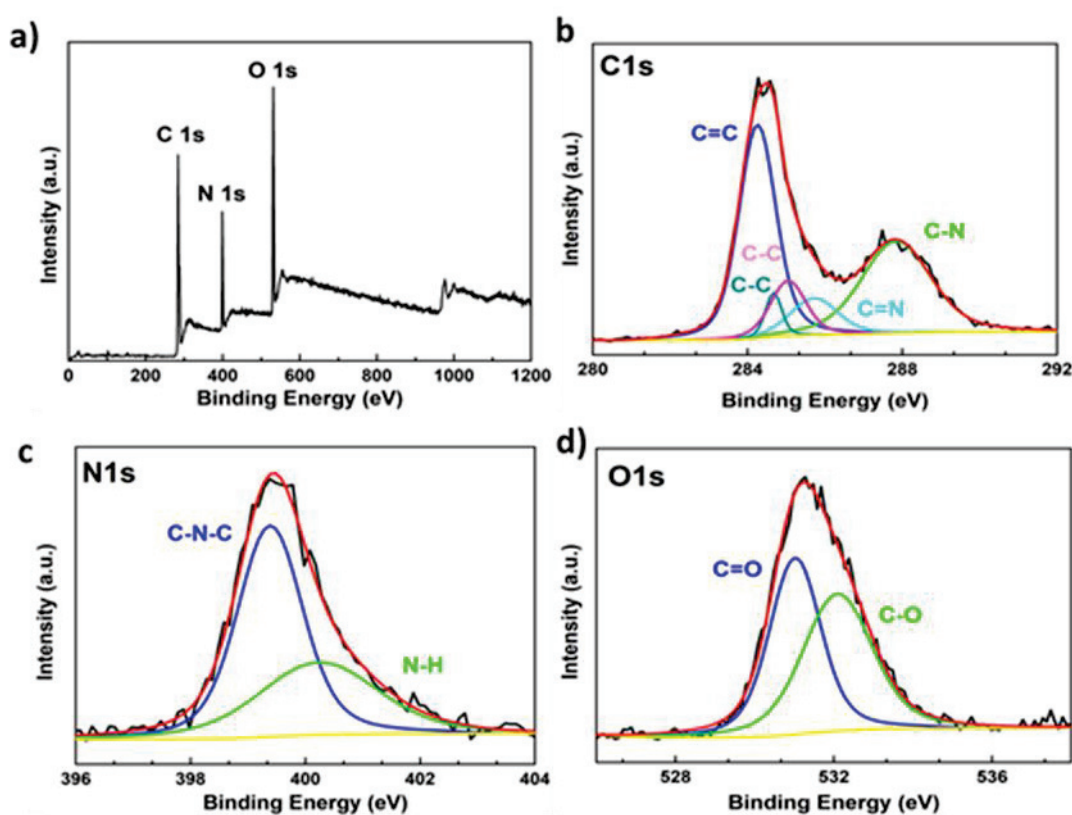
Figure 2.3. (a) Nitrogen doped CDs XPS full scan spectrum. (b) C 1s (c) N 1s (d) O 1s (high resolution) XPS spectrum of CDs with nitrogen doping.

The substance was subsequently analyzed by FT-IR spectra to confirm whether it was nitrogen-rich or not (Figure 2.4). The O-H and symmetric/asymmetric N-H bonds make up the wide band that is centered at 3346 cm^{-1} [100]. At 2787 cm^{-1}, there is a minor signal indicating the presence of C-H stretching vibration. Furthermore, the FT-IR

18

spectrum clearly shows the presence of amide bonds, as seen by their typical peaks of 1700 and 1639 cm^{-1}, which correspond to C=O and C=N stretching vibrations, respectively. At 1192 cm^{-1}, the other amide band, which is C-N stretching, can be seen. In addition, the CH2 bending and C-O-C stretching vibrations have distinctive peaks at 1400 and 1069 cm^{-1} [100, 101]. As a consequence of the XPS and FT-IR results, the material used in this investigation may be validated as nitrogen-rich carbon dots.
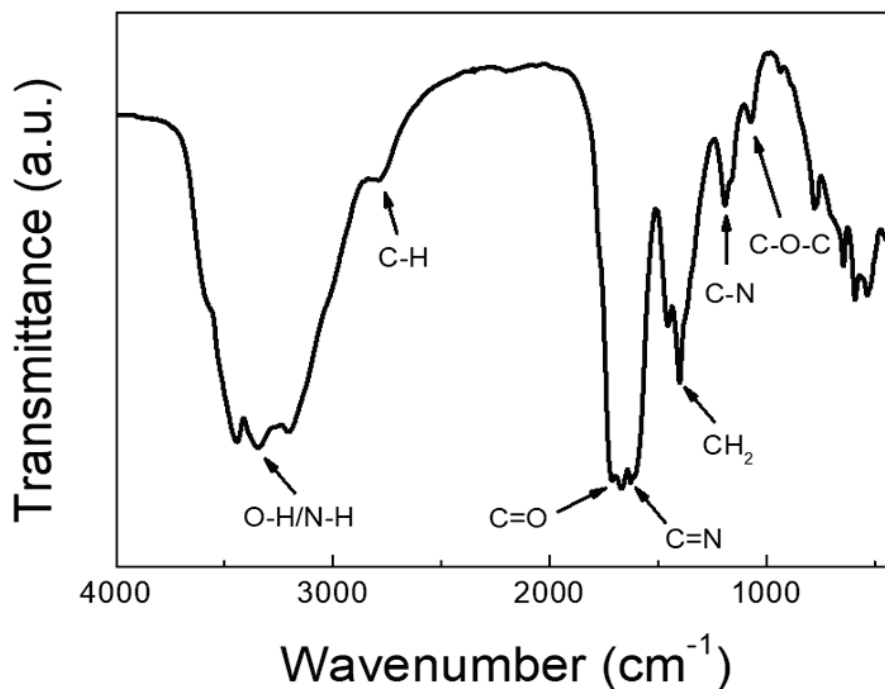
Figure 2.4. FTIR spectrum of green CDs.

Figure 2.5 shows HRTEM images of carbon quantum dots. Figure 2.5.a. shows an HRTEM image obtained from ~ 10 nm nanoparticles. The lattice spacing values of the particle are 0.24 and 0.34 nm. The lattice spacing value of 0.24 nm is reported to be generated by overlapping two (002) planes in literature[102]. Here, carbon quantum dots are more accurate to describe as graphene rather than graphite, as they are formed by stacking several layers of graphene. HRTEM images of a 9 nm nanoparticle and an 11 nm nanoparticle (Figure 2.5.d and e) show that both nanoparticles have the same lattice spacing of 0.24 nm. Figure 2.5.f shows HRTEM images of an elongated nanoparticle with dimensions of 4 nm x 9 nm, which demonstrate the existence of 0.34 nm lattice fringes in the (002) plane.
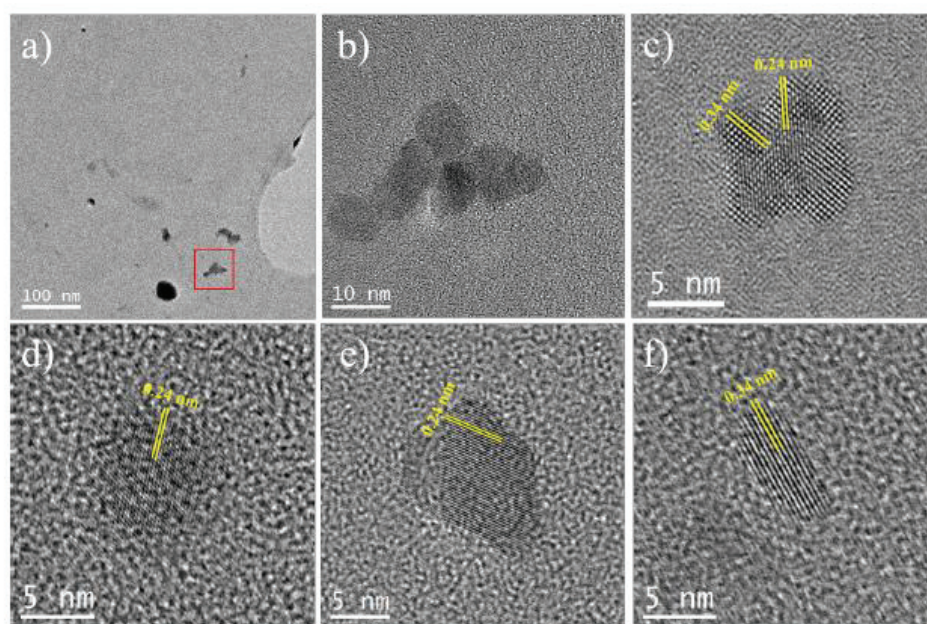
Figure 2.5. a-b) General TEM images of the green CQD sample showing the presence of small nanoparticles. c-f) HRTEM images of several individual nanoparticles identified as carbon based quantum dots. 0.34 nm lattice spacing value corresponds to the (002) plane, where 0.24 nm lattice spacing is formed by overlapping two (002) planes.

2.3.2. Spectral and Structural Characteristics Blue Luminescent Carbon Based Nanoparticles

The photophysical properties of blue luminescent carbon based nanoparticles which are supplied from Quantag Nanotechnologies are as follows (Table 2.2).

Table 2.2. The properties of blue luminescent carbon based nanoparticles

Composition:	Blue Luminescent Carbon-based NP
Quantum Dots Apperance:	Colorless solution
Maximum excitation wavelength:	355 nm
Maximum emission:	450 nm
Quantum Yield:	>60 %
Concentration:	1 mg/ml
Purity:	>80 %
Solution:	Water

It is observed that the particle has absorbance at 355 nm and emission at 450 nm (Figure 2.6). PL intensities are high and FWHMs are below 90 nm. In addition, particle quantum yields are above 60%.
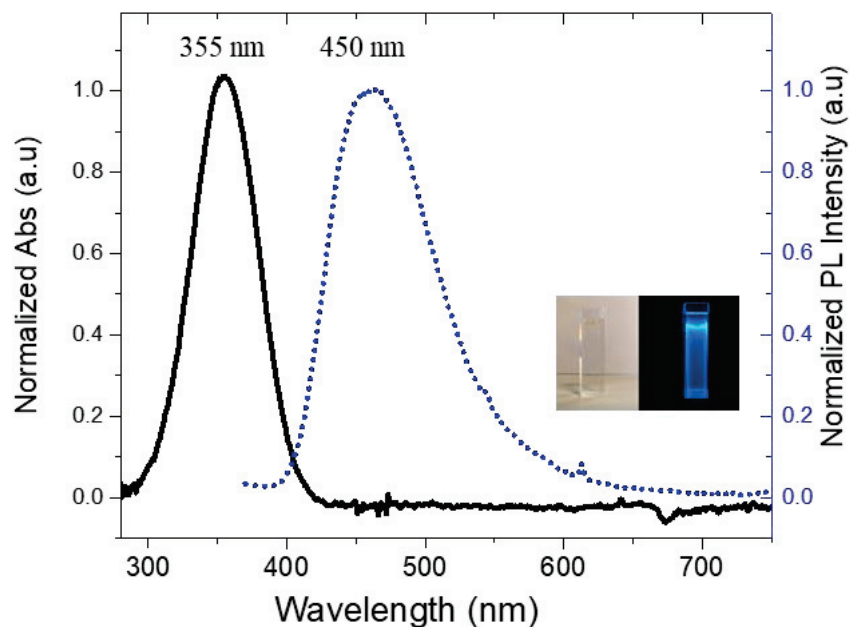
Figure 2.6. Absorption and PL spectra of blue luminescent carbon based nanoparticles.

Furthermore, according to the results of the TEM analysis, it is observed that the particle sizes are approximately 2 nm.
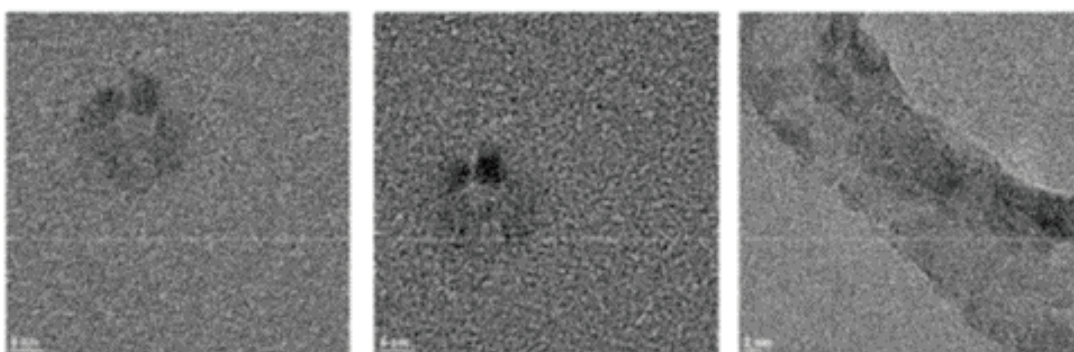
Figure 2.7. General TEM images of the blue luminescent carbon based nanoparticles.

2.3.3. Creating Luminescent Security Label with Carbon-Based Particles by Inkjet Printing

Here, we show the use of CDs to produce luminescent ink is based on the good photostability of CDs. As known, major efforts and advances are being made to combat counterfeiting in inkjet printing using luminescent nanoparticles. To date, various luminescent compounds have been developed and utilized as security inks[70]. Organic dyes, for example, were utilized as fluorescent inks in the early stages. However, low photostability and a small Stokes shift restrict them. Conjugated polymer dots, inorganic quantum dots, and rare earth compounds, due to their tunable fluorescence characteristics and narrow emission bandwidths, have been used instead of dye[103-105]. Polymer dots, on the other hand, need complex preparation procedures and are costly. Moreover, due to low biocompatibility and long-term toxicity, inorganic quantum dots or rare earth compounds are often not suited for counterfeit printing in industries like food and medicines. As a result, achieving easy and rapid anticounterfeiting printing employing biocompatible, non-toxic, and efficient luminescent materials is critical. Carbon-based nanoparticles stand out from other luminescent materials (inorganic quantum dots, organic fluorescent dyes, and rare earth compounds) because of their long fluorescent life, low toxicity, easy synthesis, and superior photostability, etc. Moreover, the small size and homogeneous distribution of carbon nanoparticles make them suitable for printing.

Since water has a high surface tension of 72 mN/m[106] and a low viscosity value of 0.89 cP, it is not possible to print an ink formulation consisting only of water and particles with an inkjet printer. Therefore, some ink mixtures were prepared by targeting the viscosity and surface tension values stated in the literature. The viscosities of available inkjet inks are quite low, ranging from 2 to 20 cP[107]. The drop should be as spherical as possible for the finest printing results and to achieve this, the surface tension of the ink must be adjusted to 25-35 mN/m[108]. Table 2.3 shows the viscosity and surface tension values of the ink formulations without added particles. The optimum surface tension value in the prepared ink formulations was measured in the sample of ink-4. Due to the orientation effects at the interfaces caused by the hydrophilic and hydrophobic parts of the surfactant added to the ink formulation, the desired surface tension value was measured.

Table 2.3. Ink formulations and their physical properties.

Content of ink	Ink-1	Ink-2	Ink-3	Ink-4
tetraethyleneglycol	0.1	0.1	0.1	0.1
ethyleneglycol	0.3	0.2	0.1	0.1
water	0.6	0.7	0.8	0.75
span 80 & Tween 80	0	0	0	0.05
Physical properties				
surface tension (mN/m)	47.5	39.5	38.6	30.3
viscosity (cP)	2.80	2.00	1.60	3.5
pH	3.81	3.33	3.67	4.62
density (g/ml)	1.058	1.061	1.043	1.074

The inkjet ink parameters (i.e. surface tension and dynamic viscosity) have been carefully adjusted and made suitable for printing with existing commercial printers to ensure that the carbon particle-containing ink we have prepared works stably with an inkjet printer. The viscosity and surface tension of the ink according to various carbon nanoparticle concentrations were examined and shown in Table 2.4. With the addition of the particles, it is observed that the viscosity (from 3.5 cP to ~4.5 cP) and surface tension (from 30.3 mN/m to ~33.5 mN/m) of the ink increase by a small amount. In addition, the change in particle concentration does not cause a significant change in viscosity and surface tension. In summary, the physical properties of the ink are compatible with the literature values[108, 109].

Table 2.4. Summary of physical properties of inks.

		surface tension (mN/m)	viscosity (cP)	pH	Density (g/ml)
	0% QD	30.3	3.50	4.62	1.074
Blue luminescent	1% QD	33.5	4.50	6.57	1.107
	2% QD	34.2	4.40	6.57	1.042
Green luminescent	0.0625% QD	33.6	4.60	4.15	1.022
	0.125% QD	33.6	4.30	4.32	1.029

The fact that the printer has an integrated ink tank instead of a cartridge allows the prepared ink to be printed easily. The prepared QD-containing ink formulations shown in Figure 2.8 were loaded into the tanks of the Epson L382 model inkjet printer with micro piezo technology to be printed on the paper, and the 0.125% QD content green luminescent ink was printed on the brown kraft paper. According to Figure 2.9, there is a

security pattern visible on the paper even in daylight, which can be explained by the large amount of particles in the ink. Apart from this, another problem is that it emits blue fluorescence from the paper under UV light. Therefore, it is more appropriate to have non-fluorescence papers on which security printing will be applied.

Figure 2.8. Inkjet printer.
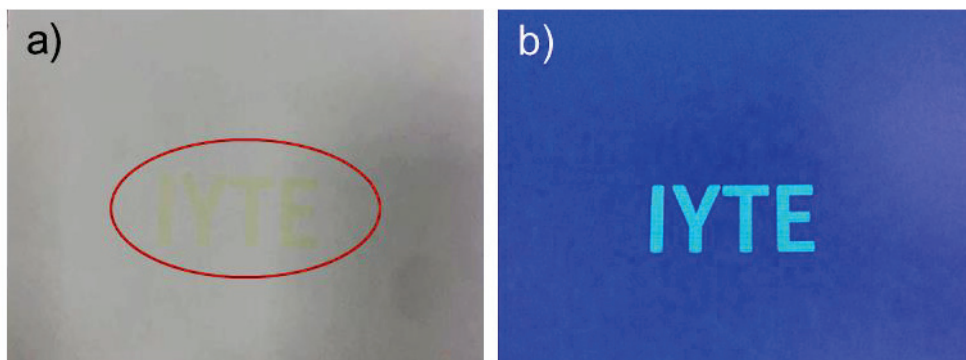
Figure 2.9. The photographs of IYTE pattern printed using CDs ink under a) visible light and b) UV light (365 nm) on the paper which has fluorescence background.

Figure 2.10 shows that the photograph of the pattern printed on paper without fluorescence background under daylight and UV light. While 2% blue luminescent carbon particles were added in the inkjet ink, 0.125% green luminescent carbon particle was added. In the photograph taken under daylight, it is observed that the concentrations of particles are high and the printed square patterns are noticed in daylight. However, it is easily observed that the patterns created with thin lines on the same printed-paper do not leave any color on the paper under daylight, and the patterns formed under UV light.
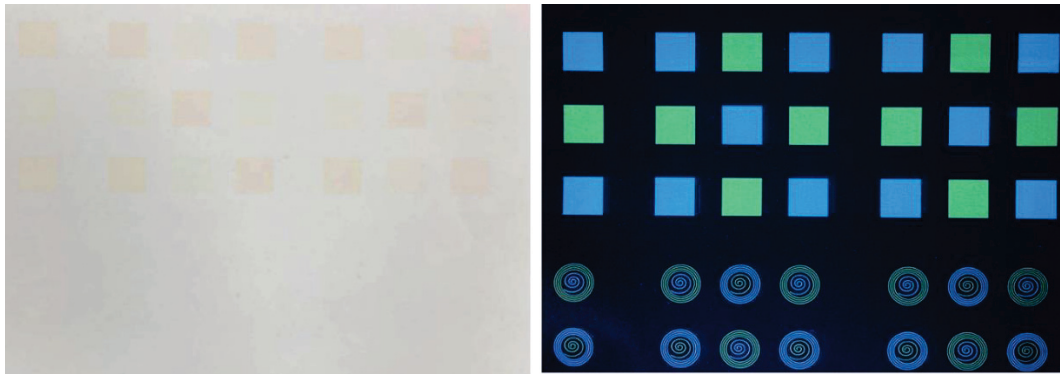
Figure 2.10. The photograph of pattern printed using CDs ink under visible light and UV light (365 nm) on the paper which has non-fluorescence background (2% blue luminescent CDs, 0.125% green luminescent CDs).

In this study, since it is essential that the security pattern on the valuable paper or document becomes visible only under UV and should not be noticed in daylight, the amount of particles added to the ink formulation has been reduced. The amount of green particles in the ink has been reduced to 0.0625%. After the particle concentrations were reduced by half, the image of the pattern written by inkjet printer under daylight and UV light is given in Figure 2.11. It is observed that although the character and volume of the printed ''quantag'' text is large, there is no coloration on the paper due to the reduced particle amount, but the hidden text is clearly read under UV light.
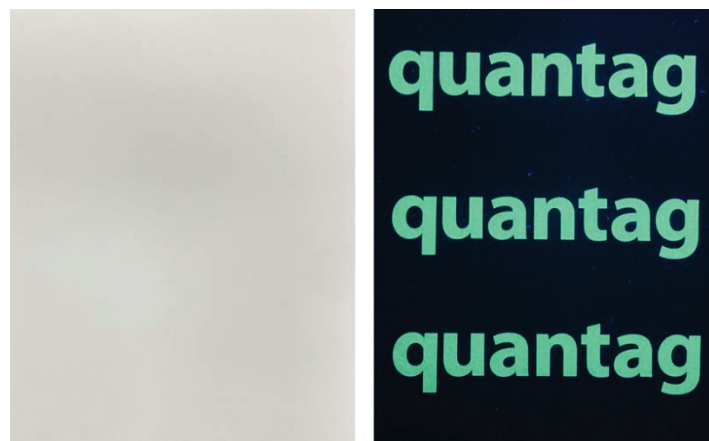
Figure 2.11. The photograph of pattern printed using CD ink (0.0625% green luminescent CDs) under visible light and UV light (365 nm).

Furthermore, in Figure 2.12, it is observed that the patterns printed with ink prepared with 1% blue luminescent carbon particle are not noticed in daylight, but they luminescence very well under UV light. In the literature, many security patterns obtained

with carbon or different luminescent nanomaterials can be created within the scope of combating counterfeiting. Similarly, the fact that a lot of published anticounterfeiting study in the literature may make the efforts' of counterfeiters easier. Recently, studies have shifted to lanthanide particles to increase the security level of such security patterns, which have become reproducible due to their easy production. Although the dual-mode luminescent obtained with two different excitation wavelengths increase the safety level a little[110], the production difficulty and cost of the material limit its widespread applicability. We consider that such security patterns, which are controlled only by human eye, would limit fighting against counterfeiting.

Figure 2.12. The photograph of pattern printed using CDs ink (1% blue luminescent CDs) under visible light and UV light (365 nm).

Therefore, controlling authenticity of security labels with the help of a device having better sensitivity than naked eyes may enhance security level of the obtained labels. In this study, the fluorescent emissions of the security labels with the hand-held sensor of Quantag Nanotechnologies was measured in Figure 2.13.a. The Quantag sensor includes one excitation fiber bringing laser to the substrate to excite the ink; and collection fibers integrated with bandpass filters transmitting selected emissions to sensor[111]. Here, the signal level of the blue-luminescent ink was read from the 450 nm channel on the sensor, while the green-emitting ink was read from the 550 nm channel. According to Figure 2.13.b, the signal values read increase linearly depending on the particle concentration.
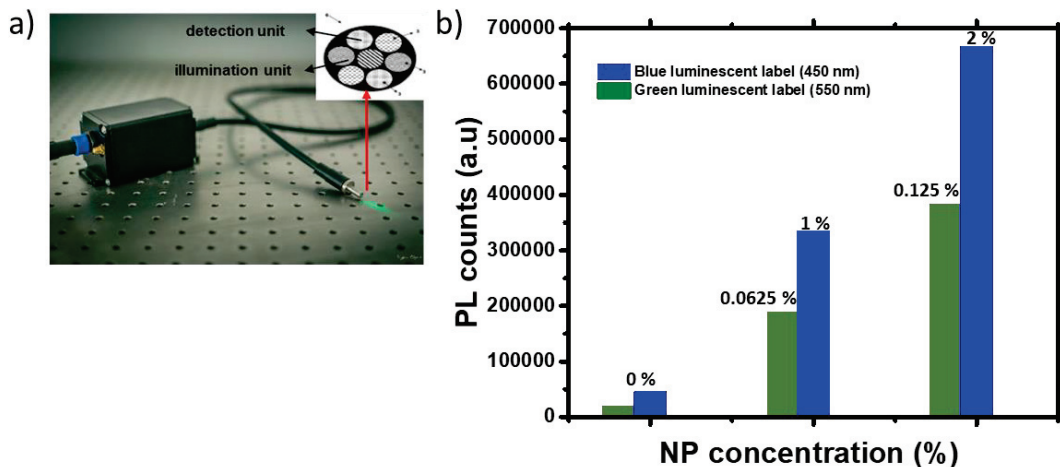
Figure 2.13. a) Quantag sensor, b) The fluorescent emissions of blue and green security labels with different nanoparticle concentrations by Quantag sensor.

At the same time, the photostability of the obtained labels was followed for 54 days. The signal values are normalized to the value read on the first day and the change in the weekly measurement results is given in Figure 2.14. As can be seen in the Figure 2.14, when looking at the sensor results obtained from the labels with both particles, it is observed that the optical stability of the printed security labels is also very good.
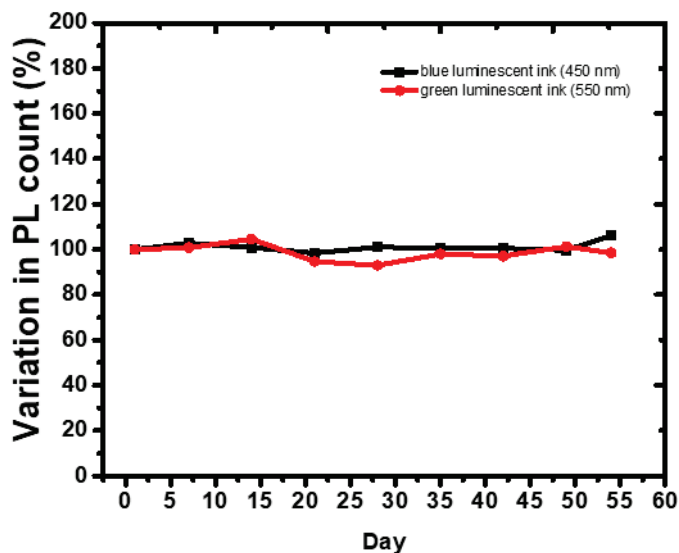
Figure 2.14. The intensity of luminescent inks monitored by the Quantag sensor for 54 days, demonstrating the photostability of security labels printed on the paper. N=3G, the standard deviation is less than 2% therefore omitted.

In summary, in this study, highly stable security labels were created with high photostability particles. In addition, since the emission intensities of the inks are read with the help of a device, the differences that the human eye cannot distinguish can be detected and the originality of the document or document can be accurately demonstrated.

2.4. Conclusion

In this study, firstly, having green emission and water-dispersible carbon nanoparticles were synthesized by a bottom-up method. Second, different concentrations of carbon particles were dispersed in a solvent mixture containing ethylene glycol, tetraethylene glycol, water, and surface agent to create a hydrophilic ink formula, resulting in water-based, environmentally safe luminescent security inks. More importantly, the security labels that would not be visible in daylight but would be visible under UV light were printed on non-fluorescent papers with inkjet printing by adjusting the amount of carbon particles. The fact that the printed labels are visible only under the 365 nm UV lamp and exhibit different colors reveal that it can be used for security printing. Furthermore, it enabled the creation of security labels with high security capacity by reading the optical response from the labels with a hand-held sensor. Here, security labels are easy to both manufacture and verify. Therefore, the technology developed in this chapter against counterfeiting is highly promising.

CHAPTER 3

DEVELOPMENT OF AN ANTICOUNTERFEITING TECHNOLOGY COMBINING In(Zn)P/ZnS NANOPARTICLES BASED FLUORESCENT INKS FOR SCREEN PRINTING AND A HAND-HELD OPTICAL DEVICE FOR VALIDATION

3.1. Introduction

Counterfeiting and adulteration of valuable documents cause economical loss and initiate societal concerns. Anticounterfeiting efforts require advanced materials and technologies to prevent counterfeiting. Fluorescent inks are commonly used as second level security features; being invisible in the daylight and detectable under UV light. In the last decade, to prevent counterfeiting security labels have been created using different printing techniques with various fluorescent inks formulated by using rare earth luminescent materials[112-116], carbon dots[57, 117, 118], organic dyes[18, 119], and quantum dots[22, 120, 121]. Among various printing methods, screen printing is preferable because it is easily applicable to various substrates[122]. Screen printing, which is a unique technique in terms of quality, is a process that uses ink or pastes pushed by a template attached or embedded in a web stretched onto a printing frame. Since an intermediate transfer tool is not required, the consistency of the ink is not limited. Long-lasting and durable prints can be produced, providing unrivaled homogeneity and color brilliance. Screen printing can be applied to a variety of substrates from papers to metals to plastics, and even glass and ceramics. These capabilities enable the production of a wide variety of products including smart identity cards, credit cards, technical and industrial parts, automobile components, flat glass and glass containers, etc.[123].

In the past several years, publications applying screen-printing techniques using lanthanide-based luminescent materials have been widely reported for anticounterfeiting[25, 28, 29]. Organic dyes as fluorescence materials are used in this field[119, 124]. Colloidal quantum dots (cQDs) are considered as alternatives to these materials

because of their unique optical properties[30, 31]. Unlike the lightfastness and cost-effectiveness of lanthanide-based materials and broad emission peaks of organic dyes[125], cQDs possess narrow, stable, and tunable photoluminescent emission features[126]. In addition, cQDs may be excited by a single wavelength light source because of their broad absorption spectra. With all these distinctive features, cQDs may be regarded as an excellent anticounterfeiting material for contemporary security ink and printing technology.

For two key reasons, the focus of QD research has recently shifted to III-V semiconductors. First, III-V materials are more covalent than ionic materials (II-VI and IV-VI materials), resulting in better optical stability and reduced toxicity. Second, the Bohr radius in III-V systems is substantially bigger than in II-VI systems, causing stronger size quantization effects. Among all III-V semiconductors, especially InP, are of great interest due to the stability and the low toxicity explained by the absence of elements of Cd and Hg[127]. In addition, the bulk InP has a bandgap of 1.35 eV (918 nm) with a relatively larger Bohr exciton radius which leads to a wider emission range between visible and near IR spectral regions due to the strong quantum confinement effect[128].

Synthesized InP core nanocrystals exhibit generally poor fluorescence quantum yield (less than 1%)[129]. They are also prone to photodegradation and surface oxidation. Coating the core with a larger band semiconductor shell such as ZnS or ZnSe is a common method for increasing and improving PL efficiency because of better surface passivation and reduction of dangling bonds[130, 131].

In the literature, two approaches to the colloidal synthesis of high quality and monodisperse InP QDs have discussed: Hot injection and heating-up techniques. In the hot injection method, at room temperature the precursor solution is quickly injected into the hot reaction medium[132]. Injection leads to sudden nucleation of NCs and the formation of new nuclei is prevented due to the drop in temperature. As a result, monodisperse NCs are obtained. The hot injection approach is a commonly used technique for the synthesis of colloidal InP NCs[133]. The heating-up approach is a method where the reaction mixture containing precursors, solvents stabilizing ligands are heated from room temperature to higher temperatures[134]. In contrast to the hot injection approach, the nucleation time in the heating-up method may be longer at the same time as the growth time. In this method, the selection of precursors and the heating rate are very important to obtain high-quality NCs[135].

To prevent counterfeiting, luminescent/fluorescent materials are turned into colorless fluorescent inks that exhibit confidential information when exposed to UV light[26, 71, 136]. However, as these materials often exhibit monochromatic emissions that are easy to imitate, these security inks offer a low-level of protection against counterfeiting. In recent years, luminescent inks made of rare-earth materials attract great attention due to their fast response time, high brightness, and efficiency[35, 137-139]. However, rare-earth materials based security inks severely limit scaled-up production due to high cost. Furthermore, it is desired to verify the authenticity of a document illuminated under UV light by visual inspection without using a device[35, 71]. However, this simplicity would make security patterns predictable and can be easily reproduced. To prevent counterfeiting, utilizing an affordable, widely-used, handy instrument such as a mobile phone or an optical device working with a specially formulated ink may enhance anticounterfeiting procedures.

In this study, we formulated a colloidal nanoparticle (colloidal quantum dot)-based security ink to authenticate valuable documents. Here, we chose indium-based alloyed nanoparticles because the cost of indium based precursors is much lower than the rare-earth element based materials. On top of that, they can be easily produced at hundreds of grams in one-pot, and thereby further lowering the ink cost. Herein, we synthesized In(Zn)P/ZnS nanoparticles to formulate security inks emitting brightly in various colors. The fluorescence properties of nanoparticles were adjusted by precursor type and reaction temperature. The In(Zn)P/ZnS colloidal nanoparticles were mixed with a commercial printing varnish to formulate security ink. The inks were used to print security patterns on various substrates including paper, polymer, and glass by applying the screen-printing technique. The security patterns printed were evaluated by using a commercial fiber-optic based spectrometer, and a low-cost, convenient handheld optical device, called Quantag sensor developed in-house by Quantag Nanotechnologies. The security patterns that were barely detectable under UV light by the naked eye were clearly detectable by the Quantag sensor. The spectral features, wavelengths, and brightness, were validated by a fiber-optic based spectrometer; verifying the readings of the Quantag sensor. It is demonstrated that the security patterns can be printed by using the specially formulated ink and detected with a low-cost, simple, and handy optical device to authenticate the originality of documents or products.

3.2. Experimental

In this study, In(Zn)P/ZnS nanoparticles were synthesized according to the hot injection approach. Then, In(Zn)P/ZnS nanoparticles at low percentage were dispersed in the commercial screen printing varnish. Nanoparticles included varnish were printed to the paper by using screen-printing process.

3.2.1. Reagents

Indium (III) chloride (InCl$_3$, 98%), indium (III) bromide (InBr$_3$, 99%), Zinc (II) iodide (ZnI$_2$, ≥99.99%), oleylamine (OA, 70%), trioctylphosphine (TOP, 97%), zinc stearate (technical grade), 1-octadecene (ODE, 90%), 1-dodecanethiol (DDT, ≥98%), and sulfur (Merck, 99%) were purchased from Sigma-Aldrich. Zinc (II) chloride (ZnCl$_2$, 97%) and tris(diethylamino)phosphine ((DEA)$_3$P, 97%) were purchased from Alfa Aesar. Printcolor series 592 varnish was used to formulate inks.

3.2.2. Synthesis of In(Zn)P/ZnS Nanoparticles

In this study, for creating new security codes we aimed to obtain InP based nanoparticles with high photoluminescence spectra in the visible region and high experimental yield.

In(Zn)P/ZnS/DDT colloidal nanoparticles were synthesized by applying a modified hot injection method[140]. Figure 3.1 shows a schematic illustration of the synthesis of In(Zn)P/ZnS/DDT particles. Briefly, 0.9 mmol of InCl$_3$ and 4.4 mmol of ZnCl$_2$ were mixed in 10.0 mL of oleylamine at 120 °C and stirred for 20 min. After indium and zinc precursors were completely dissolved under a nitrogen atmosphere, the reaction temperature was increased to a specific predetermined value (varied from 150 to 200 °C). 3.3 mmol of tris(diethylamino)phosphine ((DEA)$_3$P) was rapidly injected into the precursor solution to synthesize the core of In(Zn)P nanoparticles. To coat the nanoparticle surface with ZnS shell, TOP-S and Zn(stearate)$_2$ were prepared individually and added dropwise into In(Zn)P core nanoparticle dispersion. Firstly, 2 mL of 2.2 M TOP-S and 8 mL of 0.4 M Zn(stearate)$_2$ solutions were simultaneously injected into the reaction medium and the reaction temperature was increased to 300 °C. After one hour,

1.4 mL of 2.2 M TOP-S and 0.4 M of 8 mL of Zn(stearate)$_2$ solutions were added as the second injection. The formation of additional layers was established at 30 min. and 15 min. respectively following the second injection. After the formation of multilayered ZnS shell coating, the reaction was cooled down to 120 °C. At this temperature, DDT was injected into the dispersion to grow an organic passivation layer over the nanoparticle surface. The process was subsequently stopped by cooling the dispersion to room temperature after another 20 minutes of stirring (Figure 3.2).
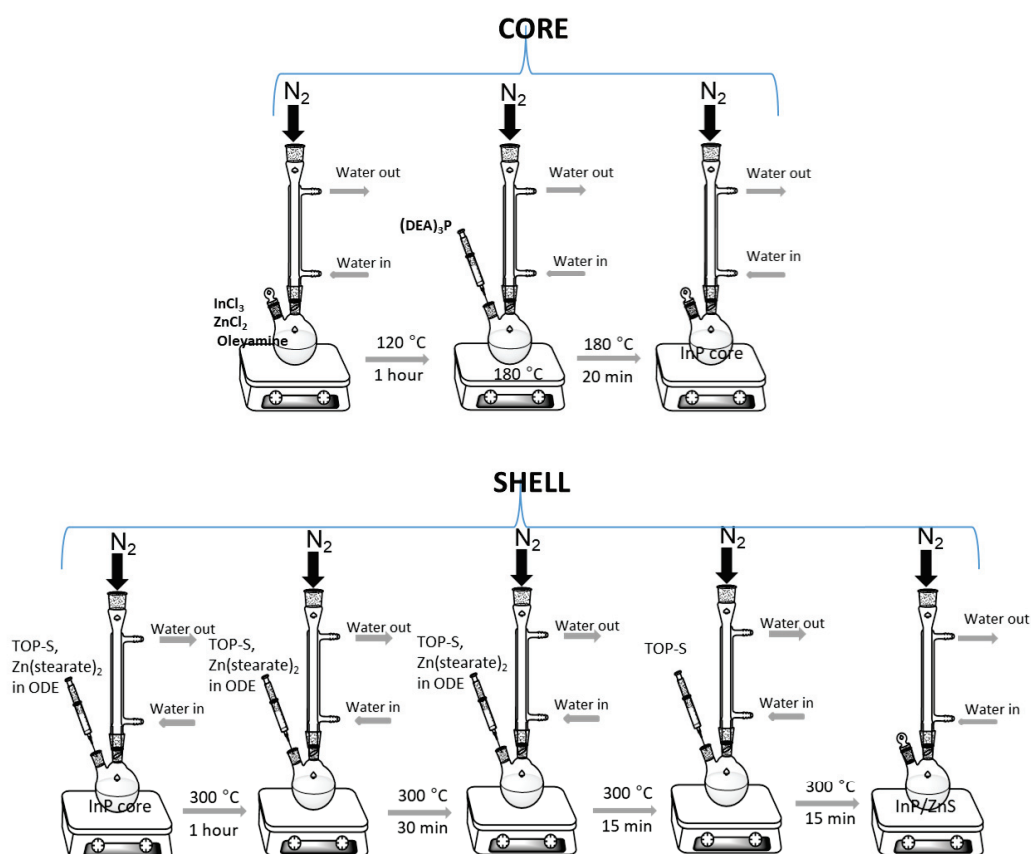
Figure 3.1. Schematic illustration of the synthesis of In(Zn)P/ZnS particles.
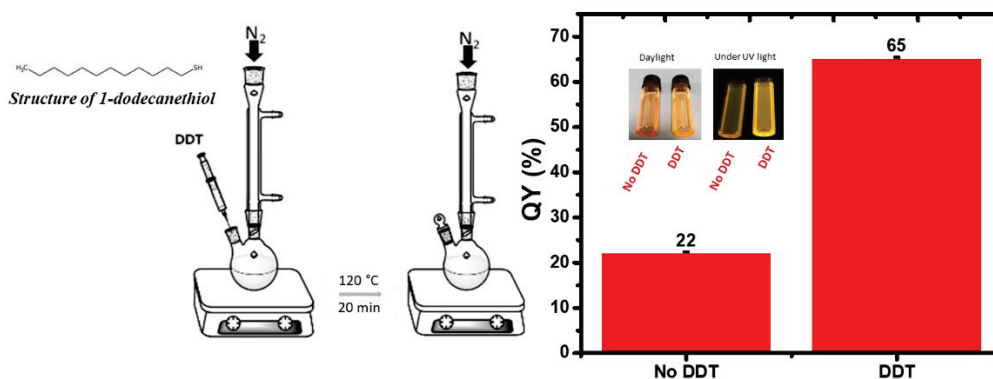
Figure 3.2. Schematic illustration of synthesis setup of DDT addition and its effect on improving quantum yield.

To purify the crude In(Zn)P/ZnS/DDT nanoparticles, the dispersion was precipitated by the addition of ethanol and then centrifugated at 6000 rpm for 15 minutes. This purification step was repeated one more time to remove remaining unreacted precursors and excessive amounts of organics. Purified In(Zn)P/ZnS/DDT nanoparticles were dried under vacuum and stored as powders.

3.2.3. Printing Process

In(Zn)P/ZnS/DDT nanoparticles were dispersed in a commercial varnish with a ratio of 0.1-0.2% v/v (1000-2000 ppm). This ink was used to print security patterns on the various substrates by using a screen-printer.

3.2.4. Characterization

Photoluminescence (PL) and quantum yields (QY %) measurements were performed by Horiba-Fluorolog with an integrated sphere or USB2000 fiber-optic based spectrometer (Ocean Optics Inc., Dunedin, FL, USA) (Koç University). Absorbance was measured by Shimadzu UV-3600 UV-VIS-NIR spectrophotometer (Koç University). Particle size measurements were taken by DLS (Malvern ZS-Zetasizer) (Quantag Nanotechnologies). SEM-EDS analysis employed FEI QUANTA 250 FEG SEM equipped with an Oxford Instruments energy dispersive X-ray analyzer (İzmir Institute

of Technology-IYTE). XRD patterns were obtained by Bruker D2 phaser–X-ray diffractometer (Koç University). Fourier transform infrared spectroscopy (FTIR; Thermo Scientific iS10 FT-IR) was used to confirm DDT coating (Koç University). The thickness of the screen-printed patterns was measured by KlaTencor MicroXM-100 optical profilometer (İzmir Institute of Technology-IYTE). Andor Revolution confocal microscope was used to determine ink homogeneity in the printed patterns (İzmir Institute of Technology-IYTE). The fluorescence intensity (brightness) and color (wavelength) of the ink embedded into labels printed on the substrates were measured with the Quantag sensor (Quantag Nanotechnologies), which was detailed in Chapter-2.

3.3. Results and Discussion

3.3.1. Spectral Properties of In(Zn)P/ZnS/DDT

In this study, we preferred to synthesize In(Zn)P/ZnS/DDT nanoparticles for anticounterfeiting application. The emission colors of these nanoparticles were adjusted by trying different indium and zinc precursors and adjusting the reaction temperature rising from 150 ℃ to 200 ℃.

Without a protective shell, the InP QDs have a poor photoluminescent quantum efficiency due to the state of the surface trap of core[135]. The solution to this problem is the epitaxial growth of another semiconductor material around the QD as the shell. Additional shell prevents trap emission by increasing the quantum efficiency of the nanocrystals but also forms a physical barrier between the core QD and the surrounding environment[141]. Here, we coated core particles with ZnS shells because of their toxicity, chemical stability, and low cost. Also, in order to reduce the lattice mismatch between ZnS and InP, Zn source was added to the structure during the core synthesis. In Table 3.1 different concentrations of zinc sources were studied at 180 ℃. According to Table 3.1 without using a zinc source in the core particle production, the photoluminescence spectrum of particles shifted further to the right, the FWHM value increased and the size distribution of particles was polydisperse. Higher concentrations of precursor led to smaller particles, but it shows that the photoluminescence properties of particles deteriorated. Increasing the amount of ZnI_2 decreased the quantum efficiency of the

sample is from 57% and 42%. The reason for this may be larger precursor concentrations make it more difficult to dissolve the solid precursors[140].

Table 3.1. Results of reactions depending on different concentration of zinc source.

Condition	PL$_{max}$ (nm)	ABS$_{max}$ (nm)	Stokes shift (nm)	FWHM (nm)	QY (%)	Core type	Atomic % Zn/In	Size (nm)
No zinc	603	550	53	71	50	$In_{0.18}Zn_{0.82}P$	-	10.8 (poly disperse)
ZnI$_2$ (2.2 mmol)	518	475	43	59	57	$In_{0.34}Zn_{0.66}P$	1.96	7.5
ZnI$_2$ (4.4 mmol)	491	440	51	60	42	$In_{0.19}Zn_{0.81}P$	4.2	5.6

Figure 3.3 shows the shifts in the absorbance peaks of the In(Zn)P core structure and the diameter information measured by DLS method. ZnI$_2$ added to facilitate shell growth also reduced the size distribution of InP nanoparticles.
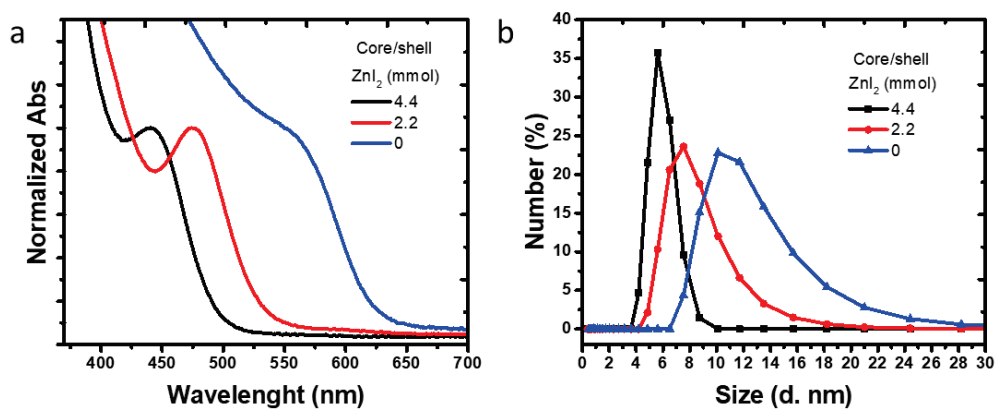
Figure 3.3. a) Absorption spectra, and b) particle size and distributions of In(Zn)P core nanoparticles, tuned by ZnI$_2$ concentration but keeping the reaction time fixed.

According to Figure 3.4, when the concentration of the zinc source was reduced, the photoluminescence spectra shifted to the red part of the spectrum. Here, the most effective parameter is the Zn content in the composition of the nanoparticles. Because increasing the Zn content in the composition results in a decrease in the PL wavelength of the nanoparticles due to the high bandgap of Zn.
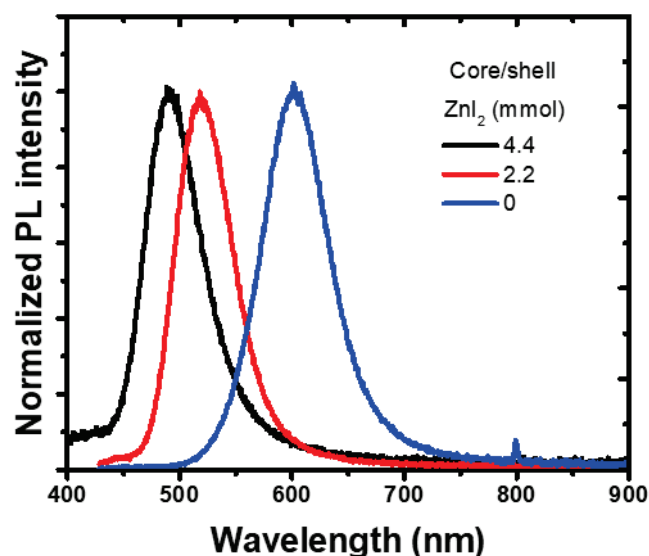
Figure 3.4. Photoluminescence spectra of In(Zn)P core nanoparticles, tuned by ZnI_2 concentration but keeping the reaction time fixed.

Then, the different indium and zinc sources were studied to obtain In(Zn)P core nanoparticles while all other reaction conditions were kept constant (Table 3.2). Table 3.2 shows that PL maxima wavelength and quantum efficiency for In(Zn)P/ZnS nanoparticles depending on different In and Zn precursor sources.

Table 3.2. PL maxima wavelength and quantum efficiency for In(Zn)P nanoparticles with different In and Zn source.

Indium source	Zinc source	
	$ZnCl_2$ (4.4 mmol)	ZnI_2 (4.4 mmol)
$InCl_3$ (0.9 mmol)	602 (75%)	491 (42%)
$InBr_3$ (0.9 mmol)	593 (70%)	496 (46%)

Table 3.3 shows that changing the precursor type and concentration is important for adjusting the particle properties. Here, the indium and zinc sources were changed when the other reaction conditions were kept constant. Using the Zn source $ZnCl_2$ and replacing $InCl_3$ with $InBr_3$, the photoluminescence shifted the wavelength from 602 nm to 593 nm (Figure 3.5). This indicates that size adjustment can be made by changing the

37

indium halide precursor type (salt). Oleylamine used in core synthesis is the hard base, it coordinates complexes containing $InCl_3$ more strongly than $InBr_3$, so $InCl_3$ is more soluble[140]. Since $InBr_3$ has poor solubility, it has led to the formation of smaller nanocrystals here.

Table 3.3. Photophysical and structural properties depending on In and Zn precursor source.

Condition	PL max (nm)	ABS$_{max}$ (nm)	Stokes shift	FWHM (nm)	QY (%)	In/(In+Zn)	Zn/(In+Zn)	Zn/In	Size (nm)
$InCl_3$ (0.9 mmol) ZnI_2 (4.4 mmol)	491	440	51	60	42	0.19	0.81	4.2	5.6
$InBr_3$ (0.9 mmol) ZnI_2 (4.4 mmol)	496	442	54	65	46	0.17	0.83	4.7	6.0
$InBr_3$ (0.9 mmol) $ZnCl_2$ (4.4 mmol)	593	525	68	68	70	0.20	0.80	4.3	8.3
$InCl_3$ (0.9 mmol) $ZnCl_2$ (4.4 mmol)	602	518	84	65	75	0.23	0.77	3.4	11.6

According to Table 3.3, when the Zn source ZnI_2 is used and studied with $InCl_3$ and $InBr_3$, it was observed that the absorbance and photoluminescence wavelength shifted further to the left. When the halides are adsorbed on the InP surface, it can cause changes in the surface reaction rate with varying steric effects. Especially the larger iodide ion can make the adsorption areas less accessible, reducing the rates of surface reaction. For this reason, it may have caused the particle sizes to remain smaller.

In summary, when $ZnCl_2$ is used instead of ZnI_2 as the source of zinc, it appears that the particle size is increased and the photoluminescence spectra of the particles move to the right. However, it is also shown that the optical quality of the particles improved. When we look at Table 3.3, it is observed that the quantum yields increase from ~40% to ~75%. Therefore, changing the zinc source is an effective method for improving the optical properties of the particle.

In Figure 3.5, it is observed that the indium and zinc sources, which provide good optical properties under these reaction conditions, are $InCl_3$ and $ZnCl_2$, respectively.

Figure 3.6 shows that FWHMs of samples synthesized using different sources of indium and zinc with different exciton positions varied between 60-68 nm.
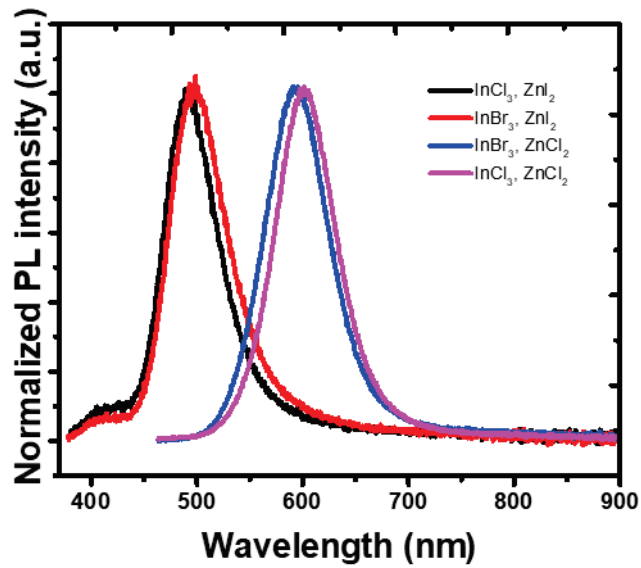
Figure 3.5. Photoluminescence spectra of In(Zn)P/ZnS core/shell nanoparticles prepared with different precursor sources.
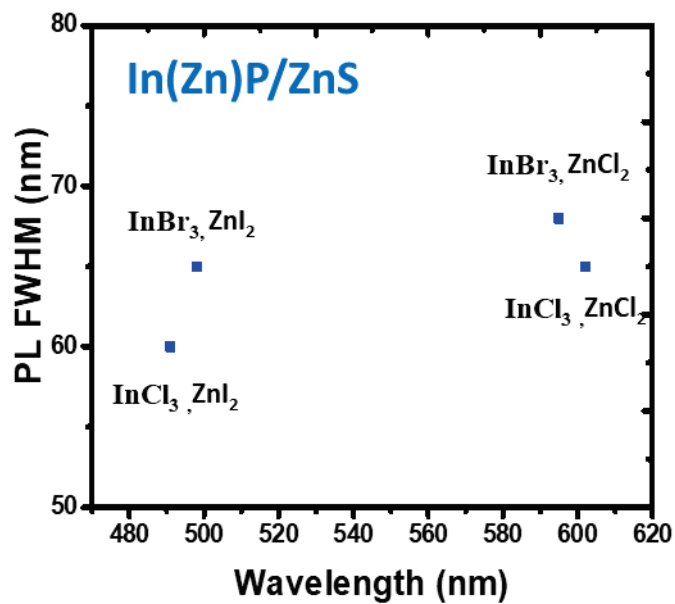
Figure 3.6. The emission line width of In(Zn)P/ZnS using different indium halides and zinc precursors.

After examining the effect of different indium and zinc sources, the effect of the reaction temperature was studied. As shown in Figure 3.7., increasing the reaction

temperature resulted in redshifts in the absorption spectra. The particle size of the nanoparticle core was measured by DLS (Dynamic Light Scattering) technique (Figure 3.7.b), confirming the increase in nanoparticle size from 5.6 to 13.5 nm was correlated to the observed red-shifted absorption spectra. Despite a well-defined absorption band of In(Zn)P core nanoparticles, weak photoluminescence was observed.
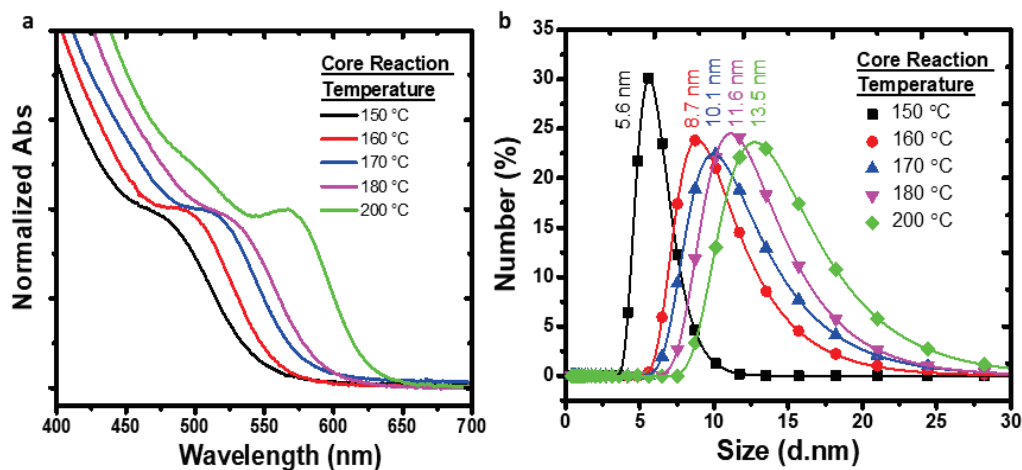
Figure 3.7. a) Absorption spectra, and b) particle size and distributions of In(Zn)P core nanoparticles, tuned by the reaction temperature but keeping the reaction time fixed.

Nonradiative relaxations due to the surface defects cause weaker emissions for InP nanoparticles unless a proper inorganic shell is coated on the surface of the core nanoparticle[142]. XRD patterns of the core nanoparticles revealed the formation of low-quality nanocrystalline structures (Figure 3.8). XRD measurements indicated the formation of ZnO layer (JCPDS: 36-1451) on the particle surface due to oxidation of Zn ions (Figure 3.8a). As demonstrated in the literature[135, 143], InP core generally generates low fluorescence emission (quantum yield <1%) and is inclined to surface oxidation and photodegradation. Coating the core with a larger bandgap semiconductor material such as ZnS is a common method to improve fluorescence efficiency by passivating the core surface and diminishing dangling bonds[130]. Herein, ZnS was chosen as the shell layer material because it has high chemical stability and wide bandgap (3.6 eV), and low-cost precursors are commercially available[144, 145]. When the core nanoparticle was coated with ZnS shell, In(Zn)P/ZnS nanoparticles emitting in the range of 535-638 nm with higher quantum yields (Figure 3.8b - Table 3.4). XRD patterns show better diffractograms

suggesting improved crystal structures and well-defined (111), (220), and (311) facets established after ZnS/DDT shell grown on the particle surface (Figure 3.8b and c).

Table 3.4. Photophysical properties of In(Zn)P/ZnS/DDT nanoparticles prepared at various reaction temperatures.

The reaction temperature	PL_{max} (nm)	Abs_{max} (nm)	Stokes shift (nm)	FWHM (nm)	QY (%)
150 °C	535	470	65	68	72
160 °C	550	490	60	65	80
170 °C	573	505	68	70	85
180 °C	602	518	84	65	75
200 °C	638	565	63	68	62
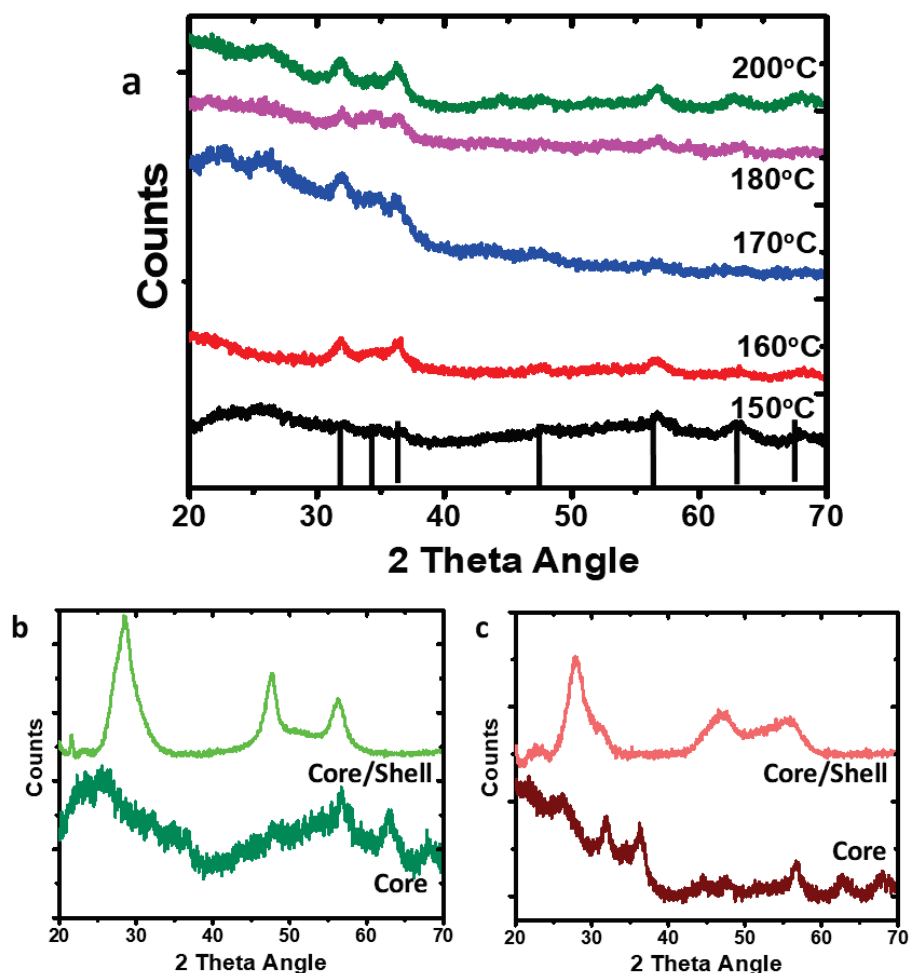
Figure 3.8. a) The XRD diffractogram of the InZnP core nanoparticles with different core reaction temperatures. The solid black lines represent the reference lines of ZnO structure (JCPDS: 36-1451). The effect of ZnS shell addition on the crystal structure of InZnP/ZnS core/shell nanoparticles was shown for b) 150 °C and c) 200 °C.

41

The fluorescent colors of the nanoparticles were tuned by adjusting the reaction temperature, which increased from 150 to 200 °C. The bright visible emission under UV illumination is an indication of the highly efficient fluorescence emission shown in the inset of Figure 3.9a. For all reaction temperatures, the FWHM of nanoparticles was comparable (Figure 3.9.b.). (DEA)$_3$P was used as the phosphorus source because its higher steric hindrance reduces chemical reactivity and consequently leads to stable and high-quality nanocrystals[130, 140]. Other phosphorus sources tris(trimethylsilyl)-phosphine ((TMS)$_3$P), and tris(dimethylamino) phosphine ((DMA)$_3$P) were not chosen because (TMS)$_3$P is highly flammable, toxic, and expensive[140] and (DMA)$_3$P has high reactivity because it has lower steric hindrance[146].
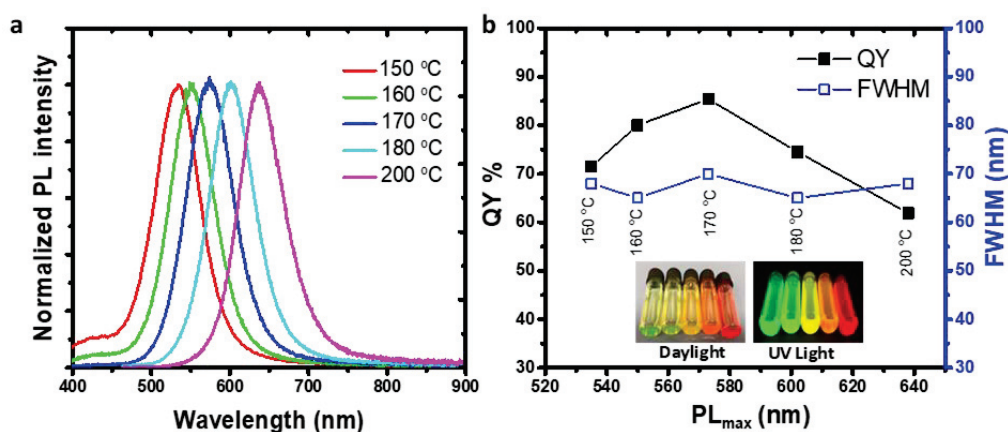
Figure 3.9. a) Fluorescence spectra of In(Zn)P/ZnS/DDT core/shell nanoparticles tuned by the reaction temperature b) Evolution of the fluorescence quantum yield (QY) percent and the FWHM of the spectra with respect to the emission wavelengths (increasing core reaction temperature resulted in red-shift in fluorescence maxima - from left to right). Highly concentrated samples were deliberately prepared to exhibit fluorescence colors under daylight and UV-light illumination.

The point of the incorporating of Zn ions into InP crystal was to reduce structural strain caused by lattice mismatch between InP core and ZnS shell layer[147, 148]. Incorporated Zn ions alleviate the lattice tension[149] between the core and the shell layers. The successful growth of the ZnS ensures higher quantum yields for the alloyed nanoparticles. Atomic % of the elements for In(Zn)P core nanoparticles was determined by SEM-EDS measurements and provided in Table 3.5.

Table 3.5. Alloy compositions and particle diameters of core In(Zn)P nanoparticles synthesized at different reaction temperatures, analyzed by SEM-EDS and DLS measurements.

The reaction temperature	Core type	Atomic %						Size (nm)
		P	Zn	In	In/ (In+Zn)	Zn/ (In+Zn)	Zn/In	
150 °C	$In_{0.18}Zn_{0.82}P$	15.8	69.3	14.9	0.18	0.82	4.7	5.6
160 °C	$In_{0.19}Zn_{0.81}P$	16.9	67.6	15.6	0.19	0.81	4.3	8.7
170 °C	$In_{0.21}Zn_{0.79}P$	14.4	67.6	18.1	0.21	0.79	3.7	10.1
180 °C	$In_{0.23}Zn_{0.77}P$	29.3	54.8	16.0	0.23	0.77	3.4	11.6
200 °C	$In_{0.18}Zn_{0.82}P$	21.9	64.1	14.0	0.18	0.82	4.6	13.5

Figure 3.10 demonstrates that the fractions of Zn and In in the alloy were not varying with the reaction temperatures. The alloy composition of the core remained unchanged by the reaction temperature. This finding suggested that the red-shifted spectra (absorption and photoluminescence) were tuned by the particle size rather than the alloy composition. Since the ionic radius of In^{3+} (80 pm) is not significantly larger than the ionic radius of Zn^{2+} (74 pm)[150], it was demonstrated that keeping reaction time fixed the reaction temperature is an effective parameter to tune the particle size and to regulate spectral properties of In(Zn)P nanoparticles.
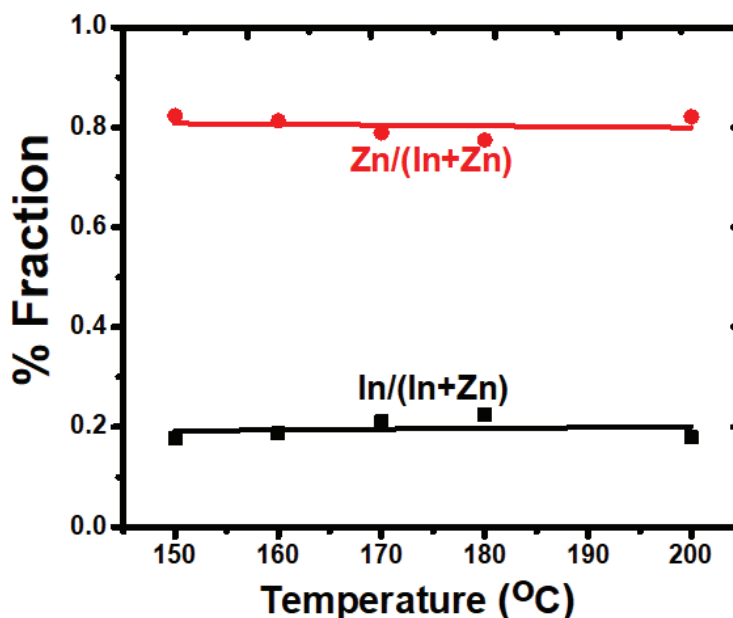
Figure 3.10. Variation of Zn and In fractions of the nanoparticles as a function of the reaction temperature, determined by SEM-EDS measurements. The compositions of the core nanoparticles remained constant.

In general, the reaction time is preferred to tune particle size keeping the reaction temperature constant. Higher reaction temperatures did not alter the zinc blende crystal structure of In(Zn)P/ZnS/DDT core/shell nanoparticles (Figure 3.11), verified by the identical XRD patterns[151]. The (111), (220), and (311) planes shown in Figure 3.11 were between the reference lines of InP (JCDS 32-452) and ZnS (JCPDS 77-2100).
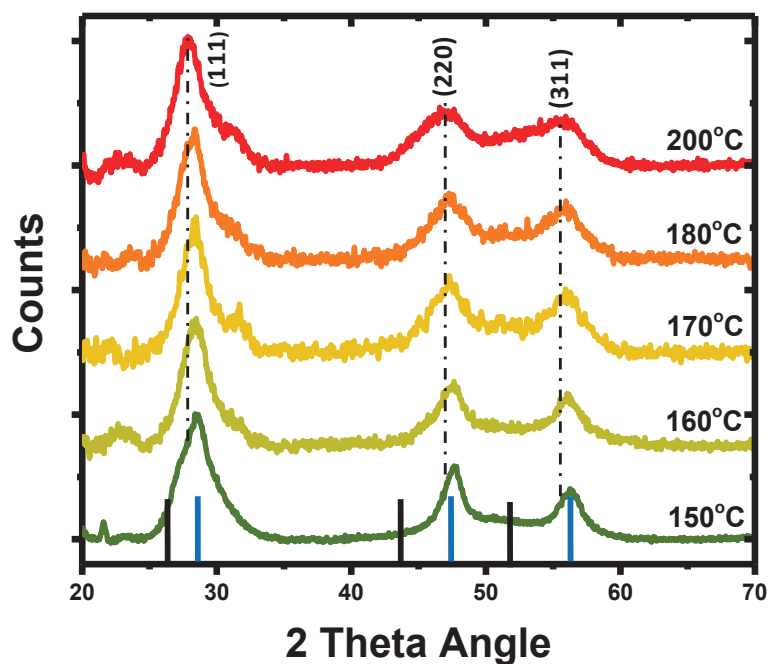
Figure 3.11. XRD patterns of In(Zn)P/ZnS core/shell nanoparticles grown at different reaction temperatures. Black and blue colored vertical lines at the bottom of the Figure were added as the reference lines for InP and ZnS, respectively. The XRD patterns of the core nanoparticles were provided in the supplement.

Real-time, in-situ PL spectra measured by Ocean Optics fiber-optic spectrometer were used to monitor the impact of the DDT coating on the fluorescence spectra. The bifurcated fiber optic probes inserted in the batch reactor shown in Figure 3.12.a was used to excite nanoparticles at 405 nm and to collect fluorescence emissions with an integration time of 100 milliseconds. Figure 3.12.b shows the time evolved fluorescence spectra of the nanoparticles with and without ZnS and DDT layers combined. The fluorescence intensity of the DDT coated nanoparticles was further monitored over 35 days to demonstrate the stability of nanoparticles (Figure 3.12.c.).
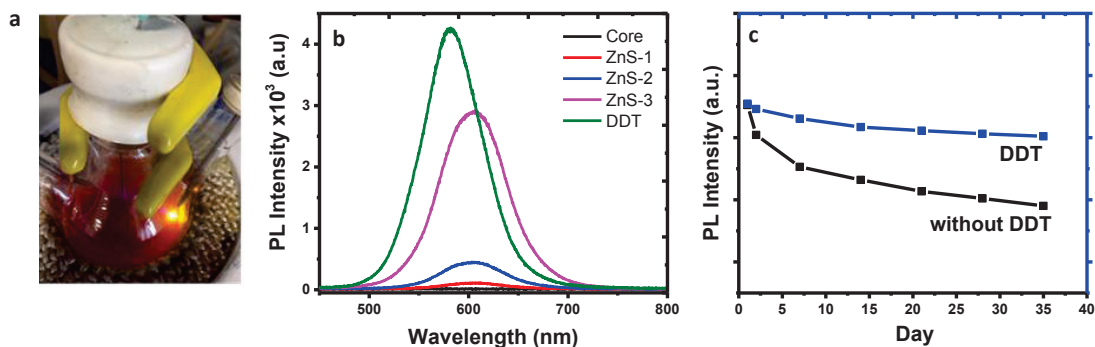
Figure 3.12. a) Photograph of the reaction set-up allowing in-situ and real-time fluorescence measurements and b) in-situ fluorescence spectra recorded by Ocean Optics fiber-optic spectrometer using bifurcated fiber optic probe. c) The time-evolved fluorescence spectra and improved photostability of the nanoparticles with and without DDT coating.

The addition of inorganic and organic layers significantly improved fluorescence emission intensity. The quantum yields of nanoparticles were significantly increased by the addition of DDT in the last step of the reaction because it provides an organic shell layer to passivate surfaces and increase particle stability[152, 153]. It was also observed that the peak position and shape of fluorescence spectra during the shell layer formation did not change. The unchanged spectral features confirm that the fluorescence emission is due to the electron-hole pairs (excitons) confined in the nanoparticle core[154]. The DDT coating increased fluorescence intensity by enabling surface passivation of the core/shell alloyed nanoparticles[155]. Since DDT has a relatively shorter alkyl chain, the steric hindrance is less than the other mostly used organic ligands, and thereby higher surface coverage of DDT may be established to prevent photodegradation of the nanoparticles (Figure 3.13). A slight blue shifting in fluorescence spectrum after DDT addition was observed and attributed to ion exchange between smaller S^{2-} ions from DDT and larger P^{3-} ions in the nanoparticle[156].
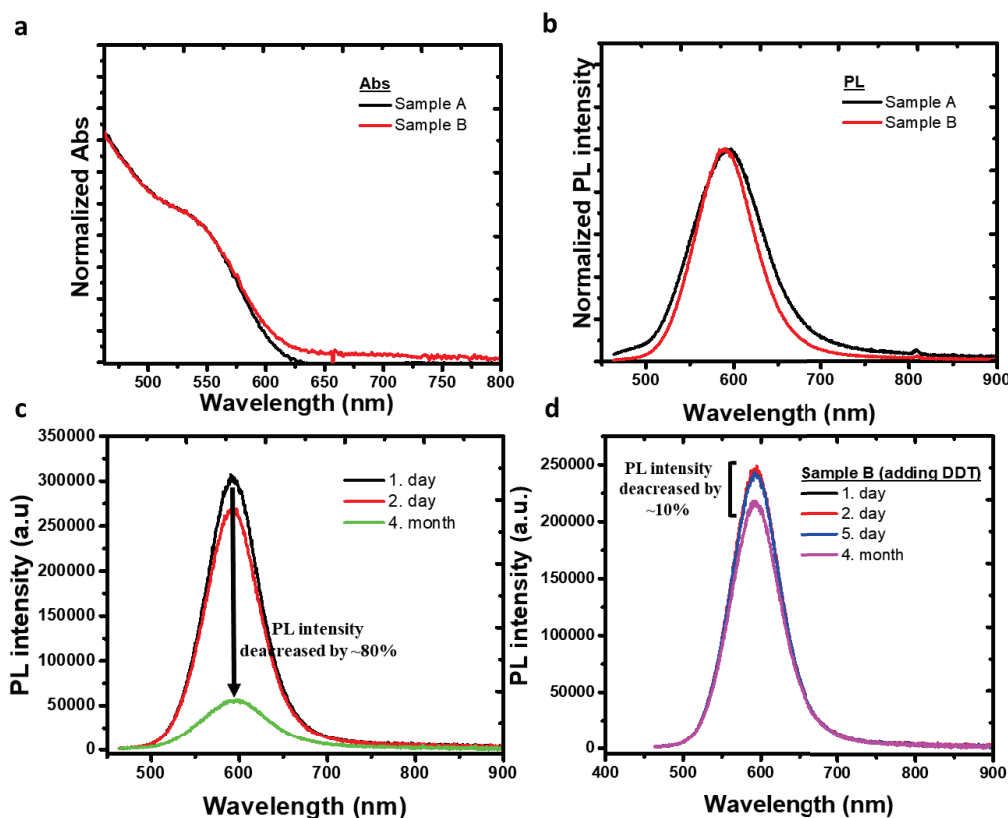
Figure 3.13. a) Absorption and b) photoluminescence spectra of nanoparticles before and after DDT. Photoluminescence spectra of c) Sample A (non-coated with DDT, core rxn temp:170 °C) and d) Sample B (coated with DDT, core rxn temp:170 °C) at different days.

FTIR spectra of DDT remnant in solution and adsorbed onto InP/ZnS nanoparticle surfaces were shown in Figure 3.14. The bands at 2985, 2930, and 2860 cm^{-1} are assigned to C-H stretching, and the band at 1467 cm^{-1} is assigned to CH$_2$ bending[157]. The absence of the band at 2565 cm^{-1} indicating the stretching vibration mode of S-H (shown with a circle) proved that the DDT ligand was bound to the nanoparticle surface successfully[158, 159]. It is assumed that DDT molecules are bonded to In or Zn atoms on the nanoparticle surface through its sulfur atom. The sharpness of the C-H stretching and CH$_2$ bending modes suggests synchronized in-phase vibrations, inferring that DDT molecules are very well aligned on the surfaces, and reducing defects and dangling bonds that increased quantum yields.
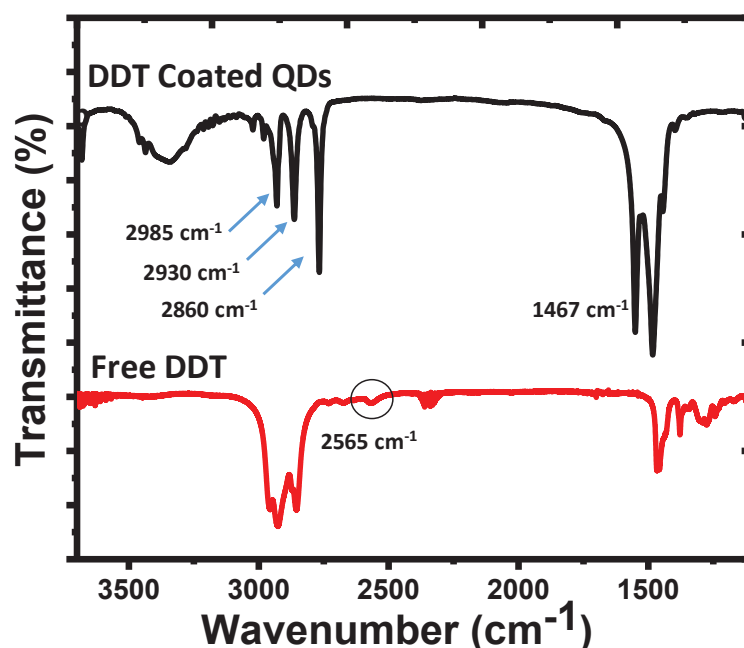
Figure 3.14. FTIR spectra of remnant DDT and In(Zn)P/ZnS nanoparticles coated with DDT. The circled area at 2565 cm^{-1} is the SH vibrational mode, which is diminished after DDT bounded to the nanoparticle surfaces.

3.3.2. Creating Luminescent Security Label with In(Zn)P/ZnS Particles by Screen Printing

In(Zn)P/ZnS/DDT colloidal nanoparticles were used as pigments for ink formula to create security patterns, by exploiting their brighter fluorescence, increased bond strength by the alloy formation, and lower cost compared to the rare earth materials. Rare earth elements based inks have been used in security patterns for anticounterfeiting[112, 113, 160, 161]. Due to the high cost of the rare earth materials, security ink made with them may not be feasible for anticounterfeiting applications. The amount of fluorescent material is the key factor to formulate ink. Generally, high amount (5-25%) of fluorescent material was required to formulate ink[28, 137, 162]. However, a significantly low amount (0.1-0.2% v/v) of highly fluorescent In(Zn)P/ZnS/DDT were used to formulate the security ink. When it is compared with the amount of fluorescent materials required in other studies, it is estimated that the printing cost would be approximately 250 times less due to the lower cost of In and lower amount of nanoparticle required to make ink.

Fluorescent security ink formula was developed by uniformly dispersing as-synthesized In(Zn)P/ZnS/DDT nanoparticles in varnish/toluene mixture. Since the nanoparticle is highly luminous, therefore, very low amount of nanoparticle about 0.2 % v/v can be utilized to formulate low-cost ink. This ink was used to print a security pattern, a logo, on a nonluminous paper to demonstrate that the ink developed may be qualified for authenticating documents. All printed patterns were dried naturally under ambient conditions. The photographs illustrated screen printing security patterns on various substrates shown in Figure 3.15.
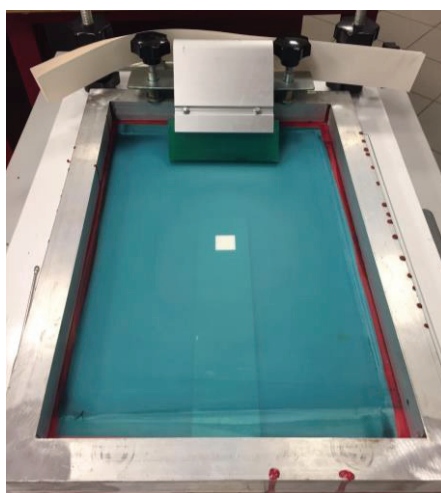
Figure 3.15. Photograph of the screen printing device.

The patterns were barely observable on the paper substrate under daylight (Figure 3.16) because the concentration of ink containing In(Zn)P/ZnS/DDT was very low. However, because of the high brightness (equal to QY*ε) of the nanoparticles, the security patterns with various fluorescence colors were easily observable under UV light (Figure 3.16). The In(Zn)P/ZnS/DDT nanoparticles may emerge as a fluorescent pigment in the security ink that is observable just under UV light[143]. Fluorescent security patterns can be created with different printing techniques[163-166], however, the security level will be lowered if the patterns are visible under UV light illumination. Since security patterns could be easily reproduced by using fake fluorescent materials having similar spectral properties, an additional level of security feature should be added for enhanced authenticity.

| | No QD | 535 nm | 550 nm | 573 nm | 602 nm | 638 nm |
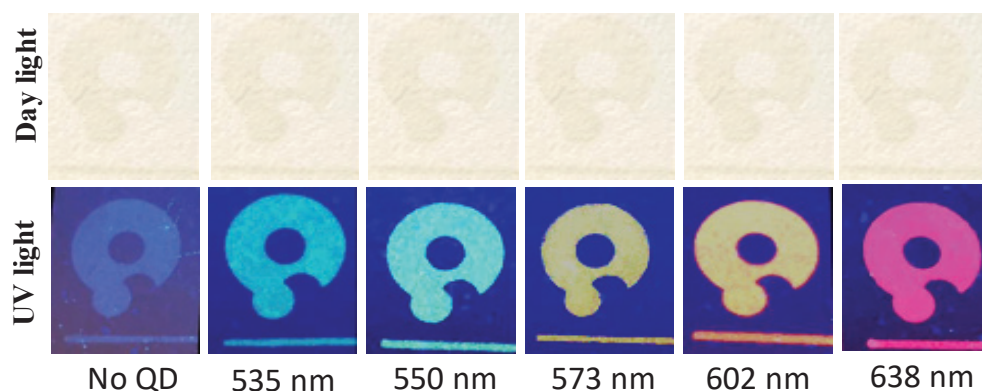
Figure 3.16. The photographs of security patterns created by the inks printed on papers under daylight and UV light. The emission wavelengths of the nanoparticles in the ink formula were given under the photographs. The concentration of the ink is % 0.2 v/v, allowing visible fluorescent patterns.

A fiber spectrometer was used to collect emission spectra originated from the security patterns printed on the papers. The fluorescence spectra of the security patterns printed on paper substrate using inks with and without In(Zn)P/ZnS/DDT nanoparticles were evaluated. While unprinted parts of the paper had almost no emission, the varnish without the nanoparticles printed on the paper substrates showed its specific broad emission at 494 nm (Figure 3.17).
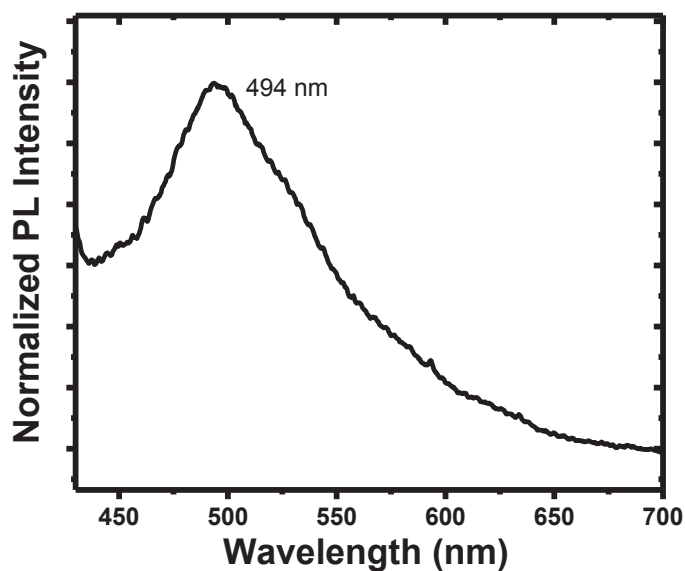
Figure 3.17. PL spectrum of the commercial varnish used.

The fluorescent emission spectra of the inks in the range from 535 nm to 638 nm (shown in Figure 3.18) were collected by using a bifurcated fiber probe. The spectral features were easily distinguished in the printed patterns.
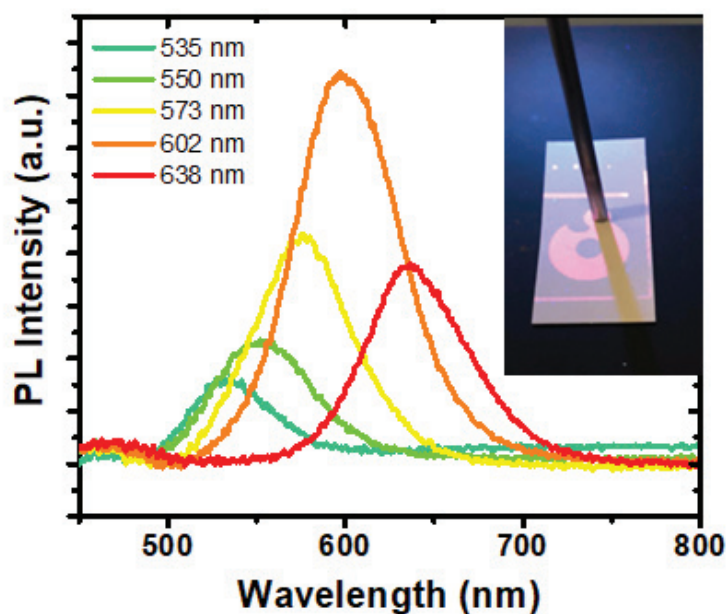
Figure 3.18. The emission spectra of In(Zn)P/ZnS/DDT nanoparticles collected from the fluorescent security patterns printed on the paper substrates. A bifurcated fiber-optic probe coupled to a spectrometer (a photograph in the inset showing the fiber optic probe) was used to collecting emissions. The emission of varnish (given in Figure 3.17) was subtracted from all the collected spectra. All samples were excited at 365 nm.

The stereomicroscope images of the security patterns under daylight and UV light illumination were also provided shown in Figure 3.19. The patterns were invisible under daylight in all photographs. However, the patterns printed on the papers were easily observable under UV illumination. The homogeneity of the patterns indicates that nanoparticles are homogeneously distributed within the printed area.
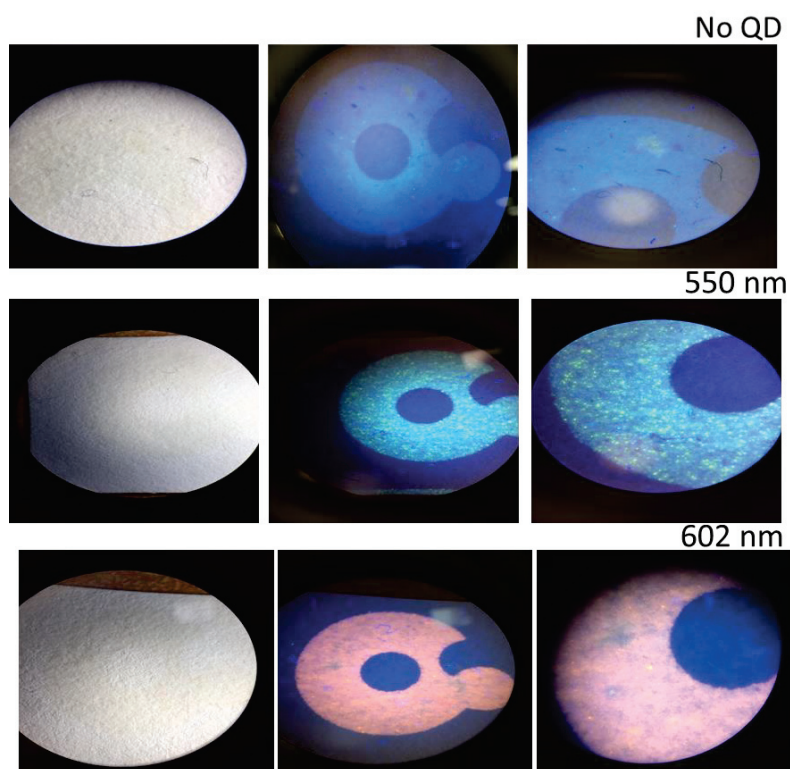
Figure 3.19. Stereo microscope photographs of the logos printed on paper. Photographs show logos without and with nanoparticles emitting at 550 nm and 602 nm, from the top to the bottom respectively.

To commercialize security inks, it is desired that security labels/codes should be produced by a low-cost ink and verified by a simple technique. Generally, the color information of fluorescent inks is encoded by tagging an anticounterfeiting pattern embedded onto substrates. To enhance the security level for anticounterfeiting, either advanced materials and/or techniques should be developed for verification of authenticity. Dual-excitation wavelength materials were used, so the security pattern could be excited at two different wavelengths[28, 57, 167]. QR codes printed on products are also used as identification through reading by a device[114]. However, since these codes can be completely duplicated, it lowers the security level. When an original QR code and a copied code are placed side by side and scanned by a smartphone, it will be very hard to identify which one is fake and which one is authentic. However, imitation can be made difficult to some extent when two different methods are applied. Herein, we developed a technology combining an optical device that reads novel security patterns/tags created with a specialty ink formula. Thus, unlike other studies, we can verify the security

51

patterns/codes with a device that has optical sensitivity beyond the visual inspection. To this end, cost-effective fluorescent ink contained indium-based nanoparticles are formulated, enabling very low amounts of nanoparticle are required in the ink. In addition, an optical device having an integrated light source and sensor is developed in house. In virtue of the novel security tags containing low amounts of nanoparticles, the ink fluorescence may not be noticeable or hardly observable under the UV light by visual inspection. The concentration of the nanoparticles in the ink was reduced to 0.1 % v/v. In Figure 3.20.a-f, the security patterns/tags created under daylight and UV light were presented. An additional varnish layer has been applied onto the security printing, as a result, the security labels were not noticed even with the naked eye. In this way, security labels that are difficult to distinguish even under daylight have been created. In addition, fluorescent security patterns with distinct colors under UV illumination were not distinguishable due to the low concentration of nanoparticles in the ink. Herein, we used a fiber optic based optical device (Quantag Sensor) that was employed to detect fluorescent emissions of the ink (Figure 3.20.g). The fluorescence intensities of the inks with different colors were detectable by Quantag sensor, shown in Figure 3.20.h, but invisible by visual inspection (Figure 3.20.a-f). Quantag sensor is highly sensitive, convenient, and specific to predetermined wavelength compared to a fiber-optic spectrometer. These features add an extra security level for anticouterfeiting efforts. The fiber-optic spectrometer collects all the emissions including ink, varnish and substrates and cannot sort out the origin of the signals coming from different sources like the nanoparticles or varnish. However, since the Quantag sensor exploits emission filters, the predetermined emissions may be employed as a higher level security code. The reduced ownership operational costs and wavelength selectivity are also the advantages of the Quantag sensor compared to a commercial fiber-optic spectrometer, on top of being handy.

The photostability of the ink (% 0.1 v/v) embedded on the paper substrate was monitored for 21 days by the Quantag sensor. The fluorescence of the security patterns monitored provided that the intensities of the patterns unchanged, shown in Figure 3.20.h. The reduction in the intensity of the red-emitting ink (638 nm) may be explained by some sort of environmental effects on the nanoparticles emitting in this wavelength.
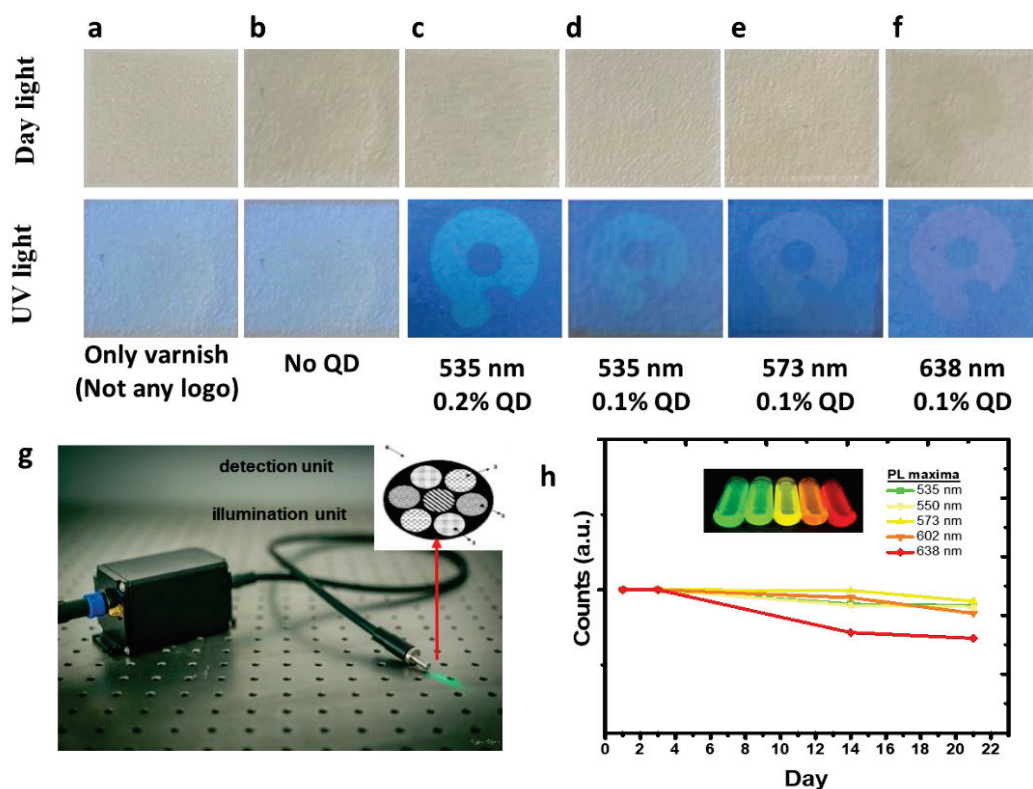
Figure 3.20. a-f) The security patterns created with fluorescent inks with and without nanoparticles printed on paper substrates. The nanoparticle concentrations are provided under the photographs. The security patterns were barely visible under daylight and slightly observable when illuminated by UV light by visual inspection. g) The photograph shows Quantag sensor having fiber optics having an integrated laser for excitation and collecting fibers as a part of optical readout unit. h) The intensity of fluorescent inks (% 0.1 v/v) monitored by the Quantag sensor for 21 days, demonstrating the photostability of security patterns printed on the paper substrates. The inset in (h) shows emission colors of highly concentrated inks.

To understand the effect of substrate on the security pattern, the inks were applied to various substrates. The thickness of the patterns screen-printed on polymer and glass substrates was measured by an optical profilometer (Figure 3.21). The thickness of the patterns was about 4.5 μm. These measurements confirmed that the security patterns form a thin film containing nanoparticles distributed homogeneously on the printed part of the substrates. The particle sizes have no effect on the film thickness.
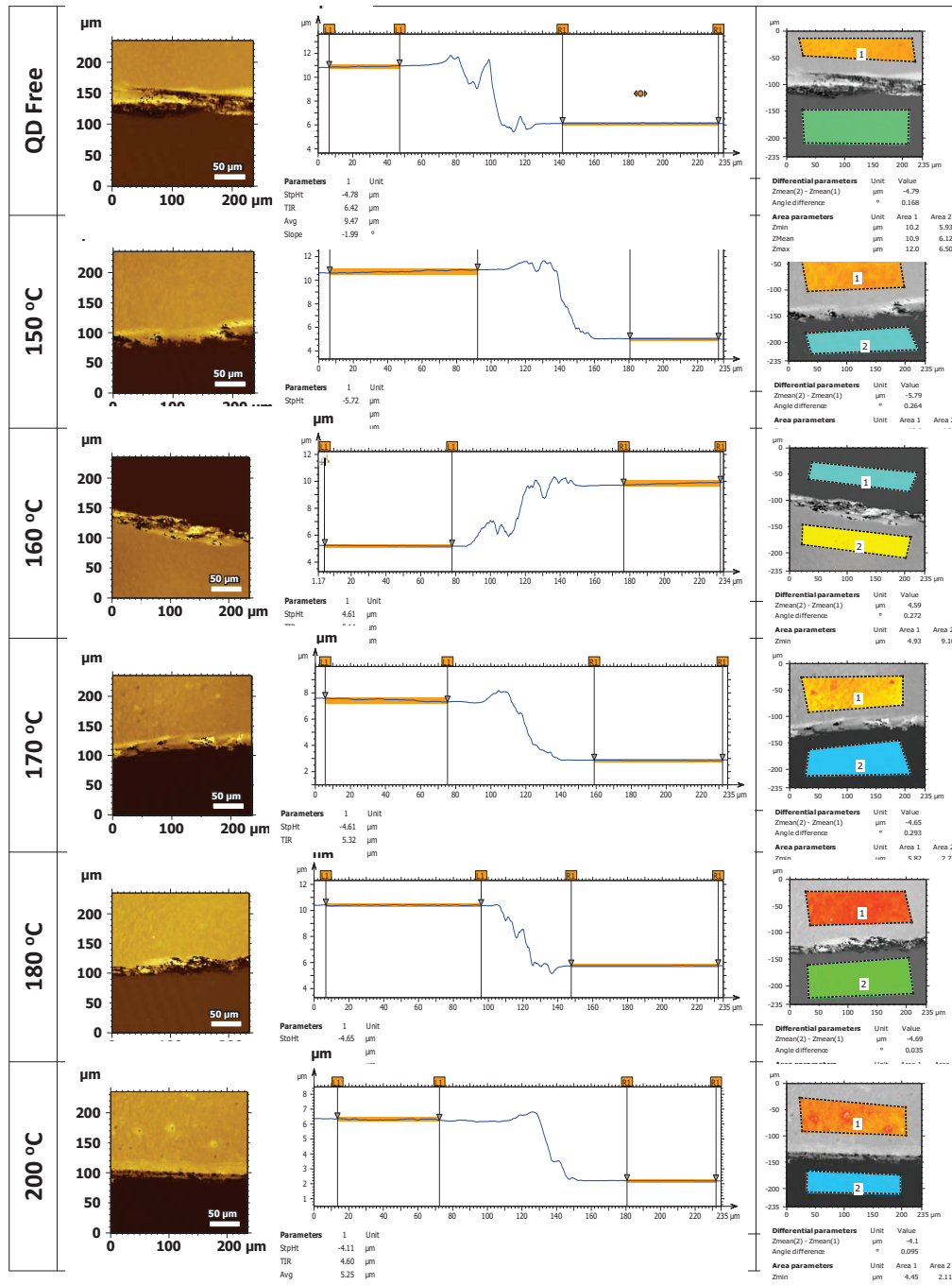
Figure 3.21. Thickness measurements of screen-printed glass substrates with and without QD incorporation by optical profilometer.

The confocal images are given in Figure 3.22 show some parts of the logo patterns printed on the polymer and glass substrates. The logos were observable on the glass and polymer surfaces. These confocal images showed that the logo patterns were homogeneously printed on the substrates.
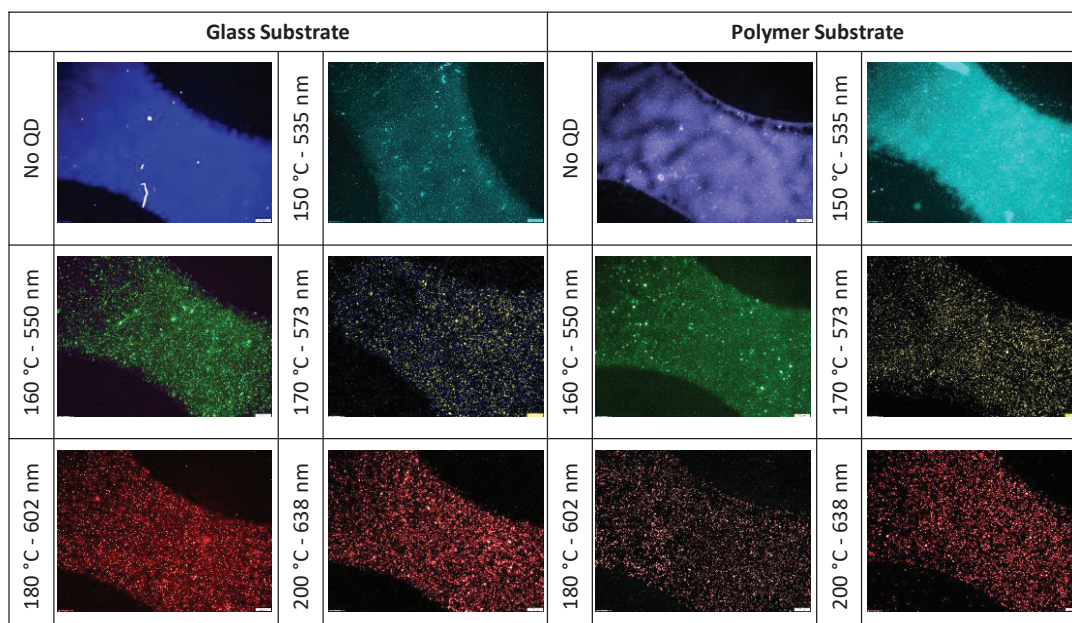
Figure 3.22. Confocal images of a part of the printed logos, excited by the Hg lamb, on both glass and polymer substrates. The reaction temperature and the emission wavelengths are provided on the left side of each photograph. The objective is 4x and the scale bar embedded in each image is 200 μm. Homogeneous distribution of the nanoparticles dispersed in the varnish are clearly seen.

In Figure 3.23, the logos printed with red fluorescent ink were imaged by using different objectives. For both polymer and glass substrates, the logos were imaged by using two different emission filters: A channel labeled as polymer channel collecting the emission/scattering coming from the varnish and substrate, and the channel labeled as QD channel collecting the fluorescent emissions of the nanoparticles. These images verify that the nanoparticles are homogeneously dispersed in the ink and uniformly printed on the substrates.
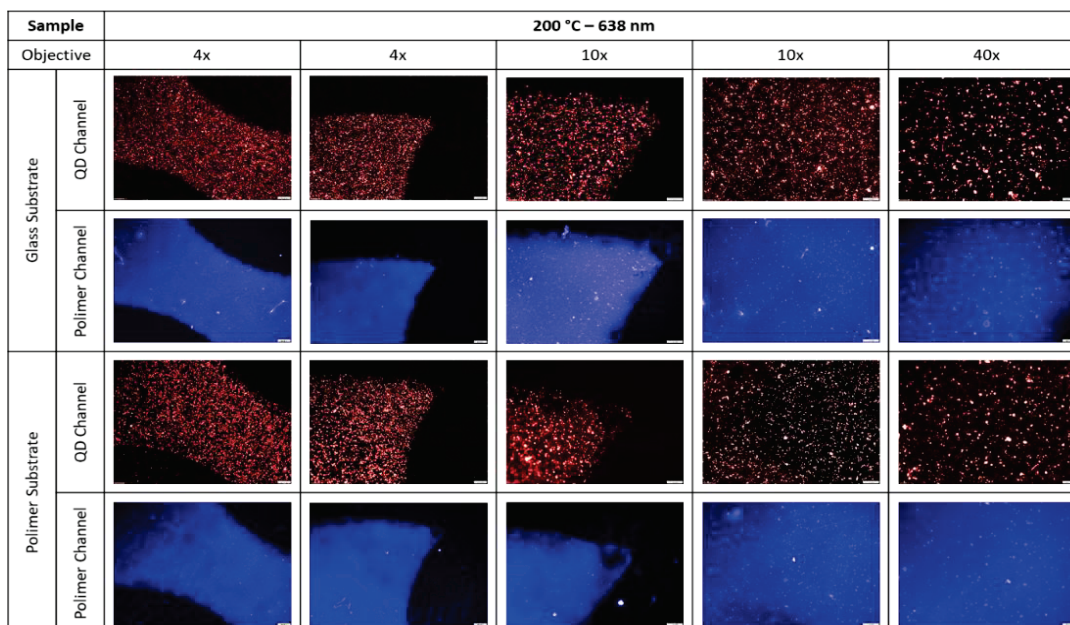
Figure 3.23. Photographs of the part of logo patterns printed with inks containing the red-emitting nanoparticles, emitting at 638 nm on the polymer and glass substrates. The images were taken by a confocal microscope with Hg lamp and red emission filter, using different objectives, to verify the homogenous distribution of nanoparticles.

3.4. Conclusion

Highly fluorescent In(Zn)P/ZnS/DDT core/shell colloidal nanoparticles are synthesized for anticounterfeiting applications. The DDT organic shell enhanced the particle stability and fluorescence brightness. The nanoparticles were homogeneously dispersed in varnish to formulate colorless security inks. The formulated inks were utilized to create security patterns by applying screen printing techniques on various substrates including paper, polymer, and glass, demonstrating the capability of the ink for anticounterfeiting. The inks are transparent in the daylight, but strongly luminous in five different colors under UV light illumination. The security patterns created on the substrates are slightly visible in the daylight but almost colorless under UV-light when the concentration of the nanoparticles was dropped to 0.1 % v/v. By using a lower amount of nanoparticles, the formula cost of the ink is substantially reduced. The invisible fluorescent inks as the security codes that cannot be perceived by visual inspection are clearly detectable by a handheld, low-cost optical device (Quantag sensor) that is developed in-house. The Quantag sensor is highly sensitive and selective to predetermined ink colors. The spectral information of the security patterns identified by the Quantag sensor is validated by a commercial fiber optic-based spectrometer. However, the Quantag sensor has an advantage to fiber-optical spectrometer, providing

56

wavelength selectivity using narrow bandwidth emission filters. In summary, an anticounterfeiting technology is developed by combining invisible fluorescent inks with a hand-held, low-cost optical device to validate authenticity.

CHAPTER 4

GENERATING PHYSICALLY NON-CLONABLE SECURITY PATTERNS USING HEAVY-ATOM FREE NANOPARTICLES BASED INK AND A TWO-STEP VALIDATION METHOD FOR AUTHENTICATION

4.1. Introduction

Counterfeiting is a global problem that causes significant economic losses and poses serious threats to society[168]. Although most of the products and printed documents (passport, ID card, etc.) are tried to be protected by anticounterfeiting techniques such as fluorescent, thermal modification, plasmonic labels, holograms or watermarks[169], the global economic loss due to product counterfeiting is expected to reach approximately USD 1.82 trillion in 2020[170]. Commonly used such anticounterfeiting methods offer low complexity and high predictability; it means that counterfeiters can easily copy the produced labels. To combat counterfeiting, making unclonable tags and using stochastic processes for this is the most appropriate way to follow. Physically non-clonable functions (PUFs) based on uncertain random structures offer advanced security techniques and are easy to generate, but difficult to regenerate because they rely on random irregularities of the object[39]. Therefore, it is the cornerstone of secure information sharing and an ideal method to prevent counterfeiting.

To prevent counterfeiting, a database is created with PUF tags, and then when the label on the product or document is read and the reading is searched in the database, it is determined whether a product is original.

In the literature, many publications using different methods and materials have been widely reported to prevent counterfeiting[13, 46, 50, 51, 63, 160, 171-173]. In recent years, it has been observed that PUF codes have been created using luminescent/fluorescent materials such as luminescent rare-earth materials and CdSe nanoparticles, which exhibit hidden patterns when exposed to UV light, to prevent counterfeiting[42, 45]. This random feature that prevents cloning will be achieved by distributing quantum dots within the

pattern by the inkjet printers. The quantum dots that are not visible to the naked eye can be detected in the security pattern with a fluorescent microscope. However, safety patterns based on rare earth materials severely limit scaled production due to high cost, while Cd-based quantum dots will be not usable due to toxicity[120]. In addition, the verification techniques used are expensive and impractical, as specialized microscopes are often used[45, 171]. In different studies, PUF tags, which consist of randomly arranged nanofibers that can be similarly detected using fluorescence microscopy, have been mentioned[43, 44]. Here the randomness is due to the angles at which the nanofibers grow and the coordinates of their end points. The suggested PUF labels, on the other hand, are made of complex organic molecules that can be difficult to mass-produce in bulk and have limited physical stability. Apart from these studies, a quantum dot-based fluorescent counterfeiting tag with physically non-clonable patterns that can be solved with powerful artificial intelligence (AI), which offers a simple recognition technique, was reported. However, the toxicity of the quantum dots used will severely limit their widespread application of these security patterns[120].

As a result, security techniques for anticounterfeiting are encountered which are either difficult to produce in terms of materials or recognition techniques are not practical. In this work, easy to manufacture but hard to reproduce even by the manufacturer; easy to read but impossible to guess; and we aimed to create PUF security codes that cannot be cloned. For this, the electrospinning technique, which is widely used in the literature to obtain polymer fibers and droplets, was used. Electrospinning provides a convenient and cost-effective way to manufacture polymeric fibers and droplets that have high surface area, uniform diameters and various composition[174]. In a typical electrospinning technique, a high voltage is delivered to a polymer droplet suspended at the tip of a syringe needle[175]. A charge builds upon this droplet, and when this charge overcomes the surface tension of the solution, the droplet expands and forms a Taylor cone[176]. The solution expelled from the Taylor cone's tip travels through the air to its target medium, where it collects as a nonwoven fiber mat or droplets. The size of the fibers or droplets is depended on electrode potential and distance between the electrodes[177, 178]. The major advantage of this technique is a simple, inexpensive and fast synthesis method to fabricate high purity fibers and is the potential of producing nano/micro scale diameter fibers or droplets, resulting in structures with a high surface area to mass ratio.

Also, here it was decided to use carbon-based and indium-based quantum dots due to their unique fluorescence properties to create non-repeatable security tags. Non-repeatable patterns resulting from the random location of the fibers and droplets and their fluorescent colors provided unique security codes suitable for anticounterfeiting purposes. With the codes developed, we aimed to create a unique fingerprint on the product or document and prevent counterfeiting. In order to check the accuracy of the unique security codes created within the scope of this study, the PUF response extracted from the random model was used to encode the identifier. A code was written in Python using OpenCV for verification. The identifier decoded during validation is compared with that stored in the database to determine the authenticity of the product. The fact that each image obtained is different from the other shows that the security codes created on the substrate are not reproducible and can be easily separated from each other.

4.2. Experimental

4.2.1. Materials

Polyvinyl alcohol 87-90% hydrolyzed (Mw 30000-70000 g/mol) and Polyvinyl alcohol 88% hydrolyzed (Mw 85000-120000 g/mol) were purchased from Sigma Aldrich. Commercially available polyacrylonitrile (PAN) (Mw: 120000-140000 g/mol) was used. *N,N*-Dimethylformamide ($\geq$99.8%) (DMF), and Dimethyl sulfoxide ($\geq$99%) (DMSO) were purchased from Merck.

4.2.2. Random Droplet Patterns by Electrospraying Process

4.2.2.1. Patterns generated with Carbon-based nanoparticles

1% wt PVA solution to contain 1000 ppm blue luminescent carbon particles was prepared. Firstly, the solid particles cleaned and dried after the reaction were dispersed in 20 ml water at a concentration of 1000 ppm. Then 0.2 g of PVA was added and mixed during 3 hours. Thus, 1% wt PVA solution containing blue luminescent carbon particles was prepared. For electrospraying process, the voltage is 20 kV and the distance between

the syringe and the metal collector was changed from 5 to 15 cm. The feed rate was changed from 0.2 to 1 ml/hour using the microsyringe pump.

Then, 1% wt PVA (Mw:30000-70000) solution with including green luminescent carbon particles was prepared in the same way. For electrospraying process, the voltage is 20 kV and the distance between the syringe and the metal collector was set to 5 cm. However, the feed rate was kept constant at 0.1 ml/hour using the microsyringe pump.

4.2.2.2. Patterns generated with In(Zn)P/ZnS/DDT nanoparticles

In(Zn)P/ZnS/DDT nanoparticles were dispersed in 2 wt.% PAN/DMF solution and mixed for 3 hours at 60°C. The nanoparticle concentration in the polymer solution was adjusted to 2500 ppm. Prepared QD-polymer solution was loaded into a plastic syringe to carry out the electrospraying process at different applied voltages (from 8 kV to 20 kV) to the tip of a syringe needle. The syringe's distance from the metal collector was fixed at 5 cm. The feed rate was changed from 0.1 to 0.4 ml/hour using the microsyringe pump.

4.2.3. Random Droplet/Fiber Patterns by Electrospinning Process

4.2.3.1. Patterns generated with Carbon-based nanoparticles

15% wt. PVA (Mw: 85000-120000) solution to contain 500 ppm green and 1000 ppm blue luminescent carbon particles was prepared. Firstly, the carbon particles were dispersed in 20 ml water. Then 3 g PVA was added and mixed during 3 hours at 60 °C. Thus, 15% wt. PVA solution containing luminescent carbon particles was prepared. For electrospinning process, prepared QD-polymer solution was loaded into a plastic syringe and the different voltages applied (from 8 kV to 15 kV). The syringe's distance from the metal collector was fixed at 10 cm. The feed rate was kept constant at 1 ml/hour using the microsyringe pump.

4.2.3.2. Patterns generated with In(Zn)P/ZnS/DDT nanoparticles

In(Zn)P/ZnS/DDT nanoparticles were dispersed in 15 wt.% PAN/DMF and 15 wt.% PAN/DMSO solution and mixed for 3 hours at 60°C. The nanoparticle concentration in the polymer solution was adjusted to 2500 ppm. Prepared QD-polymer solution was loaded into a plastic syringe to carry out the electrospinning process at different applied voltages (from 8 kV to 20 kV) to the tip of a syringe needle. The syringe's distance from the metal collector was fixed at 20 cm. The feed rate was kept constant at 1 ml/hour using the microsyringe pump.

4.2.4. Characterization

Photoluminescence (PL) spectra of droplet/fiber patterns were measured with USB2000 fiber-optic-based spectrometer (Ocean Optics Inc., Dunedin, FL, USA) (Quantag Nanotechnologies). Photographs were taken with I-phone SE mobile phone (Quantag Nanotechnologies). Images of the droplet/fibers were taken by ZEISS Axio Zoom V16 Microscope equipped with Axiocam 208 Color camera (IYTE).

4.3. Results and Discussion

4.3.1. Creating Physically Unclonable Security Patterns

Fingerprints are widely used in personal identification due to their intrinsic uniqueness[179, 180]. Based on this fact, we created security patterns that are not possible to copy but can be easily produced with a low-cost process. The security patterns can be easily produced on different substrates by using the electrospinning technique. Electrospinning is a random process that creates unique patterns that are impossible to reproduce even by the manufacturer. This non-repeatability is critical in assuring the non-clonability of anticounterfeiting tags, as well as the security level and capacity that goes with it. The luminescent nanoparticles were dispersed in the polymer solution and then random droplet/fiber structures were created using the electrospinning technique. Here, two-stage security was presented thanks to the random formation of droplet/fiber

62

structures. Figure 4.1 schematically depicts the developed two-step security technology for anticounterfeiting. The first step is to check the spectral information (PL emission profile) of the nanoparticles with a simple hand-held spectrometer, and the second is to validate the pattern created and stored in a database. By the verification to be taken in both steps, a security barrier that is very difficult to overcome against counterfeiting will be placed on the document or product. Moreover, it is proposed that the security patterns can be detected with a simple and easily accessible device such as a smartphone, instead of nonpractical imaging techniques such as electron and fluorescence microscopies demonstrated in the literature for verification.
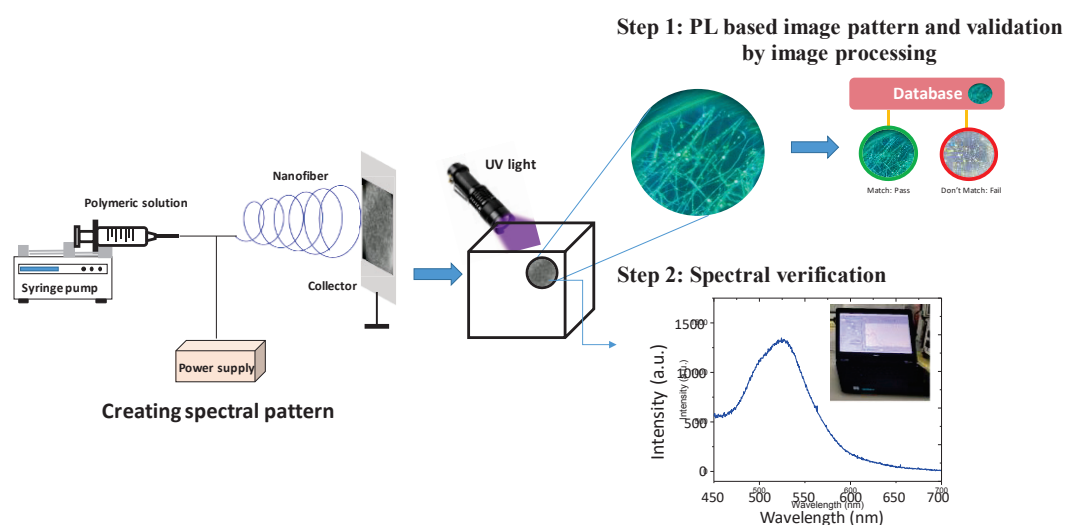
Figure 4.1. Random pattern generation and two-step optical validation for anticounterfeiting technology.

4.3.1.1. Generating Random Droplets with Carbon-based Nanoparticles

At this stage, it is aimed to create unique codes in the form of droplets on different substrates such as metal, paper and polymer, using luminescent carbon-based particles and polyvinyl alcohol.

Electrospraying, also known as electrodynamic spraying, is a widely used technique for creating droplets in biomedical and chemical applications and is considered an effective approach to depositing micro- and nano-sized small droplets on the substrate via an electric field[181, 182]. In addition, the method has several benefits such as simple device setup and low cost. This will also allow high-scale production of random droplet production, which is aimed to be used for security labels in the study. The size and

morphology of electrospray particles can be controlled by factors related to polymer solutions (eg, concentration, shear viscosity, polymer molecular weight, solvent) and by electrospray process parameters (eg. electric potential difference, distance between needle tip and collector flow rate)[183].

In this study, random droplets were created to be used as a security label by changing the flow rate and the distance between the collector and the needle tip. In addition, the polymer concentration was kept very low in order to avoid the formation of fibrillar structure. To perform the electrospraying process, the prepared solution was loaded into a plastic syringe and 20 kV voltage was applied to the tip of a needle of syringe to create droplets on the metal substrate with the electrospinning setup shown in Figure 4.2. The distance between the syringe and the metal collector was 5 cm. The feeding rate was kept constant at 0.2 ml/h using a microsyringe pump. We tried other electrospraying parameters for metal substrate (Aluminium foil) and summarized the results in Table 4.1.

Figure 4.2. Electrospinning Setup.

Table 4.1. Electrospraying parameters to obtain random droplets.

	Voltage (kV)	Flow rate (ml/h)	Distance (cm)	Results
1% wt PVA (Mw:30000-70000) & 0.1% Blue luminescent carbon dot	20	1.0	15	No spraying
	20	1.0	10	No spraying
	20	1.0	5	Spraying, forming big droplets
	20	0.5	5	Spraying, forming big droplets
	20	0.3	5	Spraying, forming big droplets
	20	0.2	5	Spraying

In Figure 4.3, it is shown that different security patterns can be created simultaneously on a large area thanks to the created mask. Here, a mask was created with aluminum foil, the areas targeted for spraying were left open. As seen in Figure 4.3, droplets of different sizes and coordination were obtained. Here, electrospraying was performed with a single needle system to a large substrate area. Therefore, very small droplets were formed in some regions while large droplets were formed in some regions. Here, the use of multi-needle systems can facilitate control of droplet formation and distribution.
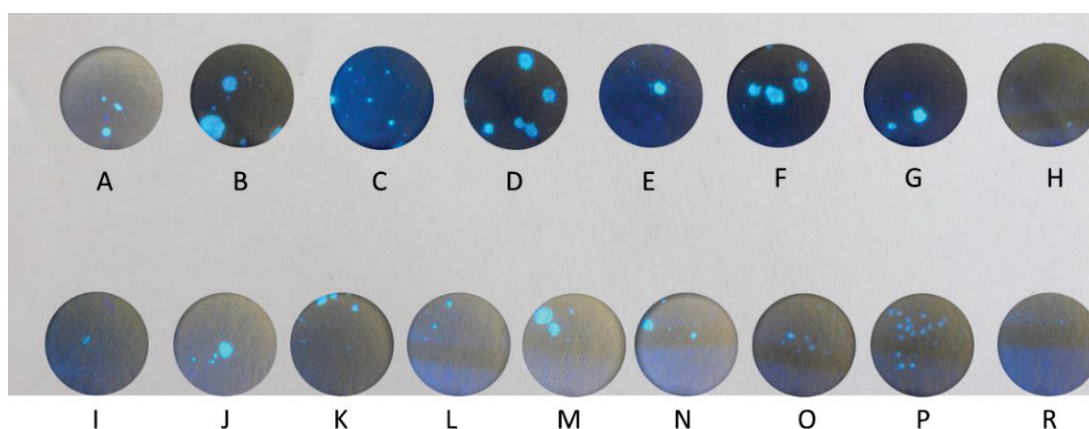
Figure 4.3. Random patterns as security codes generated on the paper substrate with 20 kV voltage and 0.2 ml/h flow rate.

The droplets can be even smaller than 100 nanometers in size, provided the appropriate parameters are provided[184, 185]. However, in this study, the droplets should be visible with a simple phone microscope, so it was more appropriate to obtain micron-sized droplets. Figure 4.4 depicts that appearance of droplets randomly formed on the different substrates under daylight and UV light. As shown in Figure 4.4, even if the droplets are in micron size, there is no trace or stain on the marked place in daylight. It was looked at the marked area in detail using I-phone SE and smartphone microscope (60X) (Figure 4.5). The actual dimensions of the substrates are 3.5x3.5 cm, the field of view of the smartphone microscope used is 1.5 cm and polymer solution was sprayed to this area. The photographs were taken at 60X magnification. Actually, a small area in the middle of the marked area is monitored. This area corresponds to approximately 0.196 cm^2 due to the diameter of the microscope's point of view is 0.5 cm. While no figure is visible on the substrate when viewed in daylight, the droplets created with blue

luminescent carbon particles under UV light become visible. Thus, with the electrospraying method, high protection against counterfeiters can be provided due to a random and uncontrollable droplet pattern.
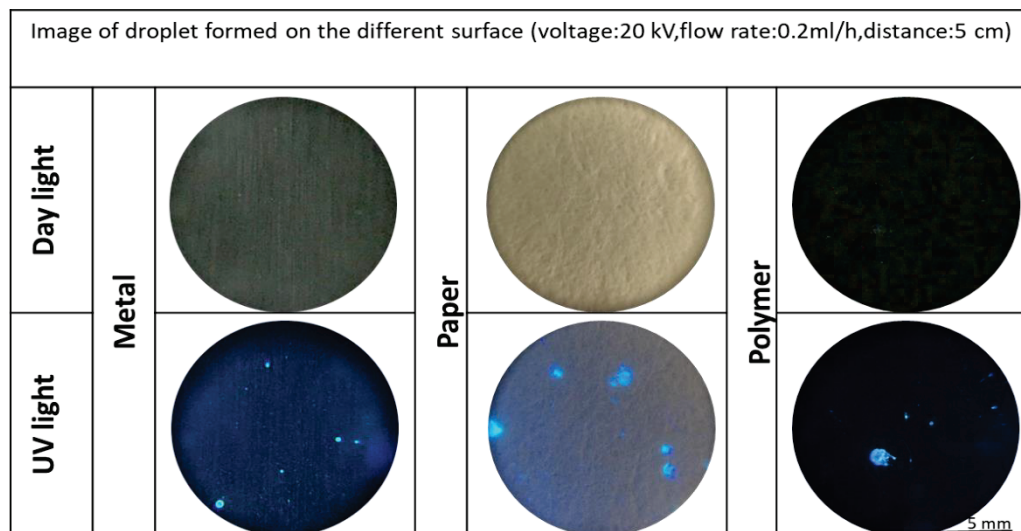
Figure 4.4. The droplet images obtained as a result of the electrospraying process with 20 kV voltage and 0.2 ml/h flow rate on the different substrates under daylight and UV light. Blue emitting (450 nm) carbon nanoparticles were used.

Figure 4.5. Smartphone microscope and an image captured with it.

Electrospraying was applied on different substrates using carbon quantum dots, which green luminescent after the blue luminescent particles. Here, while the PVA/QD solution was being prepared, 500 ppm green luminescent particle was used since we knew to color the paper substrate when applied at higher concentrations than 500 ppm. The reason for this is that the color of the product obtained after the reaction is dark. Therefore, electrospraying parameters have been updated so that no color or figure was visible on the paper substrate in daylight. In this study, when 20 kV voltage and flow rate of 0.2

ml/h was applied to the tip of a needle of syringe, it was observed that the droplet sizes were large and left a yellowish color on the surface of substrate. When the flow rate was changed to be 0.1 ml/h, it was observed that the size of the droplets formed was reduced and no color appeared on the surface of substrate in daylight (Figure 4.6). Therefore, for this application, the appropriate flow rate was decided to be 0.1 ml/hour.
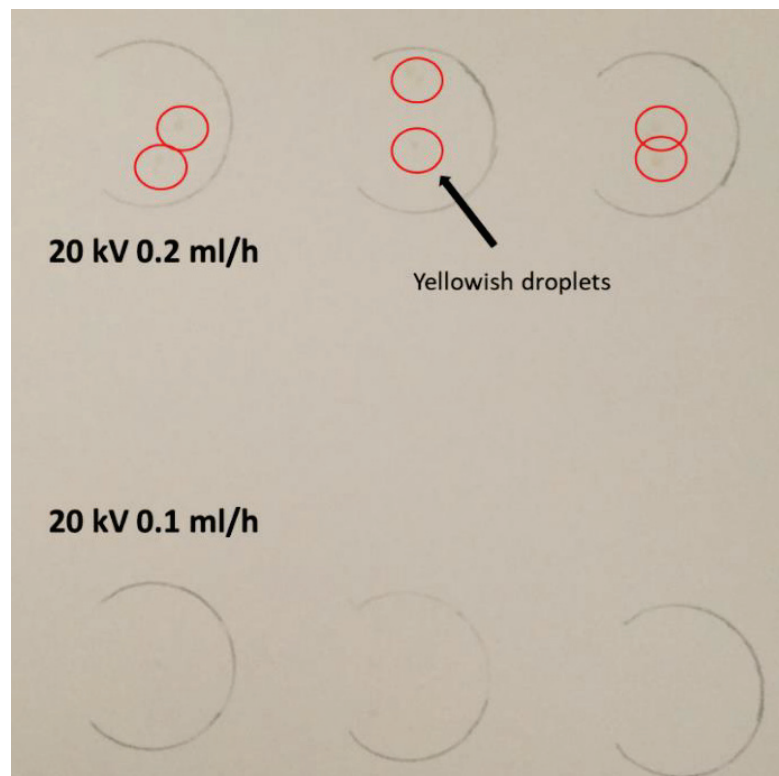
Figure 4.6. The droplet images obtained as a result of the electrospraying process with 20 kV voltage and 0.2 ml/h and 0.1 ml/h flow rate on the paper substrate under daylight. Green emitting (532 nm) carbon nanoparticles were used. The large yellowish droplets on the substrate, which are visible in daylight, are circled in red.

Figure 4.7 shows that the droplets obtained on different substrates have different sizes and coordination.
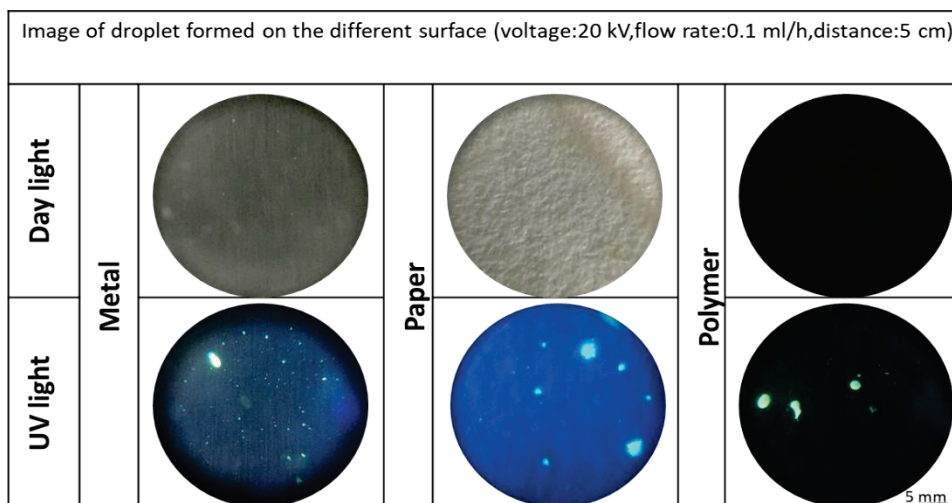
Figure 4.7. The droplet images obtained as a result of the electrospraying process with 20 kV voltage and 0.1 ml/h flow rate on the different substrates under daylight and UV light. Green emitting (532 nm) carbon nanoparticles were used.

4.3.1.2. Generating Random Droplets with In(Zn)P/ZnS/DDT nanoparticles

At this stage, it was aimed to generate unique patterns having droplets on different surfaces such as metal, paper and polymer, using luminescent indium-based particles and polyacrylonitrile.

The morphology of the electrospray object, i.e. the droplets, is determined by the viscosity of the solution[186]. Generally, electrosprayed micro-droplets are produced with low viscosity, unlike electrospun fibers that need the use of a higher viscosity solution. In this study, low viscosity PAN/DMF (Mw:120000-140000) solution was prepared to contain different color luminescent InP particles to obtain random droplet patterns. Firstly, 2 wt% PAN/DMF solution was prepared including green luminescent particles to decide electrospraying parameters.

Table **4**.**2** shows the studies performed with different electrospray parameters to obtain randomly distributed droplets on the metal substrate. Here, the size of the droplets has been tried to be adjusted by many controllable parameters, i.e. applied voltage, syringe feed rate and distance between needle tip and collector.

Table 4.2. Electrospraying parameters to obtain droplets "only patterns" on the metal substrate.

	Voltage (kV)	Flow rate (ml/h)	Distance (cm)	Results
	8	0.4	5	Rare and big droplets
	12	0.4	5	Spraying, forming big droplets
2% wt PAN (Mw:120000-140000) & 2500 ppm InP based particles	15	0.4	5	Spraying, forming big droplets
	18	0.4	5	Spraying
	20	0.4	5	Spraying
	20	0.3	5	Spraying, forming small droplets
	20	0.2	5	Spraying, forming small droplets
	20	0.1	5	No spraying

Figure 4.8 shows that the images of the patterns obtained at a constant flow rate and different voltage values under daylight and UV light. According to Figure 4.8, it was decided that the optimum voltage value for 0.4 ml/h flow rate is 20 kV. Also, it was observed that the droplet sizes increased at lower voltage values and fewer droplets fell into the area. We observed that the applied voltage has a significant impact on the polymer droplet diameter, and that as the applied voltage increases, the droplet diameter decreases. As the applied voltage increases, the polymer droplet diameter decreases. Besides, increasing the applied voltage not only significantly reduces the particle size, but also expands the particle size distribution[187].
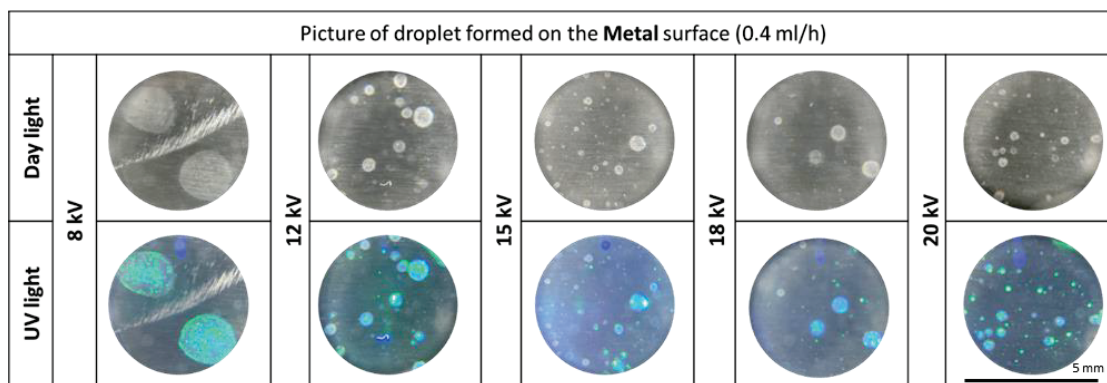
Figure 4.8. The droplet images obtained as a result of the electrospraying process performed at different voltages on the metal substrate of the 2 wt% PAN/DMF solution prepared with luminescent particles at 535 nm.

Different flow rates were tested after determining the voltage value as 20 kV for obtaining droplets on the substrate using 2 wt% PAN/DMF solution. Figure 4.9 contains patterns obtained with different flow rates. When the flow rate was reduced to values less than 0.4 ml/h, it was observed that the droplets formed on the substrate became unsuitable for image processing and even no droplets came to the substrate at a flow rate of 0.1 ml/h. It was observed that the droplet sizes increased when the flow rate was increased to 1 ml/h. As a result, it was observed that the most suitable parameter to create droplets on the substrate is 20 kV voltage and 0.4 ml/h flow rate.
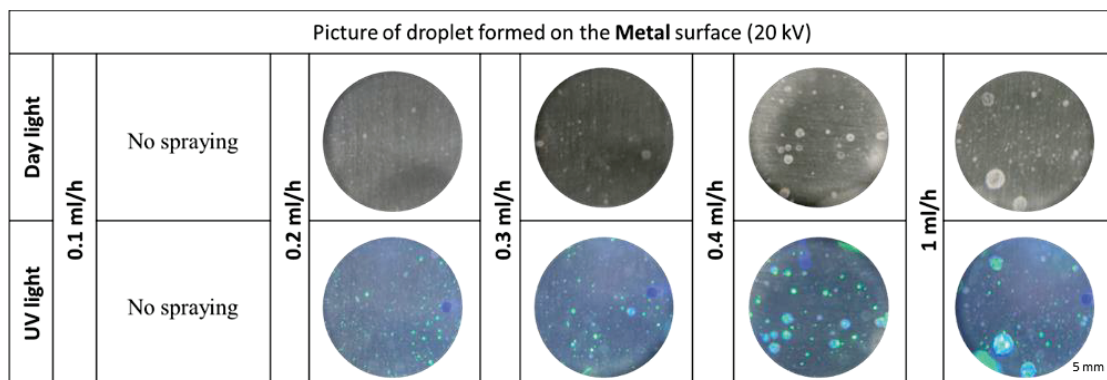
Figure 4.9. The droplet images obtained as a result of the electrospraying process performed at different flow rate on the metal substrate of the 2 wt% PAN/DMF solution prepared with luminescent particles at 535 nm.

After determining the electrospraying parameters to create security patterns containing random droplets on the substrate, electrospraying was applied to various substrates by using yellow and red luminescent particles. In Figure 4.10 and Figure 4.11,

it is shown that security patterns consisting of randomly distributed droplets can be created on different substrates (metal, cellulose paper, coated paper and polymer).
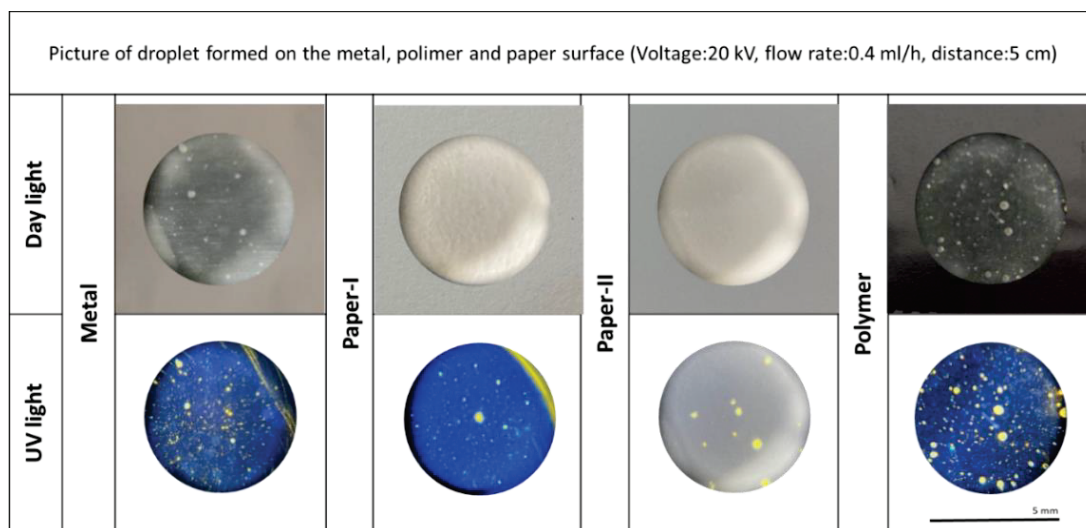
Figure 4.10. The droplet images obtained as a result of the electrospraying process performed on the different substrate with the 2 wt% PAN/DMF solution (yellow luminescent particle-573 nm).
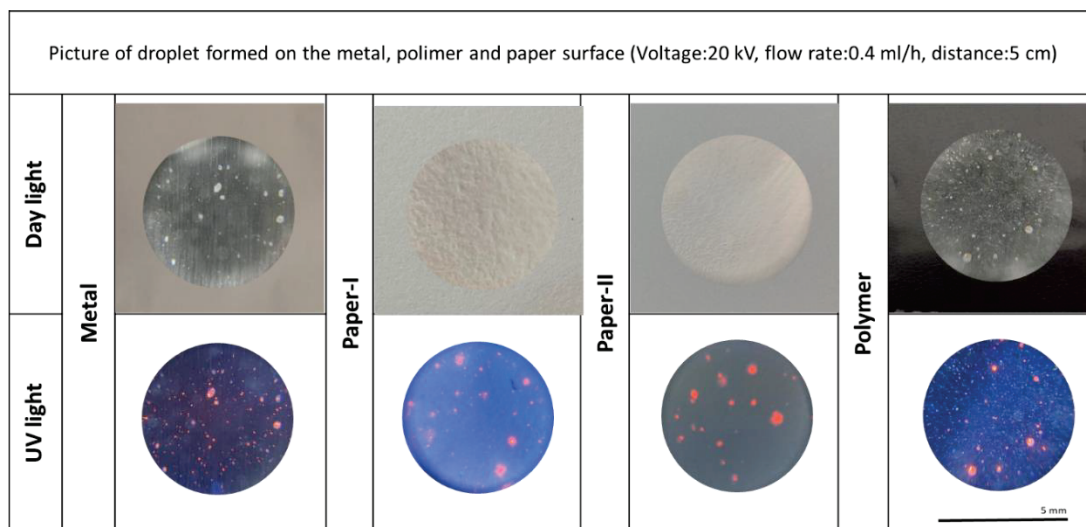
Figure 4.11. The droplet images obtained as a result of the electrospraying process performed on the different substrate with the 2 wt% PAN/DMF solution (red luminescent particle-638 nm).

To summarize, water-based and solvent-based polymer droplets that are not noticeable in daylight, but emitted in which the pattern created under UV light is visible, have been successfully sprayed on different substrates. However, due to the small number of random droplets obtained in the marked area, the wavelength of the luminescence from

the particles could not be determined. Therefore, the two-stage protection targeted in this part of the study cannot be achieved. However, the resulting randomness will still provide significant protection against counterfeiters on the product or document. Apart from this, in the in-product labeling of tablets against drug counterfeiting, fluorescent micron sized electrospun fibers have been proposed. It was mentioned that the codes in the fibers applied to the surface of the tablet can be easily resolved using a fluorescent microscope[62]. However, the need for a fluorescent microscope will make practical application difficult. Therefore, random droplets of micron size on drug tablets that can be viewed with a simple mobile phone, as in this study, will offer great flexibility in practical applications. In addition, with this simple and easy to scale strategy, desired solutions for in-product labeling of drugs can be offered. Thus, this problem can be avoided, particularly in underdeveloped nations where a large number of people are affected by low-quality counterfeit pharmaceuticals.

4.3.1.3. Generating Random Droplet/Fiber Based Security Patterns with Carbon-based Nanoparticles

Here, the real target of the study was mentioned. In this section, it was tried to create security patterns consisting of fiber and droplets to make it impossible to copy security patterns. It is not possible to copy random fibers created by electrospinning technique in the same way. Electrospinning, also known as electrostatic spinning, is a straightforward method for producing fibers from a wide range of polymers and composite materials[174]. The procedure's simplicity enables for large-scale manufacture and widespread use. Firstly, the polymer solution containing 50 ppm particles at 20 wt% concentration was prepared. PVA (Mw 30000-70000) as the polymer was used. In this study, it was started with low particle concentration (50 ppm) as it should not be observed the security pattern in daylight. After mixing the particle and polymer solution homogeneously, we took it into a syringe. By applying different voltage values to the tip of the syringe needle, we tried to create non-repeatable security patterns consisting of droplets and fibers. Table 4.3 shows the electrospinning parameter to obtain droplet/fiber with different voltages.

Table 4.3. Electrospinning parameters to obtain droplet/fiber with different voltages.

	Voltage (kV)	Flow rate (ml/h)	Distance (cm)
20% wt PVA (Mw: 30000-70000)	8	1	10
&	12	1	10
Green luminescent carbon dot (50 ppm)	15	1	10

Figure 4.12 shows the electrospinning results of the metal substrate with low molecular weight. According to Figure 4.12, droplet and fiber structures are observed. However, due to the low viscosity, fiber diameters were too thin to be distinguished at 60X magnification. It was also observed here that the smaller droplets due to the increase in voltage. However, in this study, it is expected to detect with a simple microscope to be integrated into the phone in the fiber pattern besides the spectroscopic detection of luminescent particles.
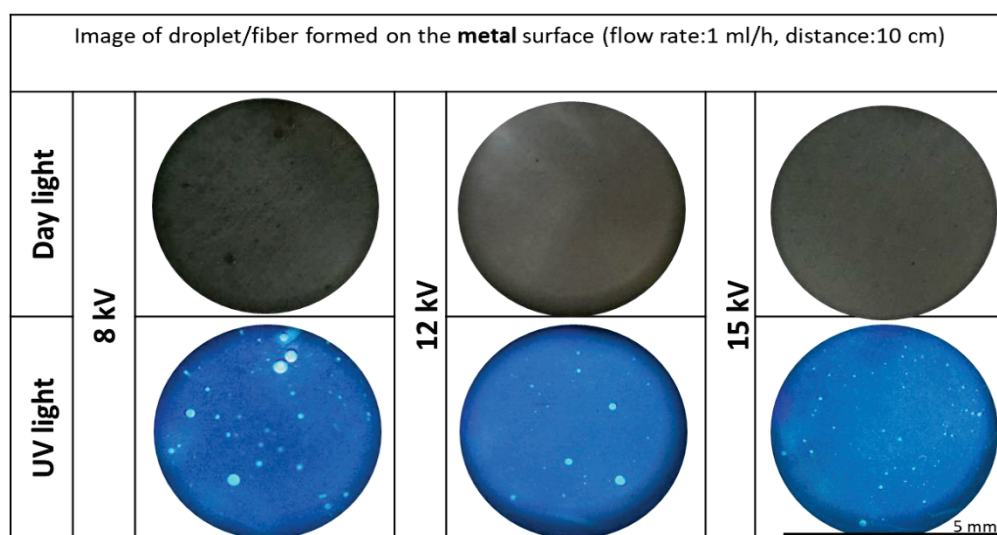
Figure 4.12. The fiber/droplet images obtained by the electrospinning process performed with the same parameters on the metal substrate with different voltages and 1 ml/h flow rate. The solutions were prepared with 20 wt% PVA/WATER (PVA Mw: 30000-70000).

The polymer concentration is critical since it determines whether or not the fibers will electrospin. Due to low viscosity, it is well known that lowering the solution concentration or molecular weight reduces fiber diameter. The solution's viscosity acts as a counterweight to the electrostatic repulsion that causes the solution jet to stretch and thin[188]. It was proceeded to work with a greater molecular weight polymer for droplet/fiber creation because it was known that increased viscosity results in a greater fiber diameter regardless of the substance utilized. Therefore, 20 wt% PVA polymer solution with Mw of 85000-120000 was prepared and spinning was attempted. However, spinning could not do because the viscosity of the polymer solution is too high. Then, the polymer concentration was reduced to 15 wt% and electrospinning was performed at different voltages (Figure 4.13). According to Figure 4.13, it was observed that droplet/fiber pattern could be created. It is observed that a thicker coating was obtained on the substrate with a flow rate of 15 kV. This makes it difficult to distinguish the fiber pattern. It was decided that 8 kV and 12 kV voltage were appropriate. Shortly, increasing the solution viscosity caused the fiber diameters to increase. This is in general accordance with those reported in the literature[189, 190]. However, the droplet dimensions were smaller with 8 kV, and whether the optical response can be detected from these small dots is the question mark. Also, the low particle concentration used here will make it difficult to determine the optical properties of the luminescent particles.
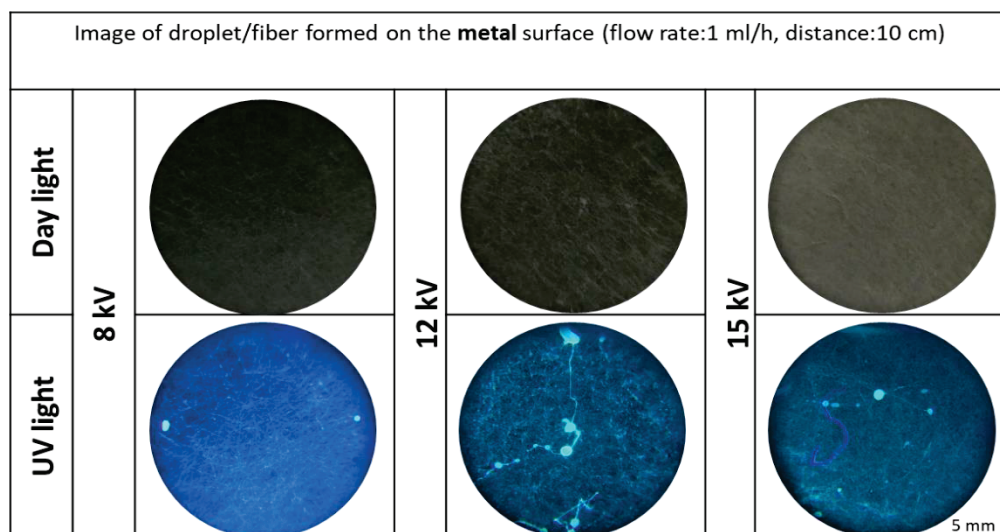
Figure 4.13. The fiber/droplet images obtained by the electrospinning process performed with the same parameters on the metal substrate with different voltages and 1 ml/h flow rate. The solutions were prepared with 15 wt% PVA/WATER (PVA Mw: 85000-120000).

Figure 4.14 shows the images of the coatings under UV light on the paper substrate using 50 ppm and 500 ppm particle concentrations (12 kV voltage and 1 ml/h flow rate). Accordingly, it was decided that increasing the particle concentration would be more suitable for taking the optical response, and studies were continued with 500 ppm particle concentration.
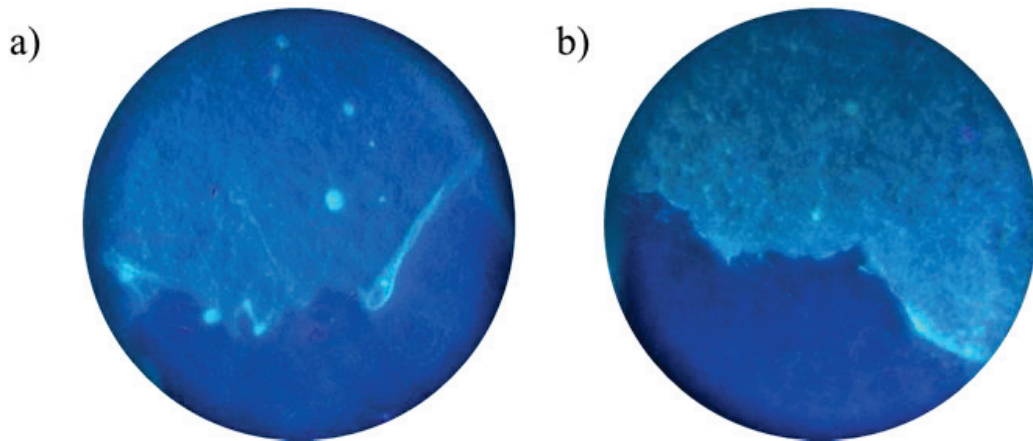
Figure 4.14. The fiber/droplet images obtained by the electrospinning process performed with (a) 50 ppm and (b) 500 ppm particle concentration on the paper substrate with 12 kV voltage and 1 ml/h flow rate. The solutions were prepared with 15 wt% PVA/WATER (PVA Mw: 85000-120000).

After increasing the particle concentration in the polymer solution, electrospinning was performed on different substrates. Figure 4.15 illustrates that the formed security patterns on the metal substrate. As a result of the electrospinning process with a voltage of 15 kV, it was observed that rarely large droplets were on the surface of the substrate. Figure 4.13 shows similarly large droplets. However, the low particle concentration was prevented it from being noticed in daylight. It is foreseen that the results obtained with 8 and 12 kV can be used as security patterns.

Figure 4.15. The fiber/droplet images obtained by the electrospinning process performed with different voltages and 1 ml/h flow rate on the metal substrate. The solutions were prepared with 15 wt% PVA/WATER (PVA Mw: 85000-120000) and 500 ppm particle concentration. Red arrows point to large droplets on the substrate.

The droplet/fiber security patterns were tried to be created by electrospinning on the polymer substrate by using the same electrospinning parameters. As shown in Figure 4.16, it was observed that the fiber pattern obtained with 12 kV voltage and 1 ml/h flow rate was showed green luminescence under UV light thanks to the presence of carbon particles in the polymer solution. By increasing the particle concentration, it was observed that not only the luminescent droplets but also the luminescent fibers. In addition, fiber patterns were clearly visible when the substrate was illuminated with daylight.
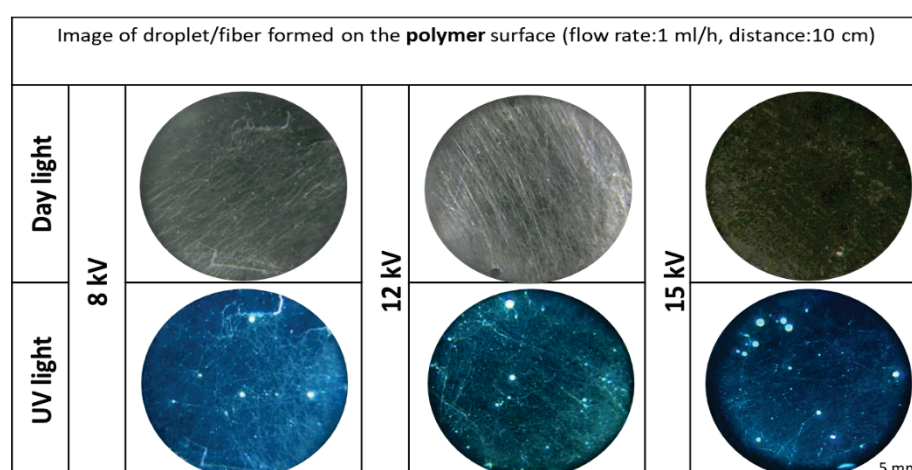
Figure 4.16. The fiber/droplet images obtained by the electrospinning process performed with different voltages and 1 ml/h flow rate on the polymer substrate. The solutions were prepared with 15 wt% PVA/WATER (PVA Mw: 85000-120000) and 500 ppm particle concentration.

Images were collected by stereomicroscope to determine the average thickness of the fibers. The created fiber/droplet patterns on the polymer substrate were also imaged by stereomicroscope in different magnifications a) 20X, b) 60X and c) 180X. However, the fibers could not be measured with ImageJ due to their low thickness. In Figure 4.17, a trend similar to Figure 4.16 was observed. It is observed that the substrate is homogeneously rich in fibers.
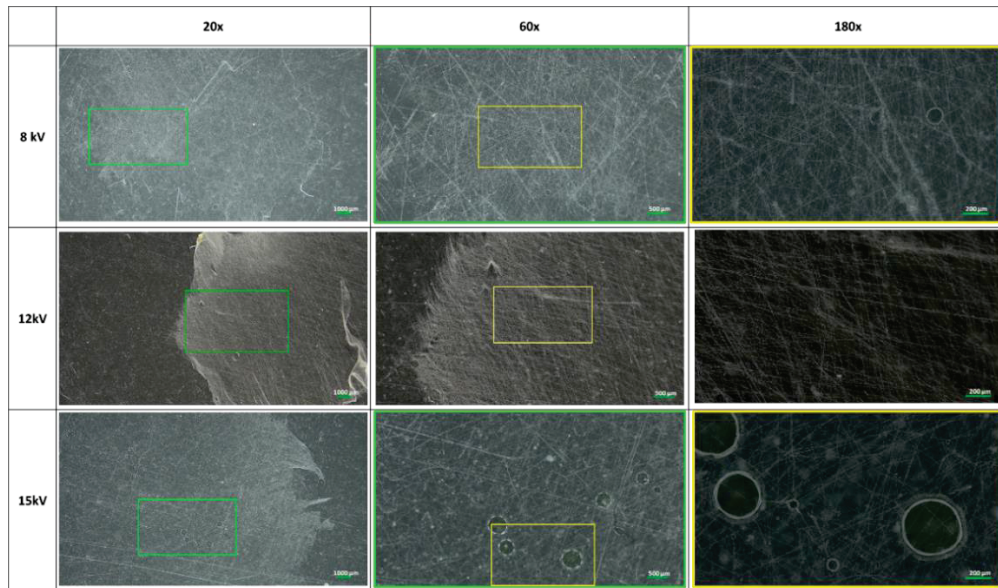
Figure 4.17. The stereomicroscope images of green luminescent droplets/fibers in %15 PVA/WATER at 8-12-15kV applied voltage. Random droplet/fiber patterns were observable in different magnifications at 20X, 60X and 180X.

Finally, the droplet/fiber pattern was generated on the paper substrate.However, as seen in Figure 4.18, the fiber pattern obtained under daylight on the paper substrate can not be clearly observed due to the fibrous structure of the substrate. Unlike day light, the presence of droplet/fiber pattern was monitorized under UV light.
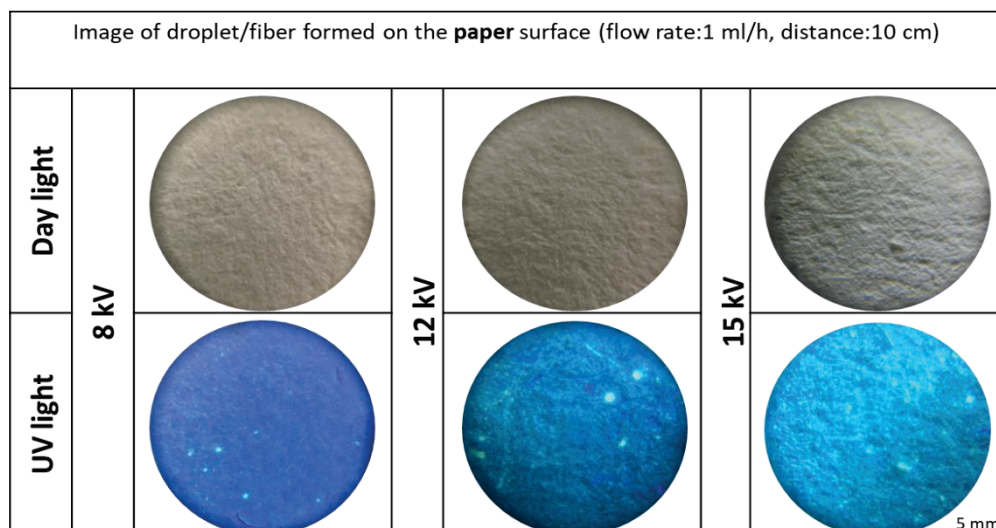
Figure 4.18. The fiber/droplet images obtained by the electrospinning process performed with different voltages and 1 ml/h flow rate on the paper substrate. The solutions were prepared with 15 wt% PVA/WATER (PVA Mw: 85000-120000) and 500 ppm particle concentration.

Several groups stated that when the flow rate increases, the fiber diameter increases[191-193]. As a result of the increased volume and beginning radius of the electrospinning jet, bending instability is decreased, and fiber diameter increases[194]. In this study, electrospinning was performed at constant voltage (12 kV) and with different flow rates to obtain larger fiber diameters (Table 4.4). Figure 4.19 shows that the image of droplet/fiber patterns obtained on the metal substrate. According to Figure 4.19, it is observed that almost no fiber was obtained at a flow rate of 0.5 ml/h. Although there was no significant change in fiber diameter with increasing flow rate, droplet sizes were observed to increase. The large droplets that can be observed in even if daylight were obtained with the flow rate of 5 ml/h. The flow rate of 1 ml/h was found to be appropriate here.

Table 4.4. Electrospinning parameters to obtain droplet/fiber with different flow rates.

	Voltage (kV)	Flow rate (ml/h)	Distance (cm)
15 % wt PVA	12	0.5	10
(Mw:85000-120000)	12	1	10
&	12	3	10
Green luminescent carbon dot (500 ppm)	12	5	10
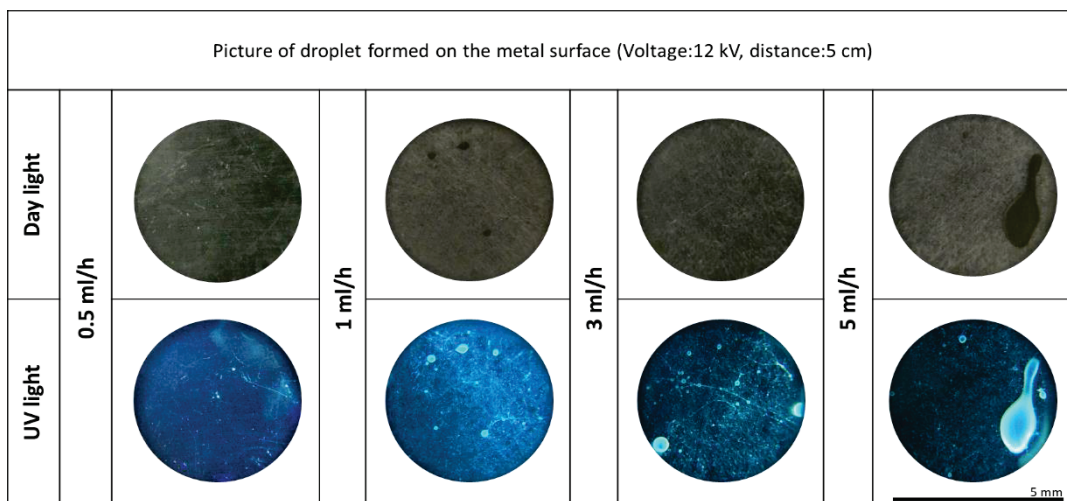
Figure 4.19. The fiber/droplet images obtained by the electrospinning process performed with 12 kV voltage and different flow rates on the metal substrate. The solutions were prepared with 15 wt% PVA/WATER (PVA Mw: 85000-120000) and 500 ppm particle concentration.

Here, the spectral signature of the security models is shown. The Figure 4.20 shows the PL spectrum of green-emitting carbon nanoparticles excited at 415 nm (emitting at 532 nm as the original model) detected with a Ocean Optics fiber spectrometer.
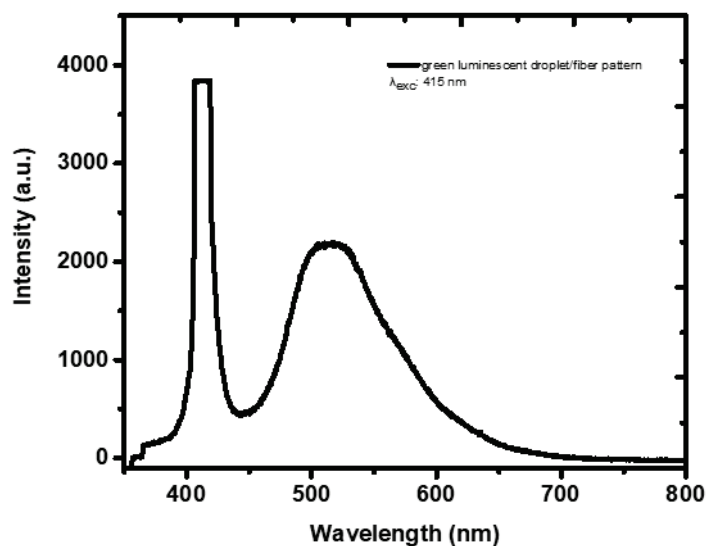
Figure 4.20. PL spectra of the green luminescence droplet/fiber pattern on the substrate.

After green luminescent particles, 15% wt PVA (Mw 85000-120000 g/mol) solution was prepared to contain 1000 ppm blue luminescent carbon particles with stirring

during 3 h at 60 °C. Electrospinning was used to create fiber and droplets on the metal substrate by loading the prepared solution into a plastic syringe and applying voltage to the tip of a syringe needle. A distance of 10 cm was fixed between the syringe and the metal collector. Using a microsyringe pump, the feed rate was kept constant at 1 ml/h. Electrospinning parameters to obtain droplet/fiber on the metal substrate (Aluminum foil) are given in Table 4.5.

Table 4.5. Electrospinning parameters to obtain droplet/fiber.

	Voltage (kV)	Flow rate (ml/h)	Distance (cm)
15% wt PVA (Mw: 85000-120000)	8	1	10
&	12	1	10
0.1% Blue luminescent carbon dot	15	1	10

Figure 4.21 shows that fiber structures and droplets obtained on metal substrate (Al foil) under daylight and UV light. According to Figure 4.21, it is observed that the droplet dimensions were more homogeneous with 12 kV voltage and 1 ml/h flow rate. In addition to this, Figure 4.21 illustrated that less droplets were observed with 8 kV voltage and 1 ml/h flow rate. Also, at 15 kV, droplet sizes were observed to be more irregular and larger.
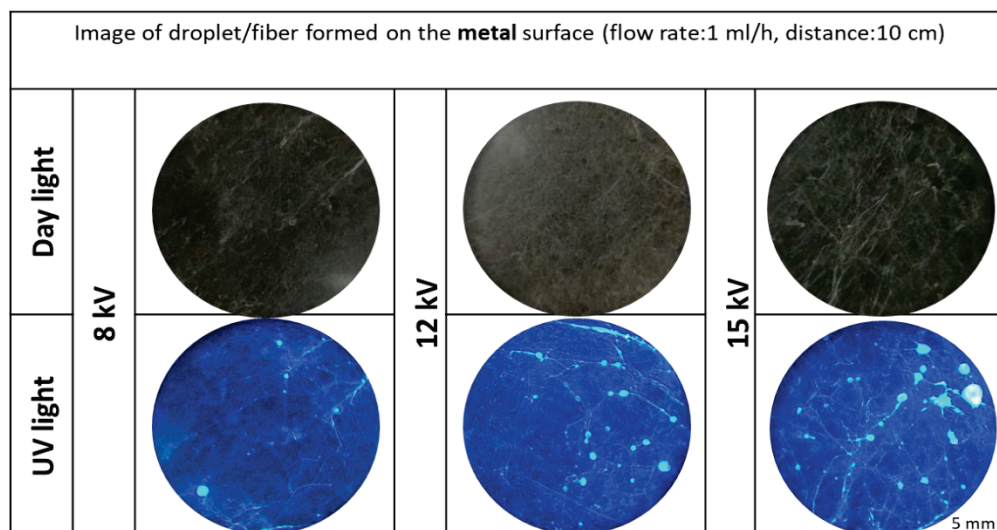
Figure 4.21. The fiber/droplet images obtained by the electrospinning process performed with different voltages and 1 ml/h flow rate on the metal substrate. The solutions were prepared with 15 wt% PVA/WATER (PVA Mw: 85000-120000) and 1000 ppm particle concentration. Blue emitting (450 nm) carbon nanoparticles were used.

Figure 4.22 shows that the images of the pattern obtained on polypropylene (PP) substrate under daylight and UV light. Since the polymer was transparent and colorless, a black background was placed behind it while imaging to prevent light reflection and see the pattern. According to Figure 4.22, the droplet/fiber pattern can be formed on the substrate with 12 kV voltage and 1 ml/h flow rate. Also as seen in Figure 4.23, the optimal voltage is 12 kV, because the presence of both droplets and fibers are clearly visible. In addition, the images obtained with the smartphone microscope and stereomicroscope from the patterns created at the same voltage values show similar droplet and fiber distributions at different magnification.
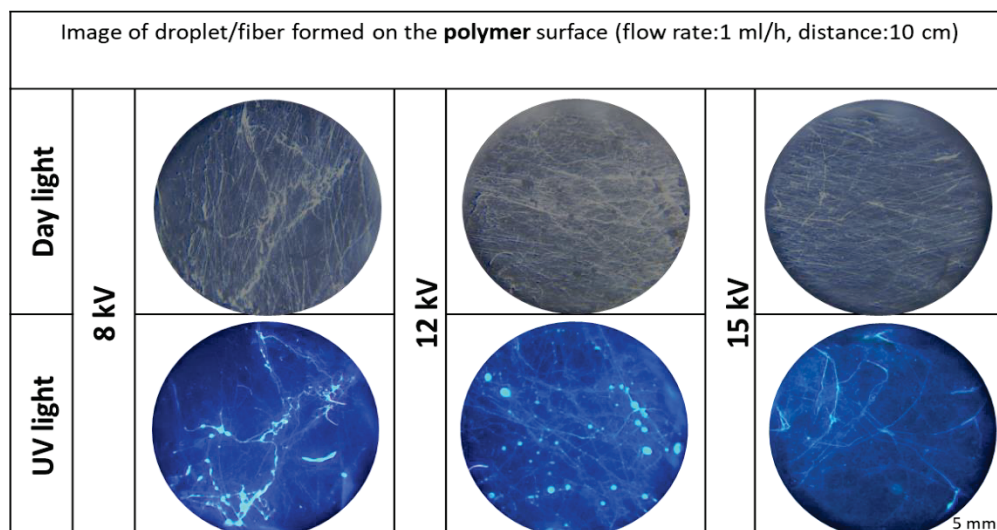
Figure 4.22. The fiber/droplet images obtained by the electrospinning process performed with different voltages and 1 ml/h flow rate on the polymer substrate. The solutions were prepared with 15 wt% PVA/WATER (PVA Mw: 85000-120000) and 1000 ppm particle concentration. Blue emitting (450 nm) carbon nanoparticles were used.
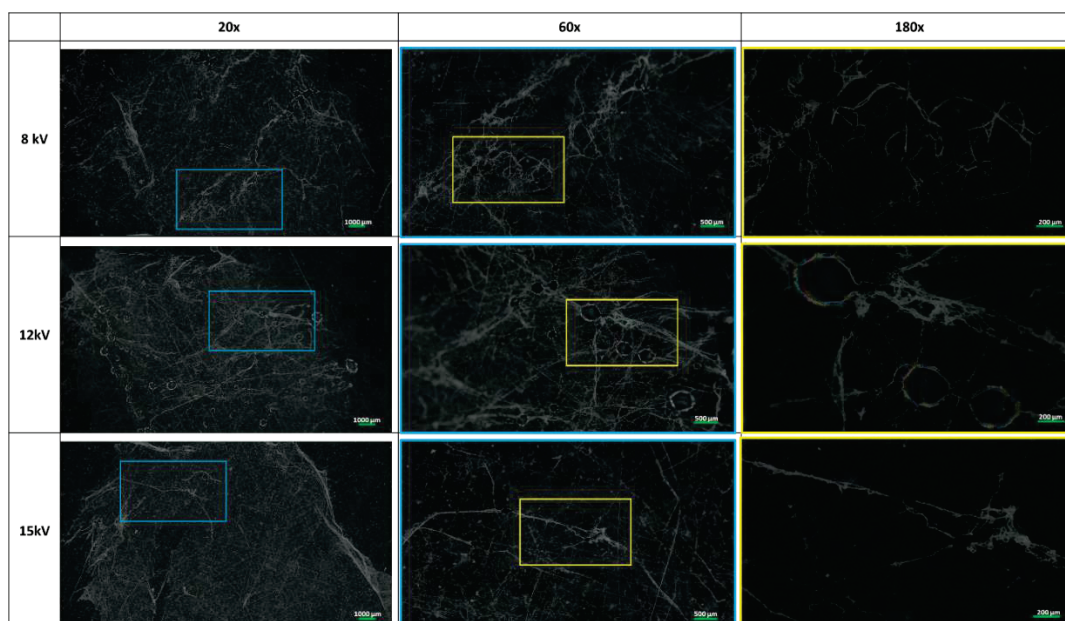
Figure 4.23. The stereomicroscope images of blue luminescent droplets/fibers in %15 PVA/WATER at 8-12-15kV applied voltage. Random droplet/fiber patterns were observable in different magnifications at 20X, 60X and 180X.

Figure 4.24 gives the results of the study for the droplet/fiber production with different voltage parameters on the paper substrate. In these images, droplet formation at 8 kV and 12 kV voltage could be clearly detected under UV light, but the polymer fiber

structures obtained could not be clearly detected even under daylight since the substrate (paper) itself consists of a fibrous structure.
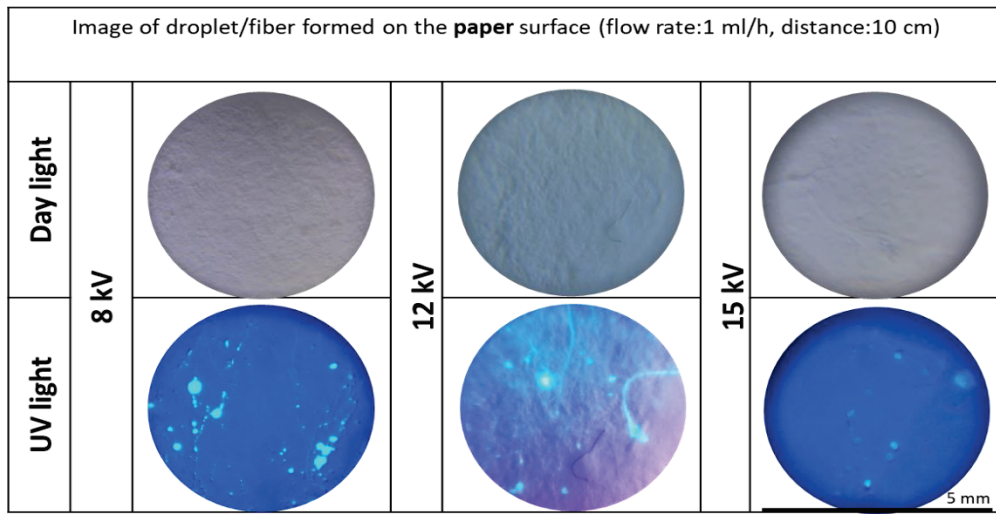
Figure 4.24. The fiber/droplet images obtained by the electrospinning process performed with different voltages and 1 ml/h flow rate on the paper substrate. The solutions were prepared with 15 wt% PVA/WATER (PVA Mw: 85000-120000) and 1000 ppm particle concentration. Blue emitting (450 nm) carbon nanoparticles were used.

In Figure 4.25, when excited with 365 nm, the PL spectrum of blue-emitting carbon nanoparticles (emitting at 450 nm as the original model) can be easily detected with the Ocean Optics fiber spectrometer. Thus, the spectral signature of the created droplet/fiber security patterns can be determined.
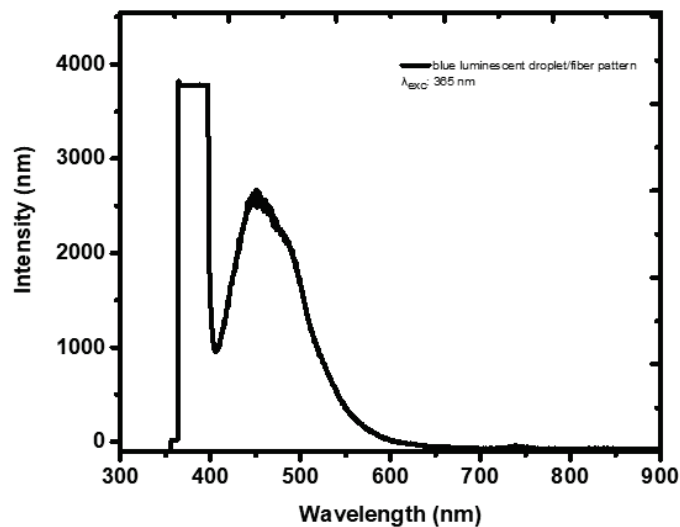
Figure 4.25. PL spectra of the blue luminescence droplet/fiber pattern on the paper substrate.

4.3.1.4. Generating Random Security Patterns Based on Droplet/Fibers with In(Zn)P/ZnS/DDT nanoparticles

Solvent plays a crucial role in electrospinning in terms of the properties of electrospun nanofibers. Solvents have various viscosity, conductivity, and evaporation times, as a result, the fiber formation and morphology of the fiber network may vary. The dipole moment determines the cohesive energy between polymer chains and solvents, whereas the dielectric constant measures the net charge deposited on the spherical droplet at the needle tip, which is a measure of fiber creation ease[195]. Therefore, solvents that have large dipole moment and high dielectric constant are preferred to adjust fiber diameter and number of droplets, and their size. *N,N*-Dimethylformamide (DMF), and dimethyl sulfoxide (DMSO), overall solubility parameters are 24.8 and 26.6 MPa$^{1/2}$, respectively, and Polyacrylonitrile (PAN) is well-soluble in both of the solvents[196]. Therefore, in this study, we decided to carry out electrospinning studies using PAN dissolved in DMF and DMSO mixture containing InZnP/ZnS/DDT nanoparticles.

The droplet/fiber pattern has been illuminated with 365-nm UV light and imaged with a smartphone having a 60X objective for magnification inserted in front of the camera of the smartphone (Figure 4.26).

Figure 4.26. Image of the pattern taken by smartphone microscope (60X objective magnification) under 365 nm UV light.

Figure 4.27 shows the microscopic images of fiber/droplet combinations created by the electrospinning process. Fiber diameters increased noticeably due to the increased viscosity of polymer concentration[197]. Because the size of the Taylor cone may remain largely stable as the solution viscosity increases, PAN fibers with large diameters may be generated as the electric jetting becomes longer and thicker[198]. In addition to this,

increasing viscosity can cause higher chain entanglements among fibers, which obstructs the flow of the solution jet, thus increasing the fiber diameters. Using an electrospinning technique with a 15% PAN/DMF solution, the effect of increasing polymer concentration on fiber diameter was investigated (Figure 4.27).
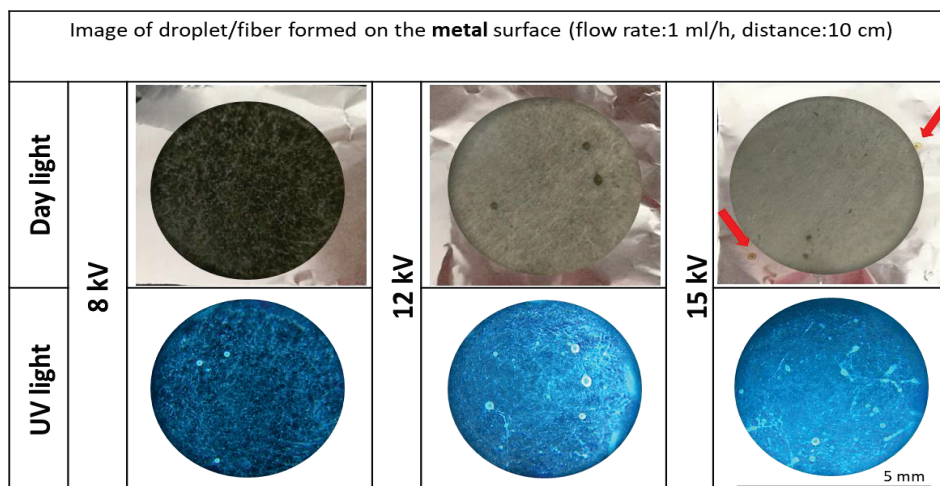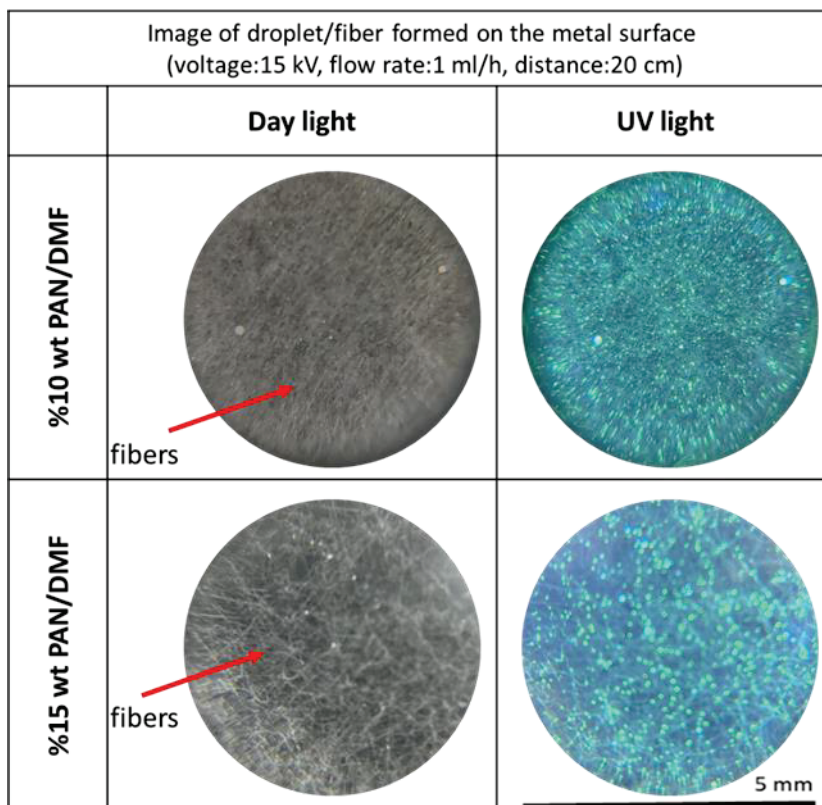

Figure 4.27. The fiber/droplet images obtained by the electrospinning process performed with the same parameters on the metal substrate of the 10 wt% PAN/DMF and 15 wt% PAN/DMF solution. Increasing the polymer concentration increased the fiber diameters. Green emitting (535 nm) InZnP/ZnS nanoparticles were used.

By increasing the PAN concentration in DMF, the fibers became easily noticeable. However, image processing requires thicker fibers to obtain visible patterns by a smartphone. Thicker fibers could be achieved by DMSO and n-methylpyrrolidone (NMP) solvents due to the properties of the solvents such as density, conductivity, dielectric properties, surface tension, and volatility[199]. Therefore, 15 wt% PAN solution was prepared with DMSO to have fibers with larger diameter. In Figure 4.28, the image of the thicker fibers in droplet/fiber structures obtained with DMSO is shown under daylight and UV light. Using DMSO rather than DMF provided easily observable fibers in the patterns that may be suitable for image processing. Additionally, upon varying

electrospinning parameters, a random distribution of luminescent droplets/fibers network is generated on the substrates, thus resulting in a unique fingerprint pattern that is unclonable.

Image of droplet/fiber formed on the **metal** surface (flow rate:1 ml/h, distance:20 cm)				
		8kV	**12kV**	**15kV**
%15 PAN/DMF	Day light			
	UV light			
%15 PAN/DMSO	Day light			
	UV light			5 mm
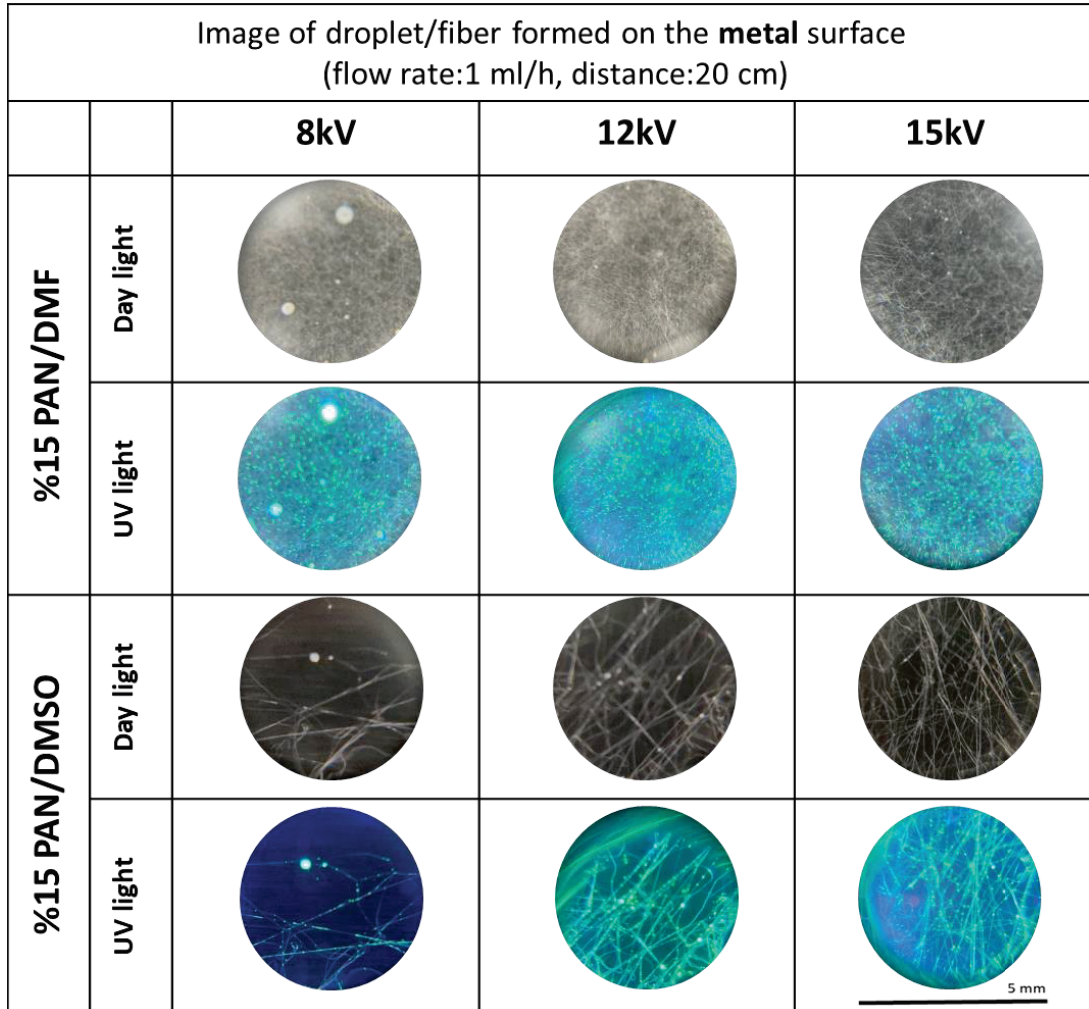
Figure 4.28. The fiber/droplet images obtained as a result of the electrospinning process with different voltages on the metal substrate. The solutions were prepared with 15 wt% PAN/DMF and 15 wt% PAN/DMSO. All the other parameters were kept constant. Green emitting (535 nm) InZnP/ZnS nanoparticles were used.

DMSO affected not only the fiber thickness but also the droplet size. Figure 4.29 shows the significant reduction in the droplet diameter when DMSO was used as a solvent. The maximum diameter of the droplets was 80 µm for all applied voltages. On the other hand, when the solvent was DMF, the droplet diameter significantly depend on the applied voltage during the electrospinning process. Increasing the applied voltage for

15% PAN/DMF solution reduces the droplet diameter from 496 μm to 380 μm and 94 μm for 8, 12, and 15 kV applied voltages, respectively.
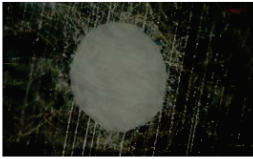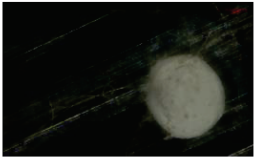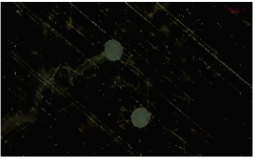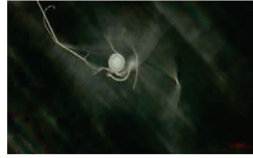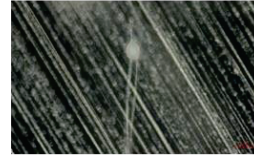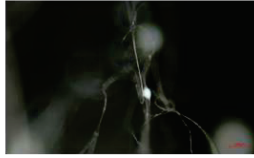
Image of droplet/fiber formed on the **metal** surface (flow rate:1 ml/h, distance:20 cm)			
	8kV	**12kV**	**15kV**
%15 PAN/DMF			
%15 PAN/DMSO			

Figure 4.29. Stereomicroscope images of the fiber/droplet images obtained as a result of the electrospinning process with different voltages on the metal substrate. The solutions were prepared with 15 wt% PAN/DMF and 15 wt% PAN/DMSO. The diameter of the droplets reduced depending on DMSO. All the other parameters were kept constant. Green emitting (535 nm) InZnP/ZnS nanoparticles were used.

After the optimization of the fiber thickness and droplet diameters, random droplet/fiber patterns were formed on diverse substrates such as metal, polymer, and coated paper (Figure 4.30). Creating the droplet/fiber patterns on paper substrates was challenging due to the surface tension of the coated paper used. Before the electrospinning process, small DMSO droplets were applied to the paper substrate to reduce the surface tension and to increase the adhesion of the fibers and droplets. After DMSO treatment the droplets' contact angle on the papers reduced (Figure 4.31) and a random pattern was created on treated paper substrates (Figure 4.30).
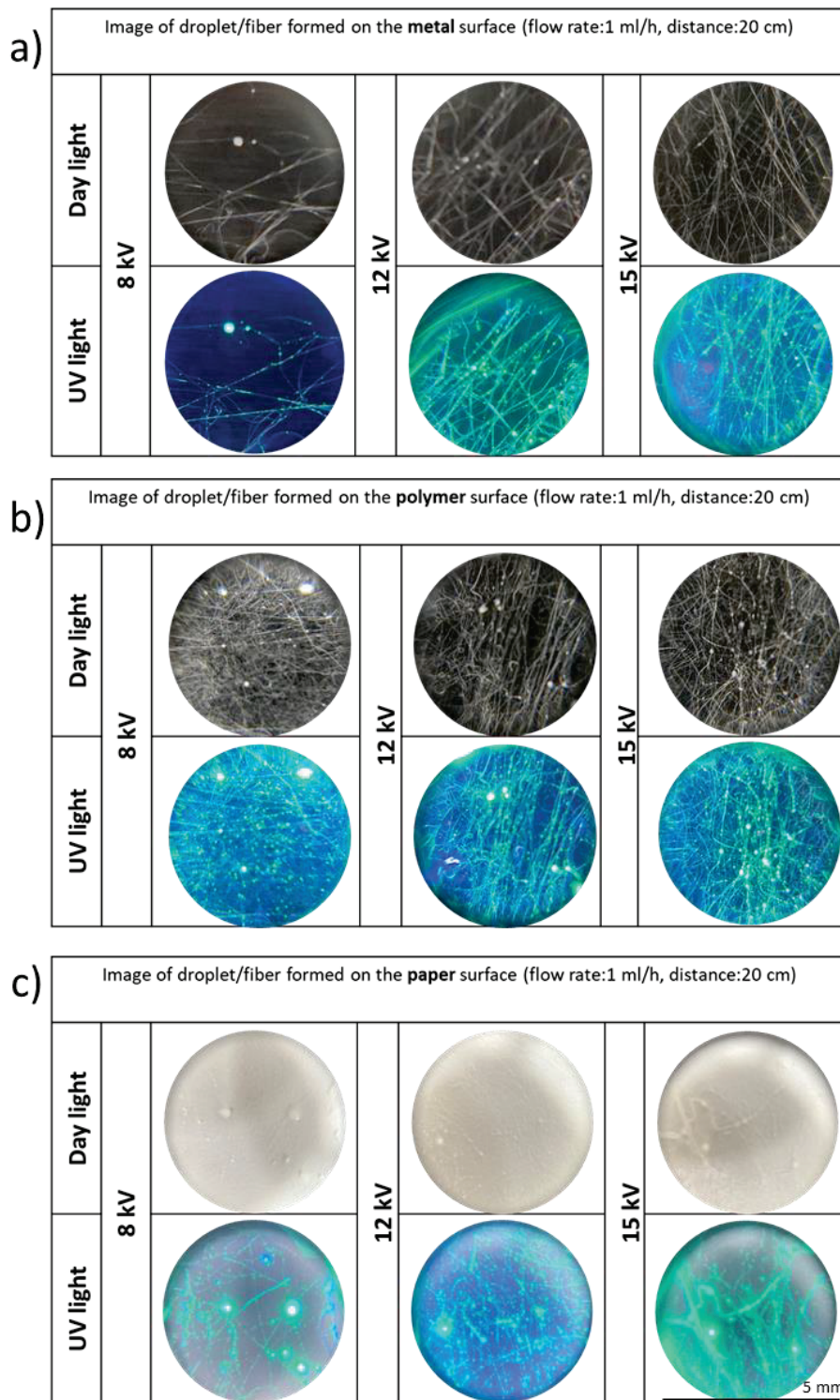
Figure 4.30. The fiber/droplet images obtained as a result of the electrospinning process performed on a) metal, b) polymer and c) the paper with the 15 wt% PAN/DMSO solution. Green emitting (535 nm) InZnP/ZnS nanoparticles were used.
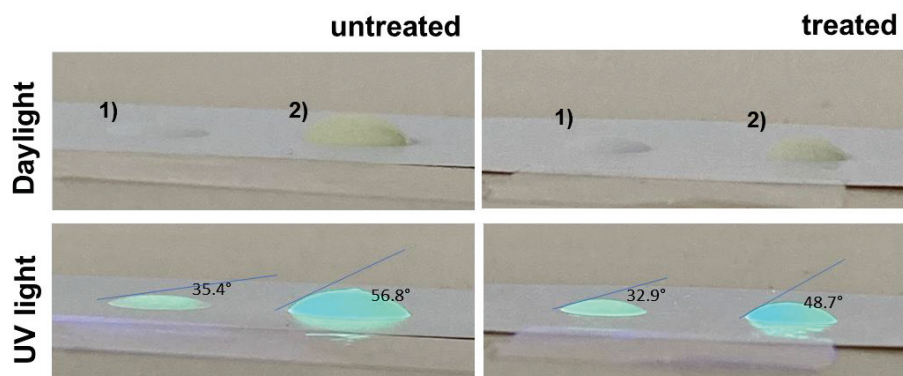
Figure 4.31. Contact angle values in the untreated and treated paper (1: QD in toluene; 2: QD in 15 wt% PAN/DMSO solution).

The created fiber/droplet patterns were also imaged by a special stereomicroscope (Zeiss Axio Zoom) with different magnifications of 20X, 60X, and 180X. Figure 4.32 depicts random droplet/fiber patterns obtained by electrospinning of nanoparticles in %15 PAN/DMSO solution at 15 kV applied voltage. Similar images were collected by the stereomicroscope to determine the average thickness of the fibers. 60X and 180X images from the selected areas were shown in Figure 4.33. The average diameter of the fibers was determined by using ImageJ as 3.98 +/- 1.62 µm. As shown in the thickness histogram of the fibers (Figure 4.34), the maximum fiber thickness is around 6.3 µm. The overlapping of the fibers in some points appears like thicker fibers and results in higher values in the histogram.
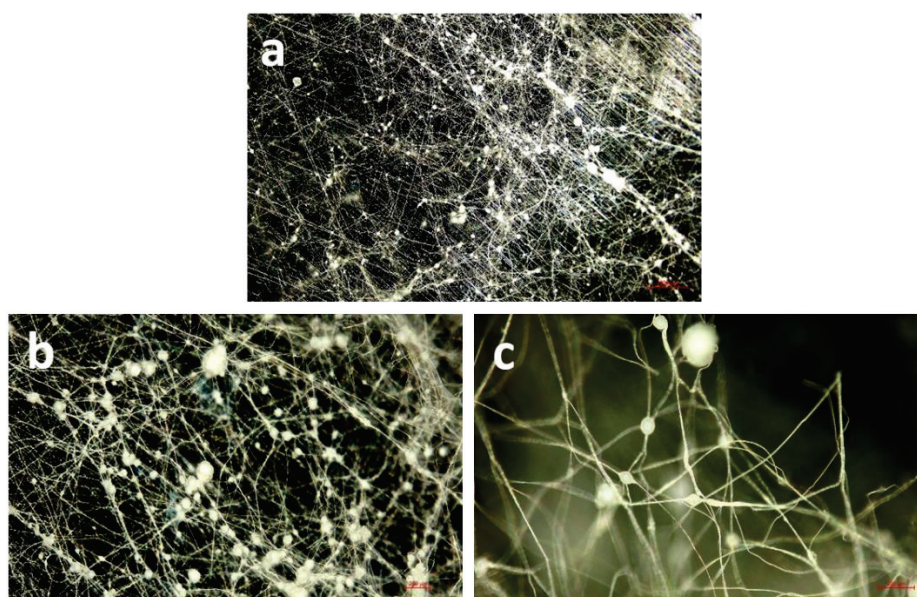
Figure 4.32. The stereomicroscope images of nanoparticles in %15 PAN/DMSO at 15kV applied voltage. Random droplet/fiber patterns were observable in different magnifications a) 20X, b) 60X and c) 180X.
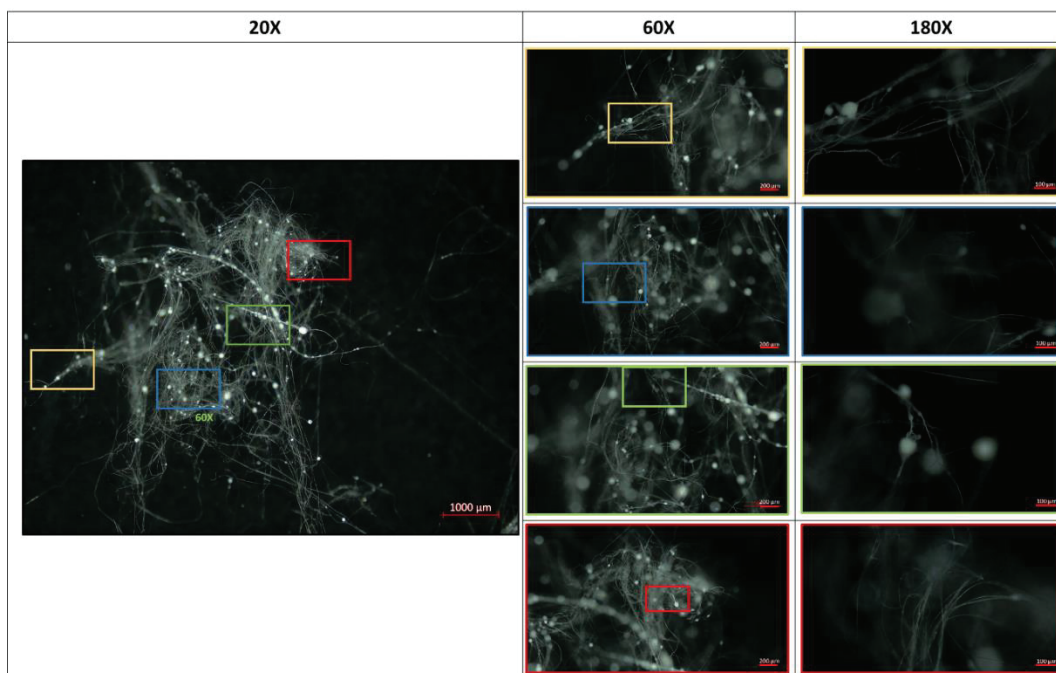
Figure 4.33. Stereomicroscope images of the nanoparticles in 15% PAN/DMSO under different magnifications. Colored rectangles in 20X and 60X magnifications represent the selected areas focussed in 60X and 180X magnification, respectively.
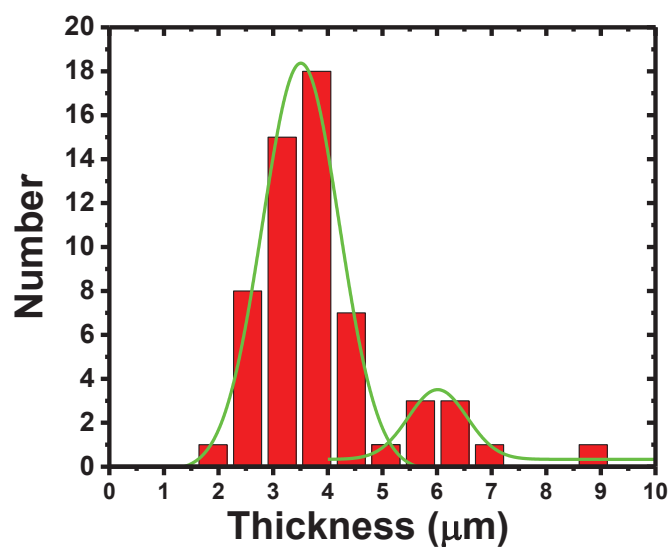
Figure 4.34. Histogram of the fiber thicknesses measured from 180X magnification images in Figure 4.33.

Security patterns were created on the treated paper substrate by applying various voltages from 8 kV to 20 kV. Figure 4.35 shows that there is no distinguishable difference in fiber diameters when the voltage is increased. The fiber thickness was also determined by the ImageJ program on the images obtained at various voltages. The histogram (Figure

4.36) of the fiber thickness confirms the same fiber diameters around 3–4 µm independent of the applied voltage. On the other hand, the luminescent area under UV illumination increased significantly due to the amount of coating deposited on the substrate with the increasing amount of jet. At all applied voltages the coated paper substrates were invisible in daylight and the coating on the substrate was indistinguishable.
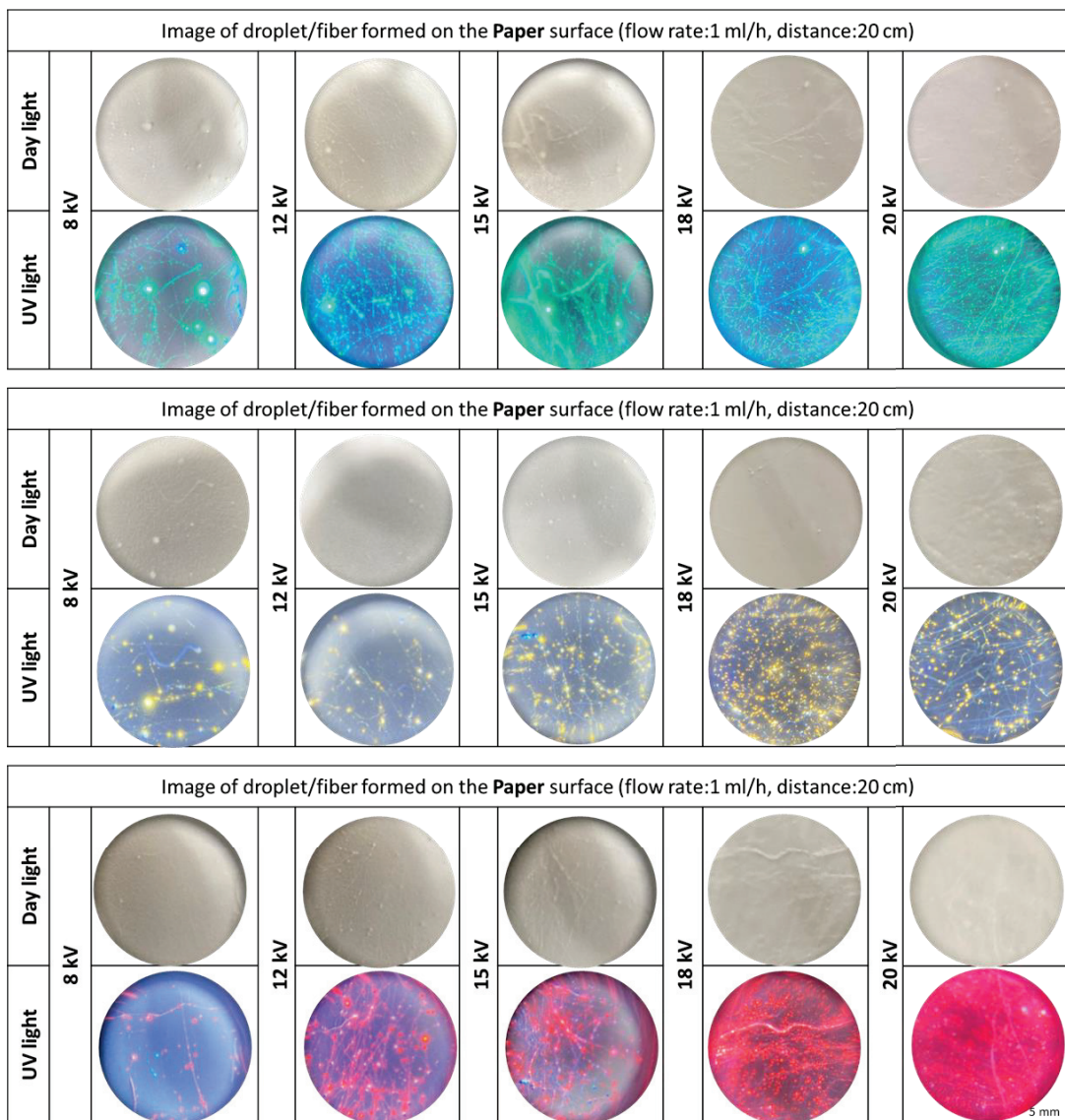
Figure 4.35. The fiber/droplet images obtained as a result of the electrospinning process performed on the coated paper substrate with the 15 wt% PAN/DMSO solution (green, yellow and red luminescent particles).
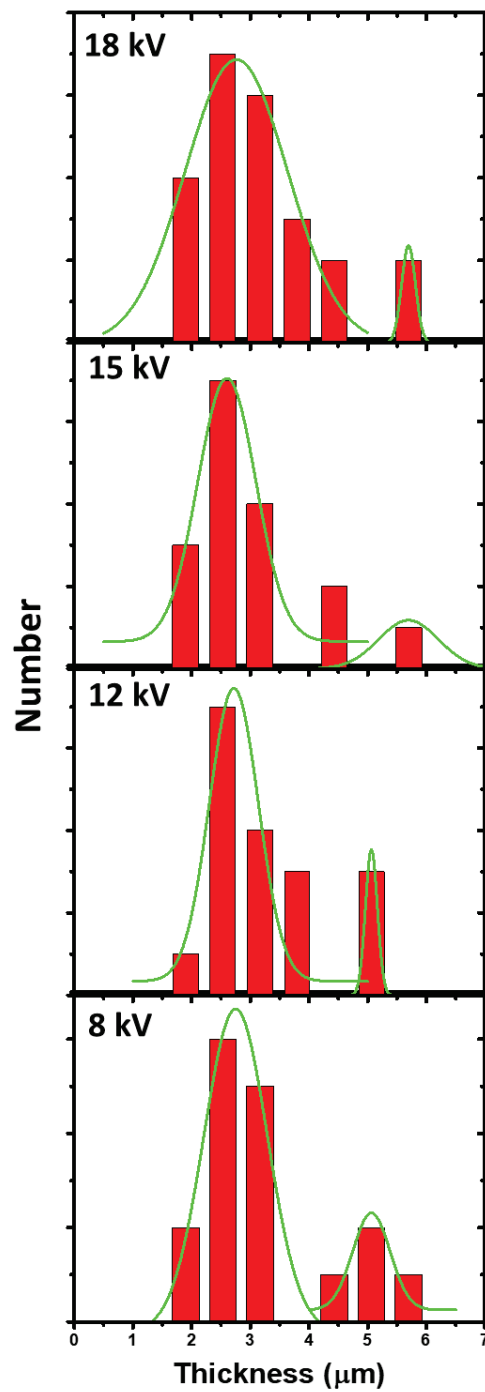
Figure 4.36. Histogram of the fiber thicknesses with respect to different applied voltages.

Figure 4.37 illustrated the optical responses of InZnP/ZnS based nanoparticles with three different PL emission wavelengths obtained from the paper substrate. Increasing applied voltage enhanced the emission intensity of the nanoparticles that after the 15 kV voltage characteristic PL peak was observed for each nanoparticle and

sufficient intensity was obtained to confirm the optical response. Increases in applied voltage to 18 kV and 20 kV did not improve PL intensity and resulted in emission intensities that were similar. These results confirmed that the whole surface of substrate was almost completely covered with luminescent droplet/fiber pattern at 15 kV and a further increase in the applied voltage created a thicker coating.
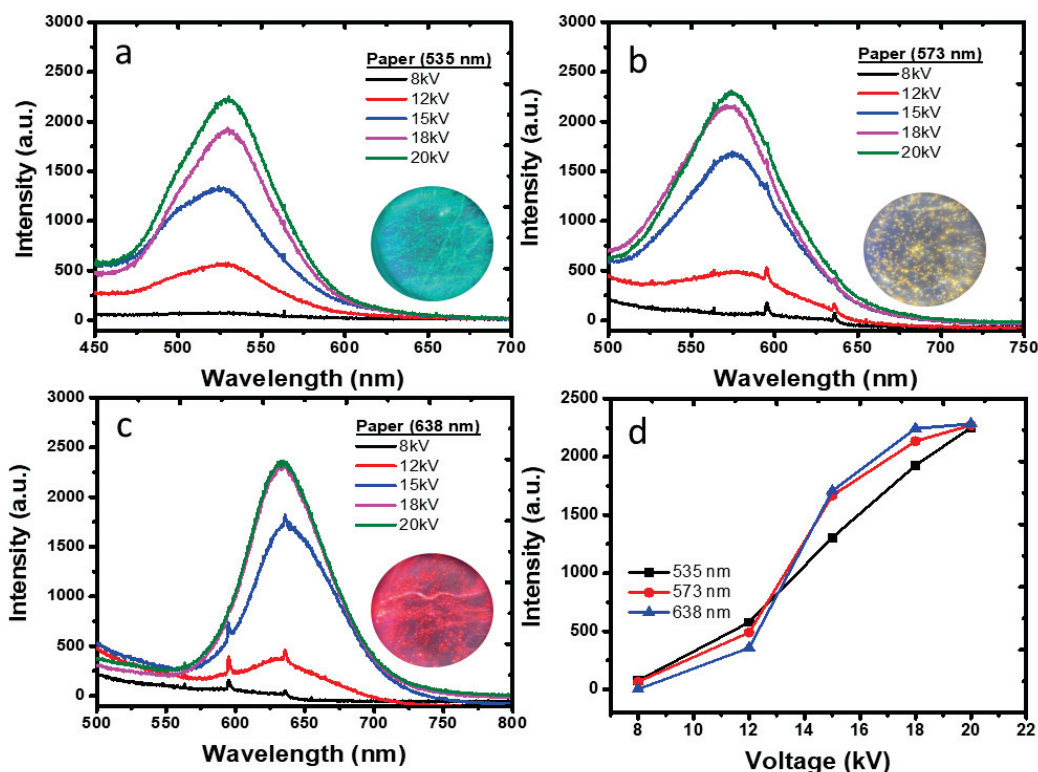
Figure 4.37. PL spectra of a) green, b) yellow, and c) red-emitting nanoparticle included droplet/fiber patterns on the paper substrate at different voltages; d) Enhanced PL intensity with increased the applied voltage. The solution concentration was 15 wt% PAN/DMSO.

Here, we would like to demonstrate the wavelength dependency (spectral signature) of the security patterns created. In Figure 4.38, PL spectra of both the InP-based nanoparticles (emitting at 638 nm – as the original pattern) and carbon dots (emitting at 666 nm – test pattern) were shown. Even if both patterns have red emission having different wavelengths, the spectral signature can not be distinguished with the naked eye. But the spectral differences could be easily detected with an Ocean Optics fiber spectrometer. Here, we see that the PL position of the non-original test model does not match with the original one. Thus, it can be said that the created security models work successfully.
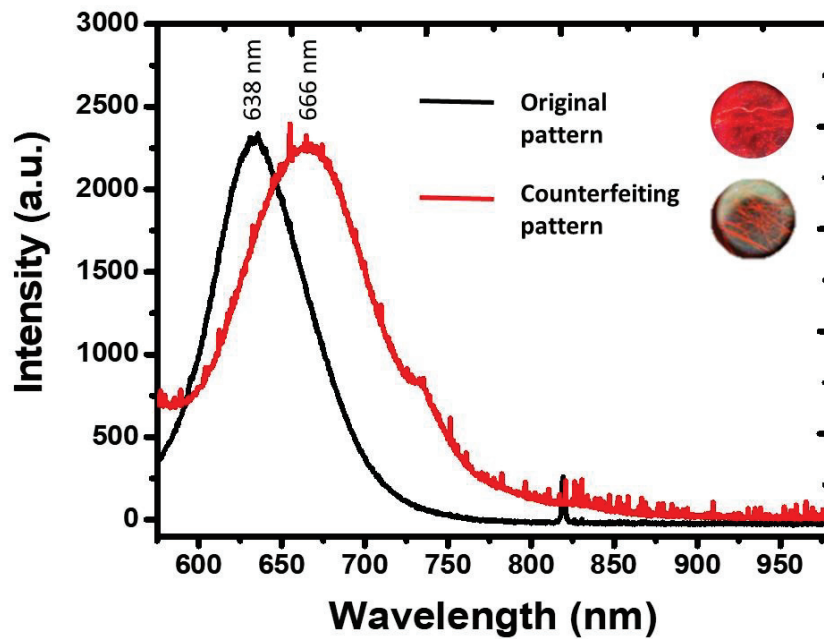
Figure 4.38. PL spectra of the original pattern and counterfeiting pattern on the paper substrate. Both patterns emit red color under UV light as shown in the inset.

In order to increase the difficulty of security codes, electrospinning process was carried out in separate layers on different substrates with three different colored luminescent particles. Figure 4.39 shows random patterns with luminescent particles of three different colors created on different substrates.
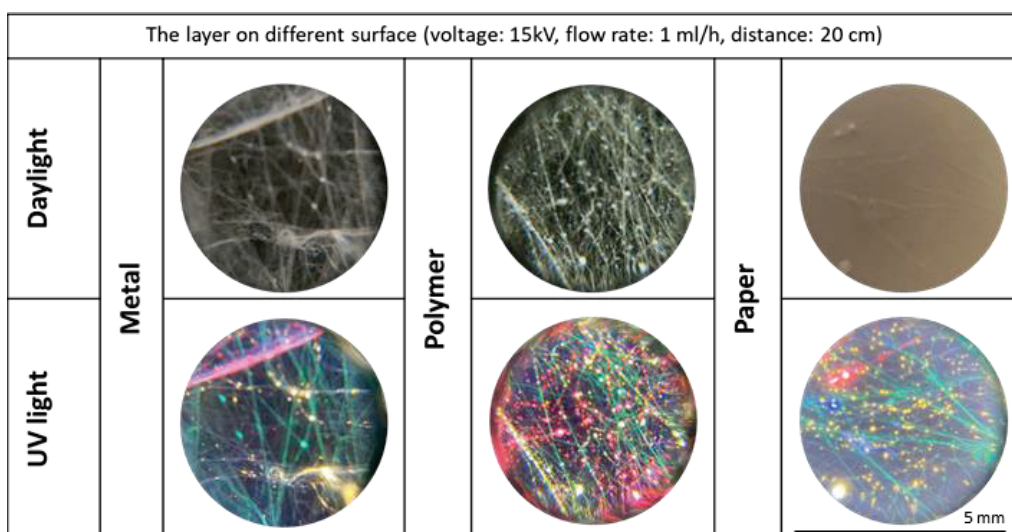
Figure 4.39. The fiber/droplet images obtained with three-layer by using green, yellow and red luminescent particles as a result of the electrospinning process performed on the different substrate.

PAN solution containing three different colors of luminescent particles was spun on the metal substrate in three different layers and then the optical response was tried to be read from the obtaining pattern with ocean optic spectrophotometer. The setup for reading (left) and the emission graph (right) obtained are shown in Figure 4.40. In the graph obtained according to Figure 4.40, peaks are observed in the regions where the emission of particles. However, due to the fact that three different colors come to the reading area at different rates, the signal levels vary depending on the ratio of the color in each new pattern. In addition, it was observed that in security patterns that were created with three different colors, sometimes three colors did not fall into the same area or they cover each other. Therefore, although the security code can be created using three different colors, it has been observed that it is more difficult to control.
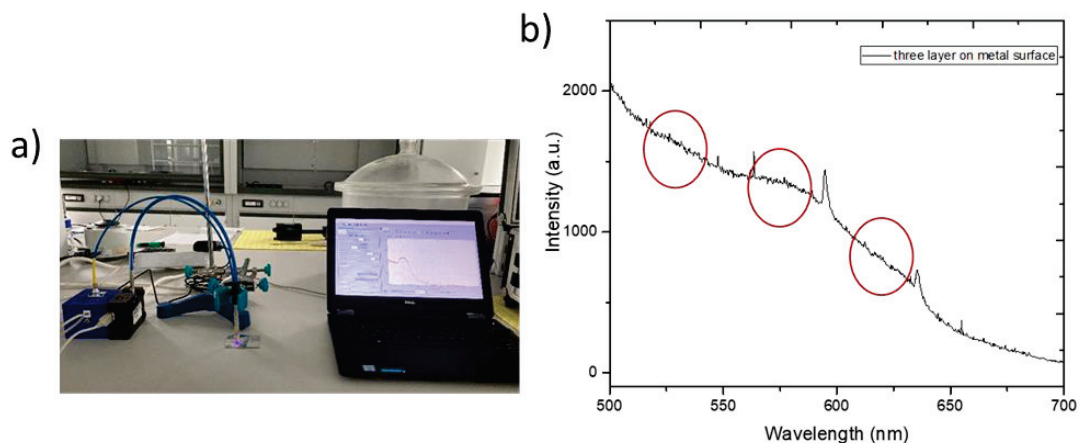
Figure 4.40. a) Detection of fluorescent information of droplet/fiber pattern with ocean optic spectrometer and b) PL spectra of the droplet/fiber pattern on the substrate.

4.3.1.5. Analysis of Image Processing

In this chapter, we propose a technology that offers security labels that are easy to manufacture but not clonable, and an inexpensive image identification method to authenticate security label created. The first part is to produce a unique security patterns by the electrospinning technique using a mixture of nanoparticles and polymer as an inexpensive. The second part has two step verification: for the first level security, the spectral originality of the pattern created by the luminescent properties of the nanoparticles is checked by using a spectrometer. For the second level security, the pattern verification is made. Here, the fiber/droplet patterns created is to be verified by

image processing. Therefore, a database was created by using the security patterns produced and an image recognition software was developed to verify patterns produced.

Each created security pattern has its own luminescence signature. Since making droplet/fiber patterns are depending on the electrospinning process, the pattern that will be formed on the substrate cannot be pre-calculated, and they will have unique patterns. The cruces here are how to use this unique pattern to get unique tagging keys for every pattern on its own. Since they are luminescent, the photographs taken under UV light show their pattern. These photographs have their unique pattern based on their emission spectrum, depending on the nanoparticle used. Since photographs are based on emission patterns they can be processed by the Canny edge detection algorithm[200].

In this study, all of the steps of Canny detection algorithm have been used the same in the OpenCV library, no changes have been made in four of them. But for the Canny algorithm, one needs to find the threshold values on his/her own, since every photograph can have different thresholds for different, sharp edges. Upon some trials, the best values for threshold have been chosen is 200 and 230 count. Also, this double threshold applies to all security codes, made on different materials, also for different spectrums. Therefore, there is no need to change by hand for each new security code made. Regardless of the used materials in the security code, same double threshold values can be used. However, there are still some minor issues. The first is, if you preprocess some photograph of security code, you need to put it exact same length and exact rotation for it. If there are some changes in angle of the photographs, or the newly taken photograph is somehow rotated by some angle, it concludes to undefined behavior and high error on these photographs. Therefore, the photograph needs to be taken at the exact rotation and exact length as before.

After the photographs have been taken for preprocessing with Canny, some minor changes need to be done on these photographs too. The first issue is the lens's radius, which can be directly observed from the photograph. If the whole photograph is processed with including lenses radius, Canny will detect it as an edge and it will result in a high error. To overcome this issue, firstly all of the taken photographs have been resized to 1024x1024 pixels, regardless of their size. Even if the camera that took the photograph has a hardware limit of taking 256x256 pixels, it will always get scaled to 1024x1024 pixels. This concludes that all of the photographs have the exact same pixel size. After the scaling process, the next issue that needs to be handled is the lens radius which can

96

be observed in the photograph. Since all of the security codes have their own unique image, there is no problem in taking only the center of the photograph, which is the main part of these photographs, that have the most density of droplet/fiber pattern, which Canny detects best. To make this, all of the photographs have been set to an offset value. This value starts from +384px from x-direction, as well as +384px from y-direction. A little note in here, the coordinates start from the bottom left, therefore the bottom left is the origin in these photographs. After this offset in both x and y directions, a fraction of the photograph, which is 256x256 pixels has been cropped from the center of the photograph. To sum up, first, the photograph has been scaled to 1024x1024 pixels. After that, a fraction of the photograph has been cropped out, which starts from both on x and y directions at 384 pixels, and goes on to 640 pixels. At last, all of the pictures have been preprocessed and ready for putting into the database.

After these operations, all of the photographs, dependent on their colors (the different quantum dot) have been saved in a different location for each type. Currently, there are yellow, green and red data folders. After photographs are preprocessed and ready to make a comparison between them, an error calculation needs to be done. Since Canny algorithms detect edges and convert the whole photograph to gray scale, only pixels left are only black and white. Since black pixels have a data of 0 in photographs, a simple Euclidian distance calculation among both preprocessed and chosen pictures will work splendidly.

In the program, color must be selected (security code luminescence color). If the color isn't selected, the program will automatically choose yellow, and if the chosen photograph is different from yellow fiber, the program will calculate enormous errors. After the correct selection of the chosen pattern, the photograph must be uploaded to the program. After it is uploaded, it will repeat the same process on the uploaded photo, like the preprocessed photographs. After the preprocessing step, the program will calculate the sum of Euclidian distance between all of the chosen fibers. For example, as in Figure 4.41, if green has been chosen, the program will compare the uploaded photograph with all of the green preprocessed fiber photographs. The total error will be the sum of Euclidian distance between them, if photographs are identical it will give 0% error and gives a 100% authentication.
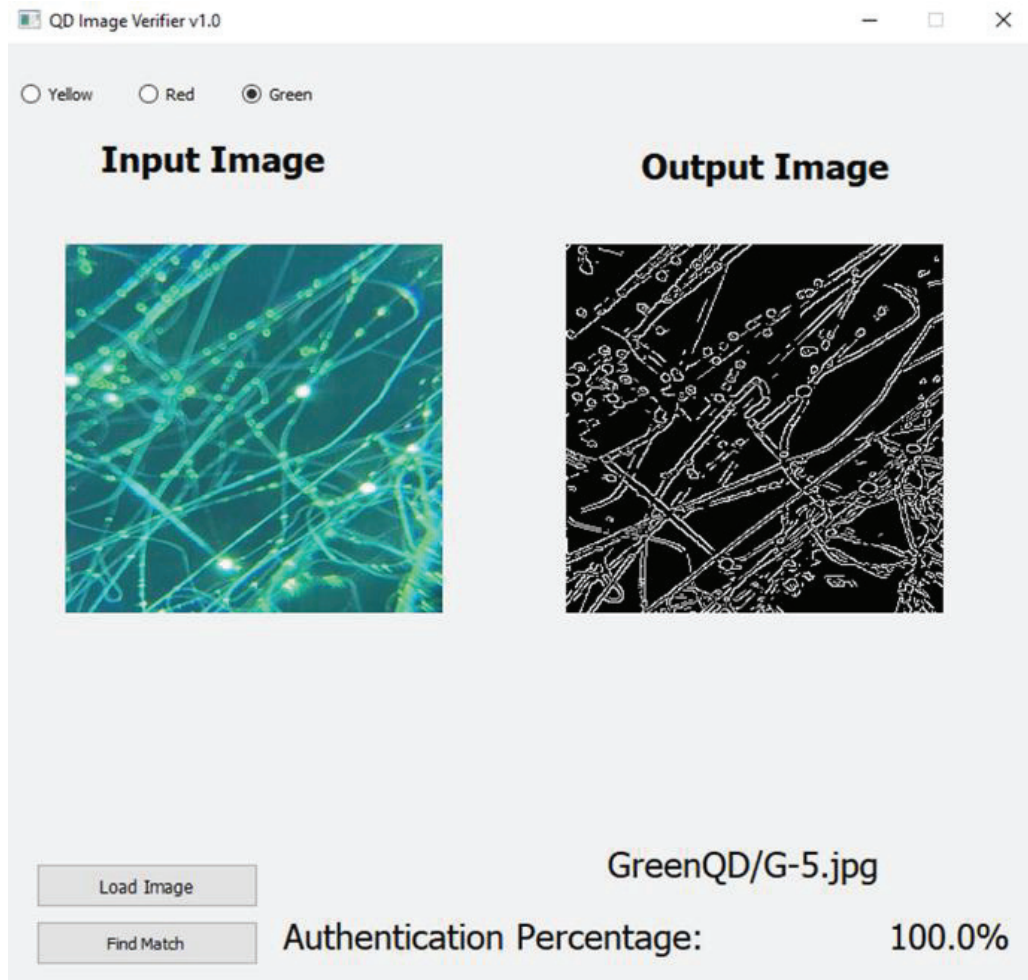
Figure 4.41. QD image Verifier Program for controlling originality of security pattern.

If there is a photograph that is not defined in the database as in Figure 4.42, the program calculates the error rate very high and gives a 0% authentication, indicating that the document or product is counterfeited. This tells us that the document or product is not original.
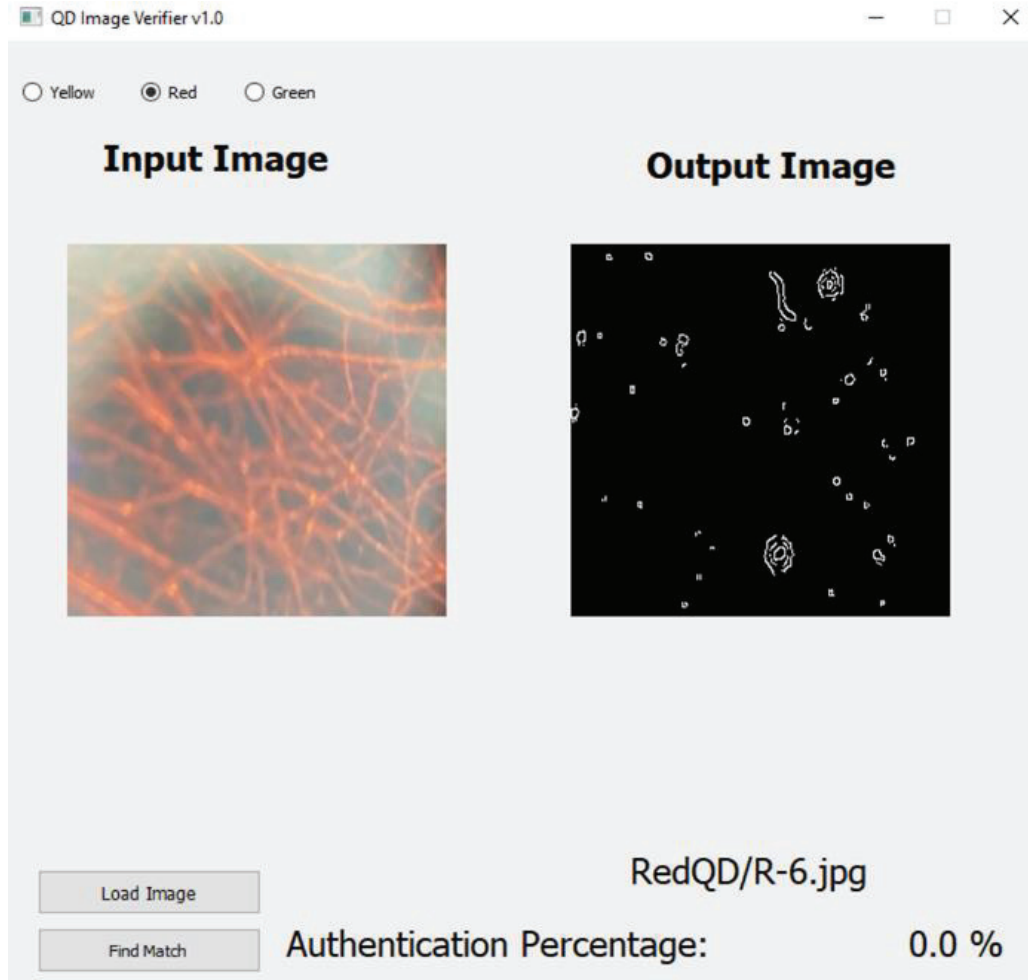
Figure 4.42. A counterfeiting pattern does not match with database in QD image Verifier Program.

The calculation is followed as below:

$$\sum_{\{i=0\}}^{216} \sum_{\{j=0\}}^{216} \sqrt{\left(x_{current}^{(i)} y_{current}^{(j)} - x_{preprocessed}^{(i)} y_{preproccesed}^{(j)}\right)^2}$$

Note that the superscript denoted on parameters indices are not powers, they are the indices of the photograph matrix which is 256x256 pixels.

This error calculation needs to be done on all of the current preprocessed photographs in the database because the minimal error is the best match for the uploaded picture. After all of the errors have been calculated, the minimal error has been chosen from the set of preprocessed photographs. After this process, the best photograph with minimal error has been put next to the uploaded picture, as well as the error. Match-no

match will have a threshold error of some value, and this threshold needs to be calculated by taking various photos of the same security pattern, then calculating the errors between these photos and the original preprocessed photograph, will give the best optimal error.

It is impossible to duplicate these security patterns through artificial manipulation, as the luminescent droplet/fiber cannot be easily manipulated due to the randomness of the patterns. Moreover, apart from the pattern image control, it is not possible to overcome two-safety steps at the same time since the emission wavelength information (the spectral signature) from the particles is also examined. Therefore, this technology will be a deterrent effect to counterfeiters who are considering producing a similar fake model. In addition, the simple and inexpensive preparation of random security labels as well as the fast and easy verification method are attractive advantages of this proposed anticounterfeiting technology. When this technology in which the proof of concept has proved, is developed the mobile application, may have a general usage by any person who does not any experience on anticounterfeiting. This technology may be applicable to many products because it is a ink based patterning that would be applied to many substrates.

4.4. Conclusion

Creating unique and non-repeatable fingerprint security patterns against counterfeiting will be an important step in the fight against counterfeiters. Therefore, in this study, high fluorescent water-based carbon and solvent-based In(Zn)P/ZnS/DDT nanoparticles were used for anticounterfeiting applications. Both water-based and solvent-based particles were homogeneously dispersed in small quantities in suitable polymer solutions, and random droplet and droplet/fiber patterns were created on different substrates (metal, polymer and paper) using the electrospinning technique which is a simple, fast and cost-effective. Due to the low amount of particles, the patterns are invisible in daylight but extremely bright under UV light. Thus, with a method that allows simple and widespread production, unique security patterns that cannot be detected in daylight but can be detected under UV light were created. Instead of expensive and hard-to-reach devices such as SEM, TEM and fluorescence microscope etc., the created security patterns were viewed with a simple smartphone microscope and a database of original patterns was created. In addition, the spectral information of the particle from the

obtained droplet/fiber pattern could be determined with a simple hand-held device (ocean optics spectrometer). In this way, a two-step protection strategy has been developed. In short, in addition to comparing the originality of the obtained random pattern with the recorded patterns in the database, an impossible and a two-step security technology was developed by reading the spectral information from the pattern. The biggest advantage of this technology is that security patterns can be created easily and quickly on high-scale different substrates and the verification method is based on simple and inexpensive systems. In this way, this technology developed has the potential for commercialization.

CHAPTER 5

CONCLUSION

Unlike traditional anticounterfeiting methods, we have developed complex and unrepeatable security labels that can be utilized in security printing and brand protection applications and systems in which their authenticity is checked simply and quickly. In this thesis, we created security labels/patterns created by nanoparticles that luminescent in the visible region and do not contain heavy metals with long-term optical stability. We synthesized water and solvent-based quantum dots that act as pigments in security labels/patterns developed for this purpose.

We synthesized colloidal monodisperse and high luminescent InP based nanoparticles with hot injection approach under an inert atmosphere. Reaction temperature, precursor type and concentration, surface agents were optimized to obtain colloidal quantum dots which have narrow full width (FWHM), high photoluminescence quantum efficiency (PL QE) and monodispersity at half maximum. Various analytical techniques have been used for both optical and structural characterization. Absorption and photoluminescence spectra were performed for optical characterization. X-ray powder diffraction (XRD), scanning electron microscopy with its x-ray energy dispersive spectroscopy detector (SEM-EDS), dynamic light scattering (DLS), fourier transform infrared spectroscopy (FTIR) were used to investigate the crystal structure and basic composition.

We synthesized water-dispersible carbon nanoparticles using a bottom-up method. Various analytical techniques for both optical and structural characterization have been used here as well. Absorption and photoluminescence spectra were made for optical characterization. To examine the basic composition and crystal structure, high-resolution transmission electron microscopy (HRTEM), X-ray photoelectron spectroscopy (XPS), fourier transform infrared spectroscopy (FTIR) were used.

We have formulated water-based carbon and solvent-based InP nanoparticles to be used in screen printing and inkjet printing, which are known methods, and security inks that emit different colors and developed security labels against counterfeiting. We also checked the authenticity of these labels with the help of a simple device. We formulated a solvent-based colloidal nanoparticle (colloidal quantum dot) based security

ink for the screen printing technique. We mixed In(Zn)P/ZnS/DDT colloidal nanoparticles with a commercial printing varnish to formulate the security ink. We printed security patterns on various substrates including paper, polymer and glass by applying the screen printing technique with inks. We evaluated the originality of the printed security patterns using a commercial fiber optic-based spectrometer (Ocean Optics spectrometer) and a handy hand-held optical device called the Quantag sensor developed by Quantag Nanotechnologies. Thus, we developed a verification method that is invisible to the naked human eye but can be distinguished by a simple detection device.

We developed a low-cost ink formulation for inkjet printer using water-based and very high optical stability carbon particles to authenticate valuable documents. We determined the optimum amount of particles in the ink by experimenting with different particle concentrations to create security patterns that cannot be detected in daylight. In addition, we paid attention to the surface tension and viscosity values of ink in the literature so that the developed ink formulations can be printed with a simple printer that is used commercially. By checking the developed security labels with a fiber optic sensor belonging to Quantag Nanotechnologies, we presented a security system that counterfeiters cannot easily imitate.

For the first time in the literature, we have obtained luminescent random droplet and droplet/fiber patterns on different surfaces with a simple and fast method such as electrospinning for use against counterfeiting. We have created unique security codes with non-repeatable patterns and their fluorescent colors resulting from the random positioning of fibers and droplets, thereby creating an important strategy to combat counterfeiting. We used carbon-based and indium-based quantum dots because of their unique fluorescent properties to create luminescent and non-repeatable security labels. We dispersed both carbon and indium particles homogeneously in low amounts in suitable polymer solutions and created random droplet and droplet/fiber patterns on different surfaces (metal, polymer and paper) using the simple and cost-effective electrospinning technique. Due to the low particle amount, we have obtained extremely bright patterns, which are not visible in daylight, are visible only under UV light. In this way, we have created unique security patterns that cannot be detected in daylight but can be detected under UV light with a method that allows simple and widespread production. To check the authenticity of the original security codes created; instead of expensive and hard-to-reach devices such as SEM, TEM, and fluorescence microscopy, we used a

simple smartphone microscope and created a database in which original patterns were recorded. We determined the originality of the obtained random pattern by comparing it with the patterns recorded in the database. In addition, we determined the spectral information of the particle from the obtained droplet/fiber model with a simple hand-held device (ocean optical spectrometer). Thus, by reading spectral information from the pattern, we determined the spectral signature of the particle and created a second security phase. In this way, we have developed a two-stage protection strategy against counterfeiting, which is impossible to imitate and surpass. In addition, the security patterns we recommend can be created quickly on high-scale different surfaces and the verification method is based on simple and inexpensive systems. This shows how high the commercialization capacity of this method we propose is.

REFERENCES

1.   Gong, G.; Xie, S. W.; Song, Y.; Tang, H. H.; Xu, J. X.; Zhang, C. F.; Xu, L. J., Synthesis of Lanthanide-Ion-Doped NaYF4 RGB Up-Conversion Nanoparticles for Anti-Counterfeiting Application. *J. Nanosci. Nanotechnol.* **2018,** *18* (12), 8207-8215.

2.   Kumar, P.; Nagpal, K.; Gupta, B. K., Unclonable Security Codes Designed from Multicolor Luminescent Lanthanide-Doped Y2O3 Nanorods for Anticounterfeiting. *ACS Appl Mater Interfaces* **2017,** *9* (16), 14301-14308.

3.   Yao, W.; Tian, Q.; Liu, J.; Wu, Z.; Cui, S.; Ding, J.; Dai, Z.; Wu, W., Large-scale synthesis and screen printing of upconversion hexagonal-phase NaYF4:Yb3+,Tm3+/Er3+/Eu3+ plates for security applications. *Journal of Materials Chemistry C* **2016,** *4* (26), 6327-6335.

4.   Choi, S. H.; Yang, B.; Cheung, H. H.; Yang, Y. X., RFID tag data processing in manufacturing for track-and-trace anti-counterfeiting. *Comput. Ind.* **2015,** *68*, 148-161.

5.   Lehtonen, M. O.; Michahelles, F.; Fleisch, E., Trust and Security in RFID-Based Product Authentication Systems. *IEEE Syst. J.* **2007,** *1* (2), 129-144.

6.   Peng, H.; Bi, S.; Ni, M.; Xie, X.; Liao, Y.; Zhou, X.; Xue, Z.; Zhu, J.; Wei, Y.; Bowman, C. N.; Mai, Y. W., Monochromatic visible light "photoinitibitor": Janus-faced initiation and inhibition for storage of colored 3D images. *J Am Chem Soc* **2014,** *136* (25), 8855-8.

7.   J. Dittmann, L. C. F., and C. Vielhauer, Hologram Watermarks for Document Authentications. *Proc. Int. Conf. Inf. Technol., Coding Comput* **2001**, 60-64.

8.   Wang, Y.; Xu, S.; Lin, J., Nuclear track anti-counterfeiting technique and its application in secure ID. *Radiation Measurements* **2008,** *43*, S659-S661.

9.   Alzahrani, N.; Bulusu, N., Securing Pharmaceutical and High-Value Products against Tag Reapplication Attacks Using NFC Tags. In *2016 IEEE International Conference on Smart Computing (SMARTCOMP)*, 2016; pp 1-6.

10.   Hyunmoon Nam, K. S., Dogyeong Ha, and Taesung Kim, Inkjet-printing-based structural coloring for anti-counterfeit applications. In *Transducers*, 2015; pp 1417-1420.

11.   Yen, C. W.; de Puig, H.; Tam, J. O.; Gomez-Marquez, J.; Bosch, I.; Hamad-Schifferli, K.; Gehrke, L., Multicolored silver nanoparticles for multiplexed disease diagnostics: distinguishing dengue, yellow fever, and Ebola viruses. *Lab Chip* **2015,** *15* (7), 1638-41.

12.   Scheuer, J.; Yifat, Y., Holography: Metasurfaces make it practical. *Nat Nanotechnol* **2015,** *10* (4), 296-8.

13.   Xie, R. S.; Hong, C. Q.; Zhu, S. Z.; Tao, D. P., Anti-counterfeiting digital watermarking algorithm for printed QR barcode. *Neurocomputing* **2015,** *167*, 625-635.

14.   Bae, H. J.; Bae, S.; Park, C.; Han, S.; Kim, J.; Kim, L. N.; Kim, K.; Song, S. H.; Park, W.; Kwon, S., Biomimetic Microfingerprints for Anti-Counterfeiting Strategies. *Advanced Materials* **2015,** *27* (12), 2083-2089.

15.   Li, L., Technology designed to combat fakes in the global supply chain. *Business Horizons* **2013,** *56* (2), 167-177.

16.   Gooch, J.; Daniel, B.; Abbate, V.; Frascione, N., Taggant materials in forensic science: A review. *TrAC Trends in Analytical Chemistry* **2016,** *83*, 49-54.

17.   Platel, R.; Palleau, E.; Vaure, L.; Raffy, S.; Guérin, F.; Nayral, C.; Delpech, F.; Ressier, L., Micropatterning of Adhesive Epoxy with Embedded Colloidal Quantum Dots for Authentication and Tracing. *ACS Applied Nano Materials* **2021**.

18.	Ju, L.; Gao, W. B.; Zhang, J. Y.; Qin, T. Y.; Du, Z.; Sheng, L.; Zhang, S. X. A., A new absorption/fluorescence dual-mode hydrochromic dye for water-jet printing and anti-counterfeiting applications. *Journal of Materials Chemistry C* **2020,** *8* (8), 2806-2811.

19.	Zhang, C.; Wang, B.; Li, W.; Huang, S.; Kong, L.; Li, Z.; Li, L., Conversion of invisible metal-organic frameworks to luminescent perovskite nanocrystals for confidential information encryption and decryption. *Nat Commun* **2017,** *8* (1), 1138.

20.	Kumar, A.; Tiwari, S. P.; Swart, H. C.; da Silva, J., Infrared interceded YF3: Er3+/Yb3+ upconversion phosphor for crime scene and anti-counterfeiting applications. *Opt. Mater.* **2019,** *92*, 347-351.

21.	Park, S. J.; Park, J. Y.; Chung, J. W.; Yang, H. K.; Moon, B. K.; Yi, S. S., Color tunable carbon quantum dots from wasted paper by different solvents for anti-counterfeiting and fluorescent flexible film. *Chem. Eng. J.* **2020,** *383*, 8.

22.	Nguyen, T. P.; Nguyen, T. P.; Lam, Q. V.; Vu, T. B., Effects of structure on photoluminescence characteristics of Mn2+-doped ZnS quantum dots for anti-counterfeiting ink application. *Solid State Sci.* **2020,** *101*, 9.

23.	Pham, H. H.; Gourevich, I.; Jonkman, J. E. N.; Kumacheva, E., Polymer nanostructured material for the recording of biometric features. *J. Mater. Chem.* **2007,** *17* (6), 523-526.

24.	Pham, H. H.; Gourevich, I.; Oh, J. K.; Jonkman, J. E. N.; Kumacheva, E., A Multidye Nanostructured Material for Optical Data Storage and Security Data Encryption. *Advanced Materials* **2004,** *16* (6), 516-520.

25.	Saraf, M.; Kumar, P.; Kedawat, G.; Dwivedi, J.; Vithayathil, S. A.; Jaiswal, N.; Kaipparettu, B. A.; Gupta, B. K., Probing highly luminescent europium-doped lanthanum orthophosphate nanorods for strategic applications. *Inorg Chem* **2015,** *54* (6), 2616-25.

26.	Gupta, B. K.; Haranath, D.; Saini, S.; Singh, V. N.; Shanker, V., Synthesis and characterization of ultra-fine Y2O3:Eu3+ nanophosphors for luminescent security ink applications. *Nanotechnology* **2010,** *21* (5), 055607.

27.	Wang, M.; Duong, B.; Fenniri, H.; Su, M., Nanomaterial-based barcodes. *Nanoscale* **2015,** *7* (26), 11240-7.

28.	Zhang, C.; Li, X.; Liu, M. L.; Li, T. T.; Yu, T. X.; Li, Y.; Zhang, J.; Asiri, A. M.; Alamry, K. A.; Zhang, K., Dual-wavelength stimuli and green emission response in lanthanide doped nanoparticles for anti-counterfeiting. *Journal of Alloys and Compounds* **2020,** *836*, 7.

29.	Huang, H.; Chen, J. K.; Liu, Y. T.; Lin, J. D.; Wang, S. X.; Huang, F.; Chen, D. Q., Lanthanide-Doped Core@Multishell Nanoarchitectures: Multimodal Excitable Upconverting/Downshifting Luminescence and High-Level Anti-Counterfeiting. *Small* **2020,** *16* (19), 12.

30.	Zhou, M.; Chang, S.; Grover, C., Cryptography based on the absorption/emission features of multicolor semiconductor nanocrystal quantum dots. *Opt Express* **2004,** *12* (13), 2925-31.

31.	Jamieson, T.; Bakhshi, R.; Petrova, D.; Pocock, R.; Imani, M.; Seifalian, A. M., Biological applications of quantum dots. *Biomaterials* **2007,** *28* (31), 4717-32.

32.	Kagan, C. B. M. a. C. R., SYNTHESIS AND CHARACTERIZATION OF MONODISPERSE NANOCRYSTALS AND CLOSE-PACKED NANOCRYSTAL ASSEMBLIES. *Annu. Rev. Mater. Sci* **2000,** (30), 545–610.

33.	Bera, D.; Qian, L.; Tseng, T.-K.; Holloway, P. H., Quantum Dots and Their Multimodal Applications: A Review. *Materials* **2010,** *3* (4), 2260-2345.

34.   Zhou, L.; Zhao, A.; Wang, Z.; Chen, Z.; Ren, J.; Qu, X., Ionic liquid-assisted synthesis of multicolor luminescent silica nanodots and their use as anticounterfeiting ink. *ACS Appl Mater Interfaces* **2015,** *7* (4), 2905-11.

35.   Wang, S. X.; Lin, J. D.; Li, X. Y.; Chen, J. K.; Yang, C. B.; Huang, P.; Cheng, Y.; Chen, D. Q., Glass-limited Yb/Er:NaLuF4 nanocrystals: reversible hexagonal-to-cubic phase transition and anti-counterfeiting. *Journal of Materials Chemistry C* **2020,** *8* (45), 16151-16159.

36.   Song, B.; Wang, H. Y.; Zhong, Y. L.; Chu, B. B.; Su, Y. Y.; He, Y., Fluorescent and magnetic anti-counterfeiting realized by biocompatible multifunctional silicon nanoshuttle-based security ink. *Nanoscale* **2018,** *10* (4), 1617-1621.

37.   Trenfield, S. J.; Tan, H. X.; Awad, A.; Buanz, A.; Gaisford, S.; Basit, A. W.; Goyanes, A., Track-and-trace: Novel anti-counterfeit measures for 3D printed personalized drug products using smart material inks. *Int. J. Pharm.* **2019,** *567*, 7.

38.   Tan, H. H.; Gong, G.; Xie, S. W.; Song, Y.; Zhang, C. F.; Li, N.; Zhang, D.; Xu, L. J.; Xu, J. X.; Zheng, J., Upconversion Nanoparticles@Carbon Dots@Meso-SiO2 Sandwiched Core-Shell Nanohybrids with Tunable Dual-Mode Luminescence for 3D Anti-Counterfeiting Barcodes. *Langmuir* **2019,** *35* (35), 11503-11511.

39.   Arppe, R.; Sørensen, T. J., Physical unclonable functions generated through chemical methods for anti-counterfeiting. *Nature Reviews Chemistry* **2017,** *1* (4).

40.   Pappu, R.; Recht, B.; Taylor, J.; Gershenfeld, N., Physical one-way functions. *Science* **2002,** *297* (5589), 2026-30.

41.   Lee, J.; Bisso, P. W.; Srinivas, R. L.; Kim, J. J.; Swiston, A. J.; Doyle, P. S., Universal process-inert encoding architecture for polymer microparticles. *Nat Mater* **2014,** *13* (5), 524-9.

42.   Ivanova, O.; Elliott, A.; Campbell, T.; Williams, C. B., Unclonable security features for additive manufacturing. *Additive Manufacturing* **2014,** *1-4*, 24-31.

43.   Johansen, S.; Radziwon, M.; Tavares, L.; Rubahn, H. G., Nanotag luminescent fingerprint anti-counterfeiting technology. *Nanoscale Res Lett* **2012,** *7* (1), 262.

44.   Radziwon, M.; Johansen, S.; Rubahn, H.-G., Anti-counterfeit Solution from Organic Semiconductor. *Procedia Engineering* **2014,** *69*, 1405-1409.

45.   Liu, Y.; Zheng, Y.; Zhu, Y.; Ma, F.; Zheng, X.; Yang, K.; Zheng, X.; Xu, Z.; Ju, S.; Zheng, Y.; Guo, T.; Qian, L.; Li, F., Unclonable Perovskite Fluorescent Dots with Fingerprint Pattern for Multilevel Anticounterfeiting. *ACS Appl Mater Interfaces* **2020,** *12* (35), 39649-39656.

46.   Zhang, Y. J.; Luan, Z. C.; Zhang, X. W.; Shu, J. P.; Wang, P. J., PbS Quantum Dots Based on Physically Unclonable Function for Ultra High-Density Key Generation. *J. Electron. Mater.* **2019,** *48* (12), 7603-7607.

47.   Zheng, Y.; Jiang, C.; Ng, S. H.; Lu, Y.; Han, F.; Bach, U.; Gooding, J. J., Unclonable Plasmonic Security Labels Achieved by Shadow-Mask-Lithography-Assisted Self-Assembly. *Adv Mater* **2016,** *28* (12), 2330-6.

48.   Han, F.; Liu, Y.; Li, F.; Lu, Y.; Cheng, H.; Lin, Y.; Zhao, T.; Ng, S. H.; Bach, U.; Zheng, Y., Self-assembly of coordination polymers on plasmonic surfaces for computer vision decodable, unclonable and colorful security labels. *Journal of Materials Chemistry C* **2019,** *7* (42), 13040-13046.

49.   Cowburn, R., Laser surface authentication – reading Nature's own security code. *Contemporary Physics* **2008,** *49* (5), 331-342.

50.   Smith, A. F.; Patton, P.; Skrabalak, S. E., Plasmonic Nanoparticles as a Physically Unclonable Function for Responsive Anti-Counterfeit Nanofingerprints. *Advanced Functional Materials* **2016,** *26* (9), 1315-1321.

51.   Carro-Temboury, M. A., R; Vosch, T; Sorensen, TJ, An optical authentication system based on imaging of excitation-selected lanthanide luminescence. *Applied Sciences and Engineering* **2018,** *4*.

52.   Arppe-Tabbara, R.; Tabbara, M.; Sorensen, T. J., Versatile and Validated Optical Authentication System Based on Physical Unclonable Functions. *ACS Appl Mater Interfaces* **2019,** *11* (6), 6475-6482.

53.   Leem, J. W.; Kim, M. S.; Choi, S. H.; Kim, S. R.; Kim, S. W.; Song, Y. M.; Young, R. J.; Kim, Y. L., Edible unclonable functions. *Nat. Commun.* **2020,** *11* (1), 11.

54.   Meruga, J. M.; Cross, W. M.; Stanley May, P.; Luu, Q.; Crawford, G. A.; Kellar, J. J., Security printing of covert quick response codes using upconverting nanoparticle inks. *Nanotechnology* **2012,** *23* (39), 395201.

55.   Kim, J.; Yun, J. M.; Jung, J.; Song, H.; Kim, J. B.; Ihee, H., Anti-counterfeit nanoscale fingerprints based on randomly distributed nanowires. *Nanotechnology* **2014,** *25* (15), 7.

56.   Liu, Y.; Han, F.; Li, F.; Zhao, Y.; Chen, M.; Xu, Z.; Zheng, X.; Hu, H.; Yao, J.; Guo, T.; Lin, W.; Zheng, Y.; You, B.; Liu, P.; Li, Y.; Qian, L., Inkjet-printed unclonable quantum dot fluorescent anti-counterfeiting labels with artificial intelligence authentication. *Nat Commun* **2019,** *10* (1), 2409.

57.   Li, M. X.; Yao, W. J.; Liu, J.; Tian, Q. Y.; Liu, L.; Ding, J.; Xue, Q. W.; Lu, Q.; Wu, W., Facile synthesis and screen printing of dual-mode luminescent NaYF4:Er,Yb (Tm)/carbon dots for anti-counterfeiting applications. *Journal of Materials Chemistry C* **2017,** *5* (26), 6512-6520.

58.   Han, S.; Bae, H. J.; Kim, J.; Shin, S.; Choi, S. E.; Lee, S. H.; Kwon, S.; Park, W., Lithographically Encoded Polymer Microtaggant Using High-Capacity and Error-Correctable QR Code for Anti-Counterfeiting of Drugs. *Advanced Materials* **2012,** *24* (44), 5924-+.

59.   Goh, X. M.; Zheng, Y.; Tan, S. J.; Zhang, L.; Kumar, K.; Qiu, C. W.; Yang, J. K., Three-dimensional plasmonic stereoscopic prints in full colour. *Nat Commun* **2014,** *5*, 5361.

60.   Gao, Z.; Han, Y. F.; Wang, F., Cooperative supramolecular polymers with anthracene. endoperoxide photo-switching for fluorescent anti-counterfeiting. *Nat. Commun.* **2018,** *9*, 9.

61.   Braeckmans, K.; De Smedt, S. C.; Roelant, C.; Leblans, M.; Pauwels, R.; Demeester, J., Encoding microcarriers by spatial selective photobleaching. *Nat Mater* **2003,** *2* (3), 169-73.

62.   Huang, C.; Lucas, B.; Vervaet, C.; Braeckmans, K.; Van Calenbergh, S.; Karalic, I.; Vandewoestyne, M.; Deforce, D.; Demeester, J.; De Smedt, S. C., Unbreakable codes in electrospun fibers: digitally encoded polymers to stop medicine counterfeiting. *Adv Mater* **2010,** *22* (24), 2657-62.

63.   Gu, Y. Q.; He, C.; Zhang, Y. Q.; Lin, L.; Thackray, B. D.; Ye, J., Gap-enhanced Raman tags for physically unclonable anticounterfeiting labels. *Nat. Commun.* **2020,** *11* (1), 13.

64.   Zhang, Y.; Huang, R.; Li, H. L.; Lin, Z. X.; Hou, D. J.; Guo, Y. Q.; Song, J.; Song, C.; Lin, Z. W.; Zhang, W. X.; Wang, J.; Chu, P. K.; Zhu, C., Triple-Mode Emissions with Invisible Near-Infrared After-Glow from Cr3+-Doped Zinc Aluminum Germanium Nanoparticles for Advanced Anti-Counterfeiting Applications. *Small* **2020,** *16* (35), 7.

65.   Areno, M. A. System and method for providing cryptographic key information with physically unclonable function circuitry 9,208,355, 2015.

66.	Eisenbarth, D.; Stoll, P.; Klahn, C.; Heinis, T. B.; Meboldt, M.; Wegener, K., Unique coding for authentication and anti-counterfeiting by controlled and random process variation in L-PBF and L-DED. *Additive Manufacturing* **2020,** *35*, 9.

67.	Zeng, Z. C.; Huang, B. L.; Wang, X.; Lu, L.; Lu, Q. Y.; Sun, M. Z.; Wu, T.; Ma, T. F.; Xu, J.; Xu, Y. S.; Wang, S.; Du, Y. P.; Yan, C. H., Multimodal Luminescent Yb3+/Er3+/Bi3+-Doped Perovskite Single Crystals for X-ray Detection and Anti-Counterfeiting. *Advanced Materials* **2020,** *32* (43), 10.

68.	Zhou, Y. S.; Zhao, G.; Bian, J. M.; Tian, X. L.; Cheng, X. J.; Wang, H.; Chen, H. Y., Multiplexed SERS Barcodes for Anti-Counterfeiting. *ACS Appl. Mater. Interfaces* **2020,** *12* (25), 28532-28538.

69.	Tang, J.; Mu, Y. X.; Du, P.; Luo, L. H., Luminescence modulation of the Eu3+ doped Srn+1SnnO3n+1 (n=1, 2, 5, infinity) ceramics based on photochromism and its application in anti-counterfeiting technology. *Ceram. Int.* **2020,** *46* (8), 11962-11969.

70.	Kumar, P.; Singh, S.; Gupta, B. K., Future prospects of luminescent nanomaterial based security inks: from synthesis to anti-counterfeiting applications. *Nanoscale* **2016,** *8* (30), 14297-340.

71.	Fu, X. J.; Li, G. Q.; Cai, S. Y.; Yang, H.; Lin, K.; He, M.; Wen, J. W.; Li, H. B.; Xiong, Y. B.; Chen, D. Z.; Liu, X. H., Color-switchable hybrid dots/hydroxyethyl cellulose ink for anti-counterfeiting applications. *Carbohydr. Polym.* **2021,** *251*, 9.

72.	You, M. L.; Zhong, J. J.; Hong, Y.; Duan, Z. F.; Lin, M.; Xu, F., Inkjet printing of upconversion nanoparticles for anti-counterfeit applications. *Nanoscale* **2015,** *7* (10), 4423-4431.

73.	Sangeetha, N. M.; Moutet, P.; Lagarde, D.; Sallen, G.; Urbaszek, B.; Marie, X.; Viau, G.; Ressier, L., 3D assembly of upconverting NaYF4 nanocrystals by AFM nanoxerography: creation of anti-counterfeiting microtags. *Nanoscale* **2013,** *5* (20), 9587-9592.

74.	Lu, Z.; Liu, Y.; Hu, W.; Lou, X. W.; Li, C. M., Rewritable multicolor fluorescent patterns for multistate memory devices with high data storage capacity. *Chem Commun (Camb)* **2011,** *47* (34), 9609-11.

75.	Bao, B.; Li, M.; Li, Y.; Jiang, J.; Gu, Z.; Zhang, X.; Jiang, L.; Song, Y., Patterning fluorescent quantum dot nanocomposites by reactive inkjet printing. *Small* **2015,** *11* (14), 1649-54.

76.	Wang, F.; Xie, Z.; Zhang, B.; Liu, Y.; Yang, W.; Liu, C. Y., Down- and up-conversion luminescent carbon dot fluid: inkjet printing and gel glass fabrication. *Nanoscale* **2014,** *6* (7), 3818-23.

77.	Wen, X.; Shi, L.; Wen, G.; Li, Y.; Dong, C.; Yang, J.; Shuang, S., Green synthesis of carbon nanodots from cotton for multicolor imaging, patterning, and sensing. *Sensors and Actuators B: Chemical* **2015,** *221*, 769-776.

78.	Campos-Cuerva, C.; Zieba, M.; Sebastian, V.; Martinez, G.; Sese, J.; Irusta, S.; Contamina, V.; Arruebo, M.; Santamaria, J., Screen-printed nanoparticles as anti-counterfeiting tags. *Nanotechnology* **2016,** *27* (9), 14.

79.	Singh, M.; Haverinen, H. M.; Dhagat, P.; Jabbour, G. E., Inkjet printing-process and its applications. *Adv Mater* **2010,** *22* (6), 673-85.

80.	Baker, S. N.; Baker, G. A., Luminescent carbon nanodots: emergent nanolights. *Angew Chem Int Ed Engl* **2010,** *49* (38), 6726-44.

81.	Hu, Y. W. a. A., Carbon quantum dots: synthesis, properties and applications. *J. Mater. Chem. C,* **2014**, 6921.

82.	Ashutosh Tiwari, H. K. P. a. A. P. F. T., *Advanced bioelectronic materials*. Scrivener Publishing LLC: 2015.

83.   Zhu, S.; Meng, Q.; Wang, L.; Zhang, J.; Song, Y.; Jin, H.; Zhang, K.; Sun, H.; Wang, H.; Yang, B., Highly photoluminescent carbon dots for multicolor patterning, sensors, and bioimaging. *Angew Chem Int Ed Engl* **2013,** *52* (14), 3953-7.

84.   Liu, W.; Li, C.; Ren, Y.; Sun, X.; Pan, W.; Li, Y.; Wang, J.; Wang, W., Carbon dots: surface engineering and applications. *Journal of Materials Chemistry B* **2016,** *4* (35), 5772-5788.

85.   Wang, Y.; Hu, A., Carbon quantum dots: synthesis, properties and applications. *Journal of Materials Chemistry C* **2014,** *2* (34).

86.   Jiang, H.; Chen, F.; Lagally, M. G.; Denes, F. S., New strategy for synthesis and functionalization of carbon nanoparticles. *Langmuir* **2010,** *26* (3), 1991-5.

87.   Sun, Y. P.; Zhou, B.; Lin, Y.; Wang, W.; Fernando, K. A.; Pathak, P.; Meziani, M. J.; Harruff, B. A.; Wang, X.; Wang, H.; Luo, P. G.; Yang, H.; Kose, M. E.; Chen, B.; Veca, L. M.; Xie, S. Y., Quantum-sized carbon dots for bright and colorful photoluminescence. *J Am Chem Soc* **2006,** *128* (24), 7756-7.

88.   Zheng, L.; Chi, Y.; Dong, Y.; Lin, J.; Wang, B., Electrochemiluminescence of water-soluble carbon nanocrystals released electrochemically from graphite. *J Am Chem Soc* **2009,** *131* (13), 4564-5.

89.   Zhao, Q. L.; Zhang, Z. L.; Huang, B. H.; Peng, J.; Zhang, M.; Pang, D. W., Facile preparation of low cytotoxicity fluorescent carbon nanocrystals by electrooxidation of graphite. *Chem Commun (Camb)* **2008,** (41), 5116-8.

90.   Zhou, J.; Booker, C.; Li, R.; Zhou, X.; Sham, T. K.; Sun, X.; Ding, Z., An electrochemical avenue to blue luminescent nanocrystals from multiwalled carbon nanotubes (MWCNTs). *J Am Chem Soc* **2007,** *129* (4), 744-5.

91.   Guo, X.; Wang, C. F.; Yu, Z. Y.; Chen, L.; Chen, S., Facile access to versatile fluorescent carbon dots toward light-emitting diodes. *Chem Commun (Camb)* **2012,** *48* (21), 2692-4.

92.   Liu, H.; Li, Z.; Sun, Y.; Geng, X.; Hu, Y.; Meng, H.; Ge, J.; Qu, L., Synthesis of Luminescent Carbon Dots with Ultrahigh Quantum Yield and Inherent Folate Receptor-Positive Cancer Cell Targetability. *Sci Rep* **2018,** *8* (1), 1086.

93.   Zhu, H.; Wang, X.; Li, Y.; Wang, Z.; Yang, F.; Yang, X., Microwave synthesis of fluorescent carbon nanoparticles with electrochemiluminescence properties. *Chem Commun (Camb)* **2009,** (34), 5118-20.

94.   Khan, W. U.; Wang, D.; Zhang, W.; Tang, Z.; Ma, X.; Ding, X.; Du, S.; Wang, Y., High Quantum Yield Green-Emitting Carbon Dots for Fe (III) Detection, Biocompatible Fluorescent Ink and Cellular Imaging. *Scientific reports* **2017,** *7* (1), 14866.

95.   Guner, T.; Yuce, H.; Tascioglu, D.; Simsek, E.; Savaci, U.; Genc, A.; Turan, S.; Demir, M. M., Optimization and performance of nitrogen-doped carbon dots as a color conversion layer for white-LED applications. *Beilstein J Nanotechnol* **2019,** *10*, 2004-2013.

96.   Chaffins Jr., S., Dekam, Kevin P., Bhatt, Jayprakash, Deardurff, Larrie, Ruud, Cory J., Thornberry, Matthew Pigment-based inkjet inks. 2017.

97.   Hauser, H., Reiniger, Karin Aqueous printing ink compositions for ink jet printing. 1992.

98.   Siddique, A. B.; Pramanick, A. K.; Chatterjee, S.; Ray, M., Amorphous Carbon Dots and their Remarkable Ability to Detect 2,4,6-Trinitrophenol. *Sci Rep* **2018,** *8* (1), 9770.

99.   Khan, W. U.; Wang, D.; Zhang, W.; Tang, Z.; Ma, X.; Ding, X.; Du, S.; Wang, Y., High Quantum Yield Green-Emitting Carbon Dots for Fe(capital I, Ukrainiancapital

I, Ukrainiancapital I, Ukrainian) Detection, Biocompatible Fluorescent Ink and Cellular Imaging. *Sci Rep* **2017,** *7* (1), 14866.

100.   Feng, Z.; Li, Z.; Zhang, X.; Shi, Y.; Zhou, N., Nitrogen-Doped Carbon Quantum Dots as Fluorescent Probes for Sensitive and Selective Detection of Nitrite. *Molecules* **2017,** *22* (12).

101.   Niu, J.; Gao, H.; Wang, L.; Xin, S.; Zhang, G.; Wang, Q.; Guo, L.; Liu, W.; Gao, X.; Wang, Y., Facile synthesis and optical properties of nitrogen-doped carbon dots. *New Journal of Chemistry* **2014,** *38* (4).

102.   Fu, M.; Ehrat, F.; Wang, Y.; Milowska, K. Z.; Reckmeier, C.; Rogach, A. L.; Stolarczyk, J. K.; Urban, A. S.; Feldmann, J., Carbon Dots: A Unique Fluorescent Cocktail of Polycyclic Aromatic Hydrocarbons. *Nano Lett* **2015,** *15* (9), 6030-5.

103.   Xie, S. W.; Tong, C.; Tan, H. H.; Li, N.; Gong, L.; Xu, J. X.; Xu, L. J.; Zhang, C. F., Hydrothermal synthesis and inkjet printing of hexagonal-phase NaYF4: Ln(3+) upconversion hollow microtubes for smart anti-counterfeiting encryption. *Mat. Chem. Front.* **2018,** *2* (11), 1997-2005.

104.   Song, Y.; Gong, G.; Du, J. J.; Xie, S. W.; Ouyang, M.; Feng, Y. H.; Xu, J. X.; Xu, L. J., Synthesis and Inkjet Printing of NaYF4:Ln(3+)@NaYF4 Core-Shell Nanoparticles with Enhanced Upconversion Fluorescence for Anti-Counterfeiting Applications. *J. Nanosci. Nanotechnol.* **2020,** *20* (3), 1511-1519.

105.   Lin, Z.; Wang, H.; Yu, M. L.; Guo, X.; Zhang, C. H.; Deng, H. T.; Zhang, P. S.; Chen, S.; Zeng, R. J.; Cui, J. X.; Chen, J., Photoswitchable ultrahigh-brightness red fluorescent polymeric nanoparticles for information encryption, anti-counterfeiting and bioimaging. *Journal of Materials Chemistry C* **2019,** *7* (37), 11515-11521.

106.   Laurén, S. Surface tension of water – Why is it so high?

107.   Magdassi, S., Ink Requirements and Formulations Guidelines. In *The Chemistry of Inkjet Inks*, Magdassi, I. S., Ed. 2010; pp 19-41.

108.   Andersson, P. Development of an Inkjet Ink to Produce Touch Sensing Surfaces. Luleå University of Technology, 2010.

109.   Yang, P.; Zhang, L.; Kang, D. J.; Strahl, R.; Kraus, T., High-Resolution Inkjet Printing of Quantum Dot Light-Emitting Microdiode Arrays. *Adv. Opt. Mater.* **2019,** *8* (1).

110.   Xie, S. W.; Gong, G.; Song, Y.; Tan, H. H.; Zhang, C. F.; Li, N.; Zhang, Y. X.; Xu, L. J.; Xu, J. X.; Zheng, J., Design of novel lanthanide-doped core-shell nanocrystals with dual up-conversion and down-conversion luminescence for anti-counterfeiting printing. *Dalton Trans.* **2019,** *48* (20), 6971-6983.

111.   Urey, H. A., Osman Vedat; Heves, Emre; Civitci, Fehmi; Can, Basarbatu A Fluorescent substance detection system. WO 2016/010494, 2016.

112.   Jung, J. Y.; Kim, J.; Shim, Y. S.; Hwang, D.; Son, C. S., Structure and Photoluminescence Properties of Rare-Earth (Dy3+, Tb3+, Sm3+)-Doped BaWO4 Phosphors Synthesized via Co-Precipitation for Anti-Counterfeiting. *Materials* **2020,** *13* (18), 12.

113.   Moon, T. O.; Jung, J. Y.; Cho, S., Synthesis and Properties of SrMoO4 Phosphors Doped with Various Rare Earth Ions for Anti-Counterfeiting Applications. *Kor. J. Mater. Res.* **2020,** *30* (8), 406-412.

114.   You, M. L.; Lin, M.; Wang, S. R.; Wang, X. M.; Zhang, G.; Hong, Y.; Dong, Y. Q.; Jin, G. R.; Xu, F., Three-dimensional quick response code based on inkjet printing of upconversion fluorescent nanoparticles for drug anti-counterfeiting. *Nanoscale* **2016,** *8* (19), 10096-10104.

115.   Zhang, J. S.; Ge, M. Q., Effects of transparent inorganic pigment on spectral properties of spectrum-fingerprint anti-counterfeiting fiber containing rare earths. *J. Rare Earths* **2012,** *30* (9), 952-957.

116.   Chen, L.; Zhang, Y.; Luo, A. Q.; Liu, F. Y.; Jiang, Y.; Hu, Q. Z.; Chen, S. F.; Liu, R. S., The temperature-sensitive luminescence of (Y,Gd)VO4:Bi3+,Eu3+ and its application for stealth anti-counterfeiting. *Phys. Status Solidi-Rapid Res. Lett.* **2012,** *6* (7), 321-323.

117.   Cheng, K.; Qi, R.; Lan, S.; Wang, H. Y.; Zheng, X. F.; Liu, C.; Jia, D. D.; Cao, L.; Wang, D. J., Tunable excitation-dependent-fluorescence of carbon dots: Fingerprint curves for super anti-counterfeiting. *Dyes Pigment.* **2020,** *174*, 10.

118.   Fatahi, Z.; Esfandiari, N.; Ranjbar, Z., A New Anti-counterfeiting Feature Relying on Invisible Non-toxic Fluorescent Carbon Dots. *J. Anal. Test.* **2020,** *4* (4), 307-315.

119.   Jiao, L. Y.; Zhang, M. N.; Li, H. B., Preparation of 1, 3, 6, 8-Pyrenesulfonic Acid Tetrasodium Salt Dye-Doped Silica Nanoparticles and Their Application in Water-Based Anti-Counterfeit Ink. *Materials* **2020,** *13* (18), 13.

120.   Liu, Y.; Han, F.; Li, F. S.; Zhao, Y.; Chen, M. S.; Xu, Z. W.; Zheng, X.; Hu, H. L.; Yao, J. M.; Guo, T. L.; Lin, W. Z.; Zheng, Y. H.; You, B. G.; Liu, P.; Li, Y.; Qian, L., Inkjet-printed unclonable quantum dot fluorescent anti-counterfeiting labels with artificial intelligence authentication. *Nat. Commun.* **2019,** *10*, 9.

121.   Platel, R.; Vaure, L.; Palleau, E.; Raffy, S.; Guerin, F.; Lagarde, D.; Cours, R.; Marcelot, C.; Warot-Fonrose, B.; Nayral, C.; Delpech, F.; Ressier, L., Synthesis of hybrid colloidal nanoparticles for a generic approach to 3D electrostatic directed assembly: Application to anti-counterfeiting. *J. Colloid Interface Sci.* **2021,** *582*, 1243-1250.

122.   Khan, S.; Lorenzelli, L.; Dahiya, R. S., Technologies for Printing Sensors and Electronics Over Large Flexible Substrates: A Review. *IEEE Sensors Journal* **2015,** *15* (6), 3164-3185.

123.   Cruz, S. M. F.; Rocha, L. A.; Viana, J. C., Printing Technologies on Flexible Substrates for Printed Electronics. In *Flexible Electronics*, 2018.

124.   Chen, L. Z.; Hu, B. A.; Zhang, J. Y.; Zhang, J. M.; Huang, S. T.; Ren, P.; Zou, Y.; Ding, F. Y.; Liu, X. H.; Li, H. B., A facile synthesis of 1,3,6,8-pyrenesulfonic acid tetrasodium salt as a hydrosoluble fluorescent ink for anti-counterfeiting applications. *Rsc Advances* **2019,** *9* (1), 476-481.

125.   Henriksen, M.; Miller, B.; Newmark, J.; Al-Kofahi, Y.; Holden, E., Laser scanning cytometry and its applications: a pioneering technology in the field of quantitative imaging cytometry. *Methods Cell Biol* **2011,** *102*, 161-205.

126.   Janke, E. M.; Williams, N. E.; She, C.; Zherebetskyy, D.; Hudson, M. H.; Wang, L.; Gosztola, D. J.; Schaller, R. D.; Lee, B.; Sun, C.; Engel, G. S.; Talapin, D. V., Origin of Broad Emission Spectra in InP Quantum Dots: Contributions from Structural and Electronic Disorder. *J Am Chem Soc* **2018,** *140* (46), 15791-15803.

127.   Brichkin, S. B., Synthesis and properties of colloidal indium phosphide quantum dots. *Colloid Journal* **2015,** *77* (4), 393-403.

128.   Mordvinova, N.; Vinokurov, A.; Kuznetsova, T.; Lebedev, O. I.; Dorofeev, S., Highly luminescent core-shell InP/ZnX (X = S, Se) quantum dots prepared via a phosphine synthetic route. *Dalton Trans* **2017,** *46* (4), 1297-1303.

129.   Xu, S.; Ziegler, J.; Nann, T., Rapid synthesis of highly luminescent InP and InP/ZnS nanocrystals. *Journal of Materials Chemistry* **2008,** *18* (23).

130.   Shen, W.; Tang, H.; Yang, X.; Cao, Z.; Cheng, T.; Wang, X.; Tan, Z.; You, J.; Deng, Z., Synthesis of highly fluorescent InP/ZnS small-core/thick-shell tetrahedral-shaped quantum dots for blue light-emitting diodes. *Journal of Materials Chemistry C* **2017,** *5* (32), 8243-8249.

131.   Yang, X.; Zhao, D.; Leck, K. S.; Tan, S. T.; Tang, Y. X.; Zhao, J.; Demir, H. V.; Sun, X. W., Full visible range covering InP/ZnS nanocrystals with high photometric performance and their application to white quantum dot light-emitting diodes. *Adv Mater* **2012,** *24* (30), 4180-5.

132.   Chang, J.; Waclawik, E. R., Colloidal semiconductor nanocrystals: controlled synthesis and surface chemistry in organic media. *RSC Adv.* **2014,** *4* (45), 23505-23527.

133.   <Synthesis of CdSe crystal using hot injection method.pdf>.

134.   Zhao, T. Designing Colloidal Nanomaterials For Electronic And Optoelectr oelectronic De onic Devices Thr vices Through Sur ough Surface Modification face Modification University of Pennsylvania, 2019.

135.   Tamang, S.; Lincheneau, C.; Hermans, Y.; Jeong, S.; Reiss, P., Chemistry of InP Nanocrystal Syntheses. *Chemistry of Materials* **2016,** *28* (8), 2491-2506.

136.   Du, F. F.; Guo, Z. H.; Cheng, Z.; Kremer, M.; Shuang, S. M.; Liu, Y.; Dong, C., Facile synthesis of ultrahigh fluorescence N,S-self-doped carbon nanodots and their multiple applications for H2S sensing, bioimaging in live cells and zebrafish, and anti-counterfeiting. *Nanoscale* **2020,** *12* (39), 20482-20490.

137.   Wang, Z. B.; Pei, P. X.; Bai, D. J.; Zhao, S. S.; Ma, X. Y.; Liu, W. S., Multicolor luminescence and triple-mode emission of simple CaTiO3:Pr3+,Er(3+)particles for advanced anti-counterfeiting. *Inorg. Chem. Front.* **2020,** *7* (13), 2506-2514.

138.   Zheng, W.; Sun, B. Y.; Li, Y. M.; Wang, R.; Xu, Y. L., Multicolor tunable luminescence and laser-sensitization induced upconversion enhancement in Ln-doped Gd2O3 crystals for anti-counterfeiting. *Mat. Chem. Front.* **2019,** *3* (11), 2403-2413.

139.   Jung, J. Y.; Song, B. K.; Kim, Y. K., Tunable color emission of transparent boron nitride nanophosphors towards anti-counterfeiting application. *Journal of Alloys and Compounds* **2019,** *791,* 81-86.

140.   Tessier, M. D.; Dupont, D.; De Nolf, K.; De Roo, J.; Hens, Z., Economic and Size-Tunable Synthesis of InP/ZnE (E = S, Se) Colloidal Quantum Dots. *Chemistry of Materials* **2015,** *27* (13), 4893-4898.

141.   Reiss, P.; Protiere, M.; Li, L., Core/Shell semiconductor nanocrystals. *Small* **2009,** *5* (2), 154-68.

142.   Thuy, U. T. D.; Thuy, P. T.; Liem, N. Q.; Li, L.; Reiss, P., Comparative photoluminescence study of close-packed and colloidal InP/ZnS quantum dots. *Applied Physics Letters* **2010,** *96* (7), 073102.

143.   Brown, R. P.; Gallagher, M. J.; Fairbrother, D. H.; Rosenzweig, Z., Synthesis and Degradation of Cadmium-Free InP and InPZn/ZnS Quantum Dots in Solution. *Langmuir* **2018,** *34* (46), 13924-13934.

144.   Haubold, S.; Haase, M.; Kornowski, A.; Weller, H., Strongly luminescent InP/ZnS core-shell nanoparticles. *Chemphyschem* **2001,** *2* (5), 331-4.

145.   Fang, X.; Zhai, T.; Gautam, U. K.; Li, L.; Wu, L.; Bando, Y.; Golberg, D., ZnS nanostructures: From synthesis to applications. *Progress in Materials Science* **2011,** *56* (2), 175-287.

146.   Zhang, J.; Gu, H., Growth of InZnP/ZnS core/shell quantum dots with wide-range and refined tunable photoluminescence wavelengths. *Dalton Transactions* **2020,** *49* (18), 6119-6126.

147. Jo, J.-H.; Jo, D.-Y.; Lee, S.-H.; Yoon, S.-Y.; Lim, H.-B.; Lee, B.-J.; Do, Y. R.; Yang, H., InP-Based Quantum Dots Having an InP Core, Composition-Gradient ZnSeS Inner Shell, and ZnS Outer Shell with Sharp, Bright Emissivity, and Blue Absorptivity for Display Devices. *ACS Applied Nano Materials* **2020,** *3* (2), 1972-1980.

148. Lim, J.; Bae, W. K.; Lee, D.; Nam, M. K.; Jung, J.; Lee, C.; Char, K.; Lee, S., InP@ZnSeS, Core@Composition Gradient Shell Quantum Dots with Enhanced Stability. *Chemistry of Materials* **2011,** *23* (20), 4459-4463.

149. Pietra, F.; De Trizio, L.; Hoekstra, A. W.; Renaud, N.; Prato, M.; Grozema, F. C.; Baesjou, P. J.; Koole, R.; Manna, L.; Houtepen, A. J., Tuning the Lattice Parameter of InxZnyP for Highly Luminescent Lattice-Matched Core/Shell Quantum Dots. *ACS Nano* **2016,** *10* (4), 4754-62.

150. Zhang, X.; Lee, H.; Kwon, J. H.; Kim, E. J.; Park, J., Low-Concentration Indium Doping in Solution-Processed Zinc Oxide Films for Thin-Film Transistors. *Materials (Basel)* **2017,** *10* (8).

151. Angel-Huerta, F.; González-Araoz, M. P.; Arias-Cerón, J. S.; Sánchez-Ramírez, J. F.; Díaz-Reyes, J.; Herrera-Pérez, J. L.; Mendoza-Álvarez, J. G., Study of the effect of the synthesis temperature on the photoluminescent properties of InP@ZnS nanocrystals. *Journal of Materials Science: Materials in Electronics* **2018,** *29* (18), 15649-15657.

152. Li, L.; Reiss, P., One-pot synthesis of highly luminescent InP/ZnS nanocrystals without precursor injection. *J Am Chem Soc* **2008,** *130* (35), 11588-9.

153. Xia, C.; Meeldijk, J. D.; Gerritsen, H. C.; de Mello Donega, C., Highly Luminescent Water-Dispersible NIR-Emitting Wurtzite CuInS2/ZnS Core/Shell Colloidal Quantum Dots. *Chem Mater* **2017,** *29* (11), 4940-4951.

154. Alemu, Y. A. Synthesis, Surface Treatment, and Characterization of Copper Indium Sulfide Quantum Dots. Oregon State University, 2016.

155. Clarke, M. T.; Viscomi, F. N.; Chamberlain, T. W.; Hondow, N.; Adawi, A. M.; Sturge, J.; Erwin, S. C.; Bouillard, J.-S. G.; Tamang, S.; Stasiuk, G. J., Synthesis of super bright indium phosphide colloidal quantum dots through thermal diffusion. *Communications Chemistry* **2019,** *2* (1).

156. Kim, T.; Kim, S. W.; Kang, M.; Kim, S.-W., Large-Scale Synthesis of InPZnS Alloy Quantum Dots with Dodecanethiol as a Composition Controller. *The Journal of Physical Chemistry Letters* **2012,** *3* (2), 214-218.

157. Watanabe, T.; Wada, C.; Iso, Y.; Isobe, T.; Sasaki, H., Preparation of Photostable Fluorescent InP/ZnS Quantum Dots Embedded in TMAS-Derived Silica. *ECS Journal of Solid State Science and Technology* **2017,** *6* (7), R75-R80.

158. Chang, J.; Waclawik, E. R., Controlled synthesis of CuInS2, Cu2SnS3 and Cu2ZnSnS4 nano-structures: insight into the universal phase-selectivity mechanism. *CrystEngComm* **2013,** *15* (28), 5612-5619.

159. Feizi, S.; Zare, H.; Hoseinpour, M., Investigation of dosimetric characteristics of a core–shell quantum dots nano composite (CdTe/CdS/PMMA): fabrication of a new gamma sensor. *Applied Physics A* **2018,** *124* (6), 1-7.

160. Yan, W.; Bai, G. X.; Ye, R. G.; Yang, X. L.; Xie, H. Q.; Xu, S. Q., Dual-mode luminescence tuning of Er^{3+} doped Zinc Sulfide piezoelectric microcrystals for multi-dimensional anti-counterfeiting and temperature sensing. *Opt. Commun.* **2020,** *475*, 7.

161. Hua, Y.; Hussain, S. K.; Yu, J. S., Ultrafast preparation of Europium(III) and Terbium(III) activated LaSr2F7 nanoparticles for white LEDs and anti-counterfeiting mark. *Journal of Alloys and Compounds* **2020,** *826*, 14.

162. Yao, W. J.; Tian, Q. Y.; Liu, J.; Xue, Q. W.; Li, M. X.; Liu, L.; Lu, Q.; Wu, W., Preparation and RGB upconversion optic properties of transparent anti-counterfeiting films. *Nanoscale* **2017,** *9* (41), 15982-15989.

163. Chen, B.; Xie, H. P.; Wang, S.; Guo, Z. Y.; Hu, Y. F.; Xie, H. Z., UV light-tunable fluorescent inks and polymer hydrogel films based on carbon nanodots and lanthanide for enhancing anti-counterfeiting. *Luminescence* **2019,** *34* (4), 437-443.

164. Yang, P.; Zhu, Z. Q.; Zhang, T.; Chen, M. Z.; Cao, Y. Z.; Zhang, W.; Wang, X.; Zhou, X. Y.; Chen, W. M., Facile synthesis and photoluminescence mechanism of green emitting xylose-derived carbon dots for anti-counterfeit printing. *Carbon* **2019,** *146*, 636-649.

165. Park, S. J.; Park, J. Y.; Yang, H. K., Luminescence of a novel cyan emitting $Sr_{10}(PO_4)(_6)OCe^{3+}$ phosphor for visualization of latent fingerprints and anti-counterfeiting applications. *Sens. Actuator B-Chem.* **2018,** *262*, 542-554.

166. Andres, J.; Hersch, R. D.; Moser, J. E.; Chauvin, A. S., A New Anti-Counterfeiting Feature Relying on Invisible Luminescent Full Color Images Printed with Lanthanide-Based Inks. *Advanced Functional Materials* **2014,** *24* (32), 5029-5036.

167. Kumar, P.; Dwivedi, J.; Gupta, B. K., Highly luminescent dual mode rare-earth nanorod assisted multi-stage excitable security ink for anti-counterfeiting applications. *Journal of Materials Chemistry C* **2014,** *2* (48), 10468-10475.

168. Development, O. f. E. C.-o. a. *The Economic Impact of Counterfeiting*; 1998.

169. Casatelli, L. M., Inks and Pigments in Security Applications. Pira International Ltd: 2011.

170. *Global Brand Counterfeiting Report 2018-2020* December 2017.

171. Jing, L.; Xie, Q.; Li, H. L.; Li, K. R.; Yang, H. T.; Ng, P. L. P.; Li, S.; Li, Y.; Teo, E. H. T.; Wang, X. N.; Chen, P. Y., Multigenerational Crumpling of 2D Materials for Anticounterfeiting Patterns with Deep Learning Authentication. *Matter* **2020,** *3* (6), 2160-2180.

172. Chong, C. N.; Jiang, D.; Zhang, J.; Guo, L., Anti-counterfeiting with a Random Pattern. In *2008 Second International Conference on Emerging Security Information, Systems and Technologies*, 2008; pp 146-153.

173. He, X. Y.; Gu, Y. N.; Yu, B. R.; Liu, Z. W.; Zhu, K.; Wu, N.; Zhao, X.; Wei, Y.; Zhou, J. M.; Song, Y. L., Multi-mode structural-color anti-counterfeiting labels based on physically unclonable amorphous photonic structures with convenient artificial intelligence authentication. *Journal of Materials Chemistry C* **2019,** *7* (45), 14069-14074.

174. George, G.; Luo, Z., A Review on Electrospun Luminescent Nanofibers: Photoluminescence Characteristics and Potential Applications. *Current Nanoscience* **2020,** *16* (3), 321-362.

175. Shi, X.; Zhou, W.; Ma, D.; Ma, Q.; Bridges, D.; Ma, Y.; Hu, A., Electrospinning of Nanofibers and Their Applications for Energy Devices. *Journal of Nanomaterials* **2015,** *2015*, 1-20.

176. Kristin J. Pawlowski, T. L. S. C., Amber C. McReynolds, Cheol Park, Zoubeida Ounaies, Emilie J. Siochi, Joycelyn S. Harrison, Electrospun electroactive polymers for aerospace applications. *Collection of Technical Papers - AIAA/ASME/ASCE/AHS/ASC Structures, Structural Dynamics and Materials Conference* **2003,** *5*, 3346-3350.

177. Xue, J.; Wu, T.; Dai, Y.; Xia, Y., Electrospinning and Electrospun Nanofibers: Methods, Materials, and Applications. *Chem Rev* **2019,** *119* (8), 5298-5415.

178. Hong, Y., Electrospun fibrous polyurethane scaffolds in tissue engineering. In *Advances in Polyurethane Biomaterials*, 2016; pp 543-559.

179. Kaushal, N.; Kaushal, P., Human Identification and Fingerprints: A Review. *Journal of Biometrics & Biostatistics* **2011,** *02* (04).

180. MD, R. M. C., How fingerprints came into use for personal identification. *Journal of the American Academy of Dermatology* **1990,** *23* (1), 109-114.

181. Khan, M. K. I.; Nazir, A.; Maan, A. A., Electrospraying: a Novel Technique for Efficient Coating of Foods. *Food Engineering Reviews* **2016,** *9* (2), 112-119.

182. Zhuoying Jiang, X. Y., Understanding of droplet dynamics and deposition area in electrospraying process: Modeling and experimental Approaches. *arXiv preprint arXiv:1809.09688* **2018**.

183. Wang, J.; Jansen, J. A.; Yang, F., Electrospraying: Possibilities and Challenges of Engineering Carriers for Biomedical Applications-A Mini Review. *Front Chem* **2019,** *7*, 258.

184. I. Wuled Lenggoro, B. X., and Kikuo Okuyama, Sizing of Colloidal Nanoparticles by Electrospray and Differential Mobility Analyzer Methods. *Langmuir* **2002,** *18* (12), 4584-4591.

185. Bock, N.; Woodruff, M. A.; Hutmacher, D. W.; Dargaville, T. R., Electrospraying, a Reproducible Method for Production of Polymeric Microspheres for Biomedical Applications. *Polymers* **2011,** *3* (1), 131-149.

186. Zhang, S.; Campagne, C.; Salaün, F., Influence of Solvent Selection in the Electrospraying

Process of Polycaprolactone. *Applied Sciences* **2019,** *9* (3).

187. Xu, Y.; Skotak, M.; Hanna, M., Electrospray encapsulation of water-soluble protein with polylactide. I. Effects of formulations and process on morphology and particle size. *J Microencapsul* **2006,** *23* (1), 69-78.

188. Eda, G. Effects of Solution Rheology on Electrospinning of Polystyrene. WORCESTER POLYTECHNIC INSTITUTE 2016.

189. Supaphol, P.; Chuangchote, S., On the electrospinning of poly(vinyl alcohol) nanofiber mats: A revisit. *Journal of Applied Polymer Science* **2008,** *108* (2), 969-978.

190. Tao, J. Effects of Molecular Weight and Solution Concentration on Electrospinning of PVA. Worcester Polytechnic Institute, 2003.

191. Zargham1, S.; , S. B.; , A. T.; , A. S. R.; , R. D., The Effect of Flow Rate on Morphology and Deposition Area of Electrospun Nylon 6 Nanofiber. *Journal of Engineered Fibers and Fabrics* **2012,** *7* (4), 42-49.

192. Xinwei WANG, J. C., Zuming HU,Wanlian PAN,Zhaofeng LIU, <Jet Shaping Nanofibers and the Collection of Nanofiber Mats in Electrospinning.pdf>. *Journal of Materials Science and Technology* **2006,** *22* (4), 536-540.

193. Milleret, V.; Simona, B.; Neuenschwander, P.; Hall, H., Tuning electrospinning parameters for production of 3D-fiber-fleeces with increased porosity for soft tissue engineering applications. *Eur Cell Mater* **2011,** *21*, 286-303.

194. TEO, W.-E. Fiber Diameter control by parameters optimization.

195. T. Senthil, S. A., Effect of Solvents on the Solution Electrospinning of Poly(styrene-co-acrylonitrile). *Kautschuk Gummi Kunststoffe* **2017,** *70* (7/8), 44-56.

196. Eom, Y.; Kim, B. C., Solubility parameter-based analysis of polyacrylonitrile solutions in N,N-dimethyl formamide and dimethyl sulfoxide. *Polymer* **2014,** *55* (10), 2570-2577.

197. Huang, C.; Soenen, S. J.; Rejman, J.; Lucas, B.; Braeckmans, K.; Demeester, J.; De Smedt, S. C., Stimuli-responsive electrospun fibers and their applications. *Chem Soc Rev* **2011,** *40* (5), 2417-34.

198.   Chi Wang, H.-S. C., Chia-Hung Hsu, Yin-Chi Wang, Cheng-Ting Wang, and Hsin-An Lu, Electrospinning of Polyacrylonitrile Solutions at Elevated Temperatures. *Macromolecules* **2007,** *40*, 7973-7983.

199.   Ucar, N.; Kizildag, N.; Onen, A.; Karacan, I.; Eren, O., Polyacrylonitrile-polyaniline composite nanofiber webs: Effects of solvents, redoping process and dispersion technique. *Fibers and Polymers* **2015,** *16* (10), 2223-2236.

200.   Canny, J., A Computational Approach to Edge Detection. *IEEE Transactions on Pattern Analysis and Machine Intelligence* **1986,** *PAMI-8* (6), 679-698.

VITA

PERSONAL INFORMATION

Surname, Name: TAŞCIOĞLU, Didem
Nationality: Turkish (T.C.)

EDUCATION

Degree	Institution	Year
PhD	İzmir Institute of Technology	2021
MSc	İzmir Institute of Technology	2013
BSc	İzmir Institute of Technology	2010

PUBLICATION

1. Optimization and Performance of Nitrogen-doped Carbon Dots as Water-based Color Conversion Layer For White-LED Applications- Beilstein J. Nanotechnol. 2019, 10, 2004–2013.

2. VOC sensors based on a metal oxide nanofibrous membrane/QCM system prepared by electrospinning-New J. Chem.**,** 38, 5761-5768, 2014.

3. An ultraviolet photodetector with an active layer composed of solution processed polyfluorene:$Zn_{0.71}Cd_{0.29}S$ hybrid nanomaterials-Applied Surface Science, 305, 227-234, 2014.

4. Humidity sensing properties of ZnO-based fibers by electrospinning-Talanta, 85, 2, 1105-1111, 2011.

Kuantag Nanoteknolojiler

Geliştirme ve Üretim A.Ş.

Barbaros Mahallesi Gelincik Sokak No: 4-28

Ataşehir 34746 İstanbul, Türkiye

T: +90 216 522 90 00

F: +90 216 522 90 13

As Quantag, we hereby declare that the sensors that are used in this academic study have been provided within the fully consent of the company and these sensors have been used in the academic study within the fully knowledge of the company.

119